RESEARCH ON THEORY AND TECHNIQUES OF ENERGY MANAGEMENT FOR ENERGY-HARVESTING POWERED WIRELESS COMMUNICATIONS

by

Xiaojing Chen

Dissertation submitted in fulfilment of the requirements

for the degree of

DOCTOR OF PHILOSOPHY

Department of Engineering
Faculty of Science and Engineering
Macquarie University
Sydney, Australia

November 2018

STATEMENT OF CANDIDATE

I certify that the work in this thesis entitled "Research on Theory and Techniques of Energy Management for Energy-Harvesting Powered Wireless Communications" has not previously been submitted for a degree nor has it been submitted as part of the requirements for a degree to any other university or institution other than Macquarie University.

I also certify that the thesis is an original piece of research and it has been written by me.

In addition, I certify that all information sources and literature used are indicated in the thesis.

Xiaojing Chen

To Marc SHE, who is learning the world now.

ACKNOWLEDGMENTS

I would like to thank to my principal supervisor, Prof. Iain B. Collings for his valuable support and supervision. I would like to extend my thanks to my co-supervisors Dr. Wei Ni in CSIRO and Prof. Xin Wang in Fudan University. This thesis would not have been possible without their help and support. My sincere thanks also go to my fellows in the office for their friendship, kindness, and all the great time we had together.

I dedicate this thesis with love to my parents for their unconditional love, to my husband for his encouragement and support, and to my son for giving me a new identity.

ABSTRACT

Energy harvesting (EH) is the process of capturing renewable energy from the environment and converting it into usable electrical energy. In wireless communication systems, collecting renewable energy from the environment is a key factor in building self-sustainable networks. In addition, EH-powered wireless communications help reduce carbon footprint and enable "green" communications to solve important issues such as haze, global warming, and climate change. Due to these ecological and economic reasons, various types of EH-powered wireless communications have become current research hotspots.

However, challenges arise in EH-powered wireless communication systems. First, the reliability of data transmissions is challenged due to the inherent randomness and instability of environmental energy sources. Second, due to the limited energy provided by environmental energy sources, how to make full use of the limited energy and ensure the systems obtain optimal performances is also a stringent subject. Therefore, for EH-powered wireless communication systems, we need to conduct reasonable energy management and resource allocation to ensure reliable and efficient communications, thus optimizing system performances.

On the one hand, for EH-powered WSN links, we optimize energy management for the transmitters, so that the collected energy is properly distributed to data transmissions. On the other hand, we introduce smart-grid technology to jointly provide renewable energy and grid's persistent energy to base stations (BSs) in

cellular networks, compensating for unstable and insufficient EH power supply. Through the optimal energy management of BSs, we make full use of renewable energy, maximize the system throughput or minimize the electricity transaction cost with the grid, while satisfying users' quality of service (QoS).

Optimal energy management is first investigated for EH-powered WSN links. A new "dynamic string tautening" algorithm is proposed to generate the most energy-efficient offline schedule for delay-limited traffic of transmitters. The algorithm is based on two key findings derived through convex formulation and resultant optimality conditions, specifies a set of simple but optimal rules, and generates the optimal schedule with a low complexity. The proposed algorithm is also extended to on-line scenarios, where the transmit schedule is generated on-the-fly.

An infinite time-horizon resource allocation problem is then formulated to maximize the time-average downlink throughput for smart-grid powered multiple-input multiple-output (MIMO), subject to a time-average energy cost budget. By using the advanced time decoupling technique, a novel stochastic subgradient based online control (SGOC) approach is developed for the resultant smart-grid powered communication system. It is established analytically that the proposed online control algorithm is able to yield a feasible and asymptotically optimal solution without a-priori knowledge of the stochastic system information.

Last, a two-scale stochastic control framework is put forth for smart-grid powered coordinated multi-point (CoMP) systems.The energy management task is formulated as an infinite-horizon optimization problem minimizing the time-average energy transaction cost. Leveraging the Lyapunov optimization approach as well as the stochastic subgradient method, a two-scale online control (TSOC) approach is developed for the resultant smart-grid powered CoMP systems.

Using only historical data, the proposed TS-OC makes online control decisions at two timescales, and features a provably feasible and asymptotically near-optimal solution.

Contents

List of Figures

List of Tables

List of Publications

Publications where the author appeared as first author.

- **X. Chen**, W. Ni, T. Chen, I. B. Collings, X. Wang, and G. B. Giannakis, "Real-time Energy Trading and Future Planning for fifth-Generation Wireless Communications," *IEEE Wireless Commun.*, vol. 24, no. 4, pp. 24–30, Aug. 2017.

- **X. Chen**, W. Ni, X. Wang, and Y. Sun, "Provisioning Quality-of-Service to Energy Harvesting Wireless Communications," *IEEE Commun. Mag.*, vol. 53, no. 4, pp. 102–109, April 2015.

- **X. Chen**, W. Ni, X. Wang, and Y. Sun, "Optimal Quality-of-Service Scheduling for Energy-Harvesting Powered Wireless Communications," *IEEE Trans. Wireless Commun.*, vol. 15, no. 5, pp. 3269–3280, May 2016.

- **X. Chen**, W. Ni, T. Chen, I. B. Collings, X. Wang, R. P. Liu, and G. B. Giannakis, "Distributed Online Optimization of Network Function Virtualization under Stochastic Arrivals of Network Service Chains," *IEEE Trans. Commun.*, accepted, 2018.

- **X. Chen**, W. Ni, I. B. Collings, X. Wang, and S. Xu, "Multi-Timescale Online Optimization of Network Function Virtualization for Service Chaining," *IEEE Trans. Mobile Comput.*, accepted, 2018.

- **X. Chen**, W. Ni, I. B. Collings, X. Wang, and S. Xu, "Distributed Placement and Online Optimization of Virtual Machines for Network Service Chains," *Proc. of ICC*, Kansas City, MO, May 20–24, 2018.
- **X. Chen**, W. Ni, T. Chen, I. B. Collings, X. Wang, R. P. Liu, and G. B. Giannakis, "Distributed Stochastic Optimization of Network Function Virtualization," *Proc. Globecom.*, Singapore, Dec. 4–8, 2017.
- **X. Chen**, X. Wang, W. Ni, and I. B. Collings, "Two-Way Energy Trading and Online Planning for Fifth-Generation Communications with Renewables," invited paper, APCC, Perth, Australia, Dec. 11–13, 2017.
- **X. Chen**, T. Chen, X. Wang, L. Huang, and G. B. Giannakis, "Two-Scale Stochastic Control for Smart-Grid Powered Coordinated Multi-Point Systems," *Proc. Globecom.*, Washington DC, Dec. 4–8, 2016.
- **X. Chen**, T. Chen, X. Wang, and G. Giannakis, "Stochastic Online Control for Smart-Grid Powered MIMO Downlink Transmissions," ICASSP, Shanghai, China, March 21–25, 2016.
- **X. Chen**, X. Wang, and X. Zhou, "Energy-Harvesting Powered Transmissions of Delay-limited Data Packets," *Proc. Globecom.*, Austin, TX, Dec. 8–12, 2014.
- **X. Chen**, X. Wang, and Y. Sun, "Energy-Harvesting Powered Transmissions of Bursty Data Packets with Strict Deadlines," *Proc. of ICC*, Sydney, Australia, Jun. 10–14, 2014.

Publications where the author is not the first author.

- X. Wang., **X. Chen**, T. Chen, L. Huang, and G. B. Giannakis, "Two-Scale Stochastic Control for Multipoint Communication Systems with Renewables," *IEEE Trans. Smart Grid*, vol. 9, no. 3, pp. 1822–1834, May 2018.

- X. Wang., T. Chen, **X. Chen**, X. Zhou, and G. B. Giannakis, "Dynamic Resource Allocation for Smart-Grid Powered MIMO Downlink Transmissions," *IEEE J. Sel. Areas Commun.*, vol. 34, no. 12, pp. 3354–3365, Dec. 2016.

Chapter 1

Introduction

1.1 Background and Motivations

Nowadays, information and communication technology (ICT) has become an indispensable part of people's daily life. However, energy consumption has raised as a big issue with the rapid proliferation of ICT, as well as greenhouse gas (CO_2) emissions. It has been estimated that, in 2012, the average annual power consumption by ICT industries exceeded 200 GW [7]; 3 percent of the world's annual electrical energy consumption and 2 percent of CO_2 emissions are caused by the ICT infrastructure. Moreover, ICT energy consumption is expected to increase by 15–20 percent annually, doubling every five years [8]. As an important field of ICT, the CO_2 emissions of wireless communication systems in 2002 accounted for 42 percent of the total ICT CO_2 emissions, and it is expected that this proportion will increase to 51 percent by 2020 [9]. In 2012, the largest mobile network in the world–China Mobile–consumed more than 14 billion kWh of energy in its network of 1.1 million base stations [10]. In the 5G era, millions of base stations with higher functionality are expected to connect with billions of smartphones and devices with higher data rates.

As people become more aware of the potentially harmful effects of CO_2 emissions and non-renewable energy consumption on the environment, it is urgent to develop green and energy-efficient telecommunications systems. From the perspective of telecom operators, reducing power consumption is not only a matter of being green and responsible, it is also a very important economic issue. A large portion of the operational expenditure (OPEX) of a telecommunications network are used to pay the electricity bill. The global mobile network OPEX for electricity has exceeded 10 billion US dollars [11]. To achieve economic efficiency and out of social responsibility for coping with global climate change, green energy-efficient communication is bound to become an important trend of the next generation wireless communication networks.

Several research groups and consortia have been investigating green and energy-efficient communications for wireless communication systems, including Mobile VCE, EARTH, and Green-Touch. Mobile VCE has focused on the hardware, architecture, and operation of BSs, achieving energy saving gains of 75–92 percent in simulations [10]. EARTH has devised an array of new technologies including low-loss antennas, antenna muting, and micro direct transmission based on traffic fluctuations, realizing energy savings of 60–70 percent with less than 5 percent throughput degradation [11]. GreenTouch has set up a more ambitious goal to improve energy efficiency 1000 times by 2020 [12]. In addition, some operators have been actively developing green technologies, e.g., green BSs powered solely by renewable energy, and green access infrastructure such as cloud/collaborative/clean radio access network (C-RAN) [13]. Communication equipment manufacturers, e.g., Huawei, are also working on the research and development of green communication technologies. Academic research on green communications is also very active. The Institute of Electrical and Electronics Engineers (IEEE) has organized discussions on green-communication related topics in international conferences such as ICC and Globecom; and in major international journals and magazines on communications, research outcomes related to green

energy-efficient communications from all over the world have been published [14].

As one of the key technologies for achieving green communications, energy harvesting (EH) is the process of capturing renewable energy from the environment and converting it into usable electrical energy [15]. In wireless communication systems, collecting renewable energy from the environment is a key factor in building self-sustainable networks, such as wireless sensor networks (WSNs) in remote human-unfriendly environments [16]. It helps communication networks get rid of the limits of the grid, enabling people to provide network services in remote areas without grid coverage or in harsh areas. Various types of EH-powered wireless communications have increasingly become current research hotspots.

However, challenges arise in EH-powered wireless communication systems. First, the reliability of data transmissions is challenged due to the inherent randomness and instability of environmental energy sources. Second, due to the limited energy provided by environmental energy sources, how to make full use of the limited energy and ensure the systems obtain optimal performances is also a stringent subject. Therefore, for EH-powered wireless communication systems, we need to conduct reasonable energy management and resource allocation, and develop optimal data transmission schedules to ensure reliable and efficient communications, thus optimizing system performances.

On the one hand, for EH-powered WSN links, we optimize energy management for the transmitters, so that the collected energy is properly distributed to data transmissions. We propose optimal transmission schedules to deliver delay-sensitive data packets before their deadlines, and minimize energy consumption, thus achieving green communications. On the other hand, based on the use of traditional energy sources, we introduce smart-grid technology to jointly provide renewable energy and grid's persistent energy to wireless communication facilities (i.e., base stations) in cellular networks, compensating for unstable and insufficient EH power supply. Through the optimal energy management of base stations, we make full use of renewable energy, maximize the system throughput

or minimize the electricity transaction cost with the grid, while satisfying users' quality of service (QoS).

1.1.1 Energy Harvesting

Energy harvesting technology mainly includes three aspects: energy conversion, energy storage and energy management. Energy conversion uses special materials (e.g., piezoelectric materials) to sense potential energy changes, and convert the input signal into a weak energy output. The energy conversion of piezoelectric sensors is the most common application. Energy storage is to store weak electrical energy through rechargeable batteries or capacitors. Energy management is responsible for the rational use of collected energy. The following describes the harvesting and storage of environmental energy.

Harvesting of Environmental Energy

With the development of energy technology, the implementation methods of harvesting environmental energy tend to be diversified. A large number of external energy sources have potential to be harvested. They are [17]:

- natural (renewable) energy, e.g., wind, water flow, ocean currents and the sun;
- mechanical energy, e.g., vibration, and mechanical stress and strain;
- thermal energy, e.g., waste energy from furnaces, heaters, and friction;
- light energy, e.g., natural and artificial light;
- electromagnetic energy, e.g., inductors, coils and transformers;
- energy from the human body, e.g., a combination of mechanical and thermal energy naturally generated by people when walking, sitting, climbing and running;
- energy from other sources, such as chemical and biological sources.

However, the amount of energy available for collection in the environment varies over space and time. Solar energy is available during the day and it vanishes at night. Ur-

Energy source	Power density	Advantages	Disadvantages
Solar	15 mW/cm^3	Sufficient energy in the daytime, high output voltage	Disappear at night
Vibration	200 uW/cm^3	Without voltage source	Brittle materials
Thermoelectric	40 uW/cm^2	Long life, reliable with low maintenance	Low energy conversion efficiency
Acoustic noise	960 nW/cm^3	High energy conversion efficiency	Rare environments with high acoustic noise levels
Airflow	1 mW/cm^2	Sufficient in certain place and time	Big size
Radio frequency	1 uW/cm^2	Simultaneous wireless information and power transfer	Attenuate rapidly over distance

Figure 1.1: Power densities, advantages, and disadvantages of different energy sources.

ban areas provide radio frequency (RF) energy, while open areas provide wind energy. Therefore, it is important to select the appropriate energy harvesting method based on the energy harvesting environment of the communication system. Fig. 1.1 lists the power densities, advantages, and disadvantages of different energy sources [4].

Fig. 1.2 shows a practical model diagram for EH systems [4]. The energy harvester is the most important device in the energy harvesting process. It can be an energy conversion sensor made of a specific material, an integrated chip with energy conversion function, or an energy conversion circuit composed of different components. The energy harvester converts ambient energy into electrical energy, which is to be stored in a rechargeable battery or capacitor (referred to as an energy buffer). A rechargeable battery or capacitor provides power to the micro-controller and transmitter module. The micro-controller can manage the entire node, including the supply, information to transmit or receive. Typically, there is a data storage device called a data buffer storing collected data.

Solar energy is typically harvested by solar panels. According to the size and power consumption of the equipment in communication systems, the size of the solar panels equipped can be designed and adjusted [18]. For electronic tags that can communicate

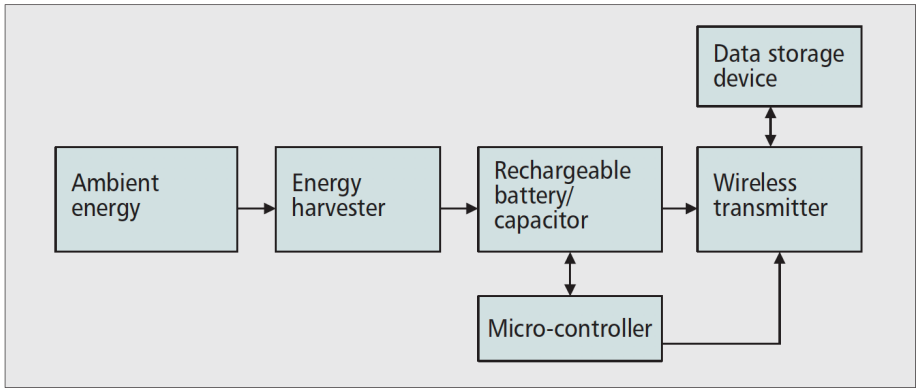

Figure 1.2: A practical model diagram for EH systems [4].

autonomously, due to the size limitation of the transmitters and the design of low power consumption, the size of the solar panels equipped must also be reduced, while meeting the basic power requirements of signal transmission. For large relay base stations, the solar panels are relatively large in size to provide more power supply and meet the high power consumption requirements, provided that the deployment of equipment is not affected. Compared with wind energy, solar energy provides relatively less, but more stable energy supply, and is easy to predict in the short term. Generally, a communication device with relatively low reliability requirements can select an independent power supply scheme based on solar energy provision, along with a rechargeable battery [19].

Wind energy harvesting is the process of converting the energy of air streams, such as wind, into electrical energy. Wind energy is usually harvested by wind turbines with appropriate size [20]. Micro wind turbines can generate enough energy to power WSN nodes [21]. However, the efficient design of small-scale wind energy harvesting still needs to be studied, which is challenged by low flows, fluctuating wind intensity, and unpredictable flow sources. In general, the advantage of wind power is that it can provide sufficient energy more effectively, but the flexibility of its deployment is limited [22]. Wind energy powered communication facilities are usually deployed outdoors, due to the

characteristics of wind energy harvesting and the limitations of the power generation units. To meet the reliability requirements, in addition to rechargeable batteries, the wind energy powered system also consumes energy from traditional power grids in many cases to compensate for the instability of wind energy. This approach not only reduces energy costs and negative impacts on the environment, but also guarantees QoS.

RF energy harvesting falls into the category of wireless energy harvesting. It is a process of converting electromagnetic waves into electrical energy through rectifying antennas. The harvesting of RF energy may come from RF power in the environment such as radio and television broadcasts, cell phones, wireless communications, and microwaves, or electromagnetic signals generated from specific wavelengths. As the signal is further away from the source, the energy is rapidly reduced. Therefore, although there is a large amount of potential ambient RF power, the energy of existing electromagnetic waves is very low. In order to efficiently collect RF energy from existing environmental waves, the harvester must be deployed close to the RF source. Another solution is to use dedicated RF transmitters or power beacons to generate more powerful electromagnetic signals to power sensor nodes. This kind of RF energy harvesting can effectively increase power from microwatts to a few milliwatts, depending on the distance between RF transmitters and harvesters.

Storage of Environmental Energy

Batteries are often considered as ideal energy storage devices to cope with the instability of environmental energy. It contains a given amount of energy units. A node operation (such as sending or receiving a data packet) uses a certain amount of energy units, based on the energy cost of the operation. After an operation is performed, the remaining energy in the battery is decreased by the amount of energy required for the operation. In practice, however, the battery experiences self-discharge. Even batteries that are not

being used suffer from a charge reduction incurred by internal chemical activity. Moreover, batteries have (dis)charge efficiency, which is smaller than 1, that is, some energy is lost during (dis)charging. In addition, batteries have some nonlinear characteristics [23]. They are: rate-based capacity, that is, as the discharge rate increases, the delivered capacity of the battery decreases in a nonlinear manner; temperature effect, in that operating temperature affects battery discharge behavior and directly affects self-discharge rate; recovery effect, for which if discharge and idle time alternate (pulse discharge), the lifetime and delivery capacity of a battery will increase. Besides, rechargeable batteries reduce their capacity during each recharge cycle, and their voltage is dependent on the charging level of the battery and also varies during discharge. These characteristics should be properly considered when designing and simulating EH systems.

Different types of batteries have different energy (dis)charge characteristics and self-discharge loss. Among them, lithium batteries have higher (dis)charge efficiency, generally up to 95 percent or more; capacitor-based batteries have large self-discharge loss, thus not suitable for long-term storage of electrical energy; lead-acid batteries can provide large capacity for energy storage; however, they have high (dis)charge loss [24].

1.1.2 Wireless Sensor Networks

The emerging concept of the Internet of Things (IoT) is considered to be the next technological revolution, enabling many types of objects, machines and devices to communicate on an unprecedented scale. WSNs can be seen as an essential part of IoT, because they help users (people or machines) interact with their environment and react to real-world events. WSNs are made up of a large number of sensors networked in unattended applications. These sensors measure environmental conditions and convert these measurements into signals, to reveal certain features of the area around these sensors.

There are various applications of WSNs. For example, one of the earliest applications

of WSNs is environmental monitoring, ranging from tracking fauna to monitoring hard-to-reach areas. WSNs can also be used in military for detecting and tracking snipers, intruders. In addition, the deployment of WSNs can address the challenges of logistics management, such as maintaining the quality of the cargo by monitoring the temperature of the container to improve logistics efficiency.

Furthermore, WSNs can also be used to improve gaming experience by using wearable and implantable camera sensors to enhance the interaction between the physical world and the virtual world. Medical and health applications form another important set of WSNs applications. WSNs enable paramedics to monitor the conditions of patients in the hospital or at home. Radiation level control, explosive gas level and leakage detection are also part of the potential safety and emergency applications of WSNs.

As enablers of applications ranging from health control to environmental monitoring, WSNs have played an important role in multi-hop wireless network research. Research in this area covers a wide range of topics, and has significant advantages in energy management, node hardware, and tracking techniques [25].

Research on WSNs is driven by a common focus: energy efficiency. WSN nodes are typically powered by batteries. The nodes are usually small in size, and the batteries can only store limited energy. The energy of the nodes determines the lifetime of the entire network. The batteries can only be replaced or recharged in very particular applications. Even though, the replacement or recharging operations are time consuming, expensive, and can degrade network performance. Therefore, different techniques for slowing down the depletion of battery energy have been proposed, including power control and the use of duty cycle-based operation [25].

Power control refers to the proper allocation of available energy by adjusting the transmission rates of data packets. According to theoretical and practical statistics, most of energy in sensor nodes is consumed by data transmission. In many modulation coding

schemes, the transmission power is an increasing convex function with respect to the transmission rate [26]. This means that to transmit the same amount of data, the energy consumed at a low rate in a longer period of time is less than the energy consumed at a high rate. However, data is often delay-sensitive. In order to meet the quality of service (QoS) requirements, the transmission time cannot be arbitrarily long and should meet the deadline constraint. Therefore, how to construct data transmission schedules in WSN links, and make full use of the limited energy in sensor nodes, while meeting the QoS requirements, is an important and challenging research topic.

Duty cycle-based operation uses the low power modes of wireless transceivers, whose components can be switched off to save energy. When a node is in low power (or sleep) mode, its power consumption is much lower than when the transceiver is on. However, the node cannot transmit or receive data packets while asleep. The duty cycle represents the ratio between the time when the node is on and the total time when the node is on and asleep. To enable a long-lasting WSN, adopting a protocol operating at a very low duty cycle is the primary solution [27]. But this approach has two main drawbacks [25].

1) This approach has an inherent tradeoff between EE and data latency, and

2) battery-powered WSNs cannot meet the requirements of many emerging applications that require decades or even longer network lifetimes. The presence of battery leakage can deplete batteries within a few years even if they are rarely used.

Out of these reasons, recent research on long-lasting WSNs has taken a different method, combining energy harvesters with rechargeable batteries and super capacitors as a key enabler of WSN operations. EH powered WSNs enable WSN nodes to extract energy from the surrounding environment. EH subsystems continuously collect energy from the environment and store it for future use, which enables a long-lasting WSN.

QoS, such as delay and packet error rate, is crucial to data transmission on WSN links.

Many sensory data are delay intolerant, especially in bushfire or flood monitoring, and security/safety surveillance applications. Three critical challenges arise in providing QoS to EH powered wireless transmissions.

- The first critical challenge is to generate QoS-guaranteed transmit schedules, given the unreliable and unstable power supply of EH. The harvested energy is time-varying. It can become insufficient to transmit data by their deadlines, if the transmissions are inadequately scheduled.

- The second critical challenge is to increase the EE of transmissions, especially in short-range wireless sensor networks where the energy consumed on the circuits (e.g., signal processing, digital-to-analogue conversion, and power amplification) is non-negligible [28]. It is important to make the insufficient energy meet the transmission requirement, reducing outage probability and QoS violations.

- The third critical challenge of providing QoS to EH powered transmissions is to reduce the computational complexity of generating schedules and in turn the energy consumption [29]. General convex optimization solvers (such as interior point methods [30]) may not be computationally efficient to solve this specific problem. Developing low-complexity specialized solvers may be required.

1.1.3 Smart-Grid Powered 5G Cellular Networks

Fifth-generation (5G) cellular networks are anticipated to be densely deployed with a significantly reduced coverage area per cell. Along with its reduced per-cell size, the number of cells will dramatically increase due to the explosively increasing mobile traffic and the limited availability of high-frequency spectrum [31]. Consequently, the total energy consumption of all base stations (BSs) would be high. It would contribute overwhelmingly to the operational expenditure of cellular networks, and adversely to global carbon footprint.

For economical and ecological purposes, an increasing number of BSs are now equipped with energy harvesting devices, e.g., solar panels or wind turbines. Renewable energy up to 10,000 KW has been used to power cellular systems, supplementing to persistent supplies from power grid [32]. Efficient techniques, such as ON/OFF BS switching [33], online scheduling [1, 34] and power control [35], have been proposed to reduce the power consumption and delay, or achieve a near-optimal throughput region for energy harvesting powered users.

While cellular networks are evolving, the revolution of power grid is also under the way. The next-generation smart grid, equipped with advanced smart meters and control capability, will be flexible, versatile, and able to support many new functionalities such as distributed energy generation, two-way energy flows, energy trading and redistribution, and energy demand management [36]. Traditional energy users, such as cellular networks, are potentially becoming an integral part of the smart grid, helping generate and redistribute energy.

From a management and productivity point of view, cellular networks are uniquely positioned to interoperate with smart grid. In particular, the sheer scale and ubiquity of cellular networks result in a significant amount of energy, either purchased off the grid or harvested from ambient environments. The amount is non-negligible to the load of the entire smart grid. Moreover, the centralized close control of cellular networks resembles to that of the smart grid. This can provide efficient redistribution of energy, and effective price negotiation with the smart grid [37].

Fig. 1.3 illustrates the new interoperable framework of 5G and smart grid, where BSs equipped with energy harvesting devices are connected to the smart grid through smart meters. The BSs are also connected to the core network (i.e., the gateway and Internet) through broadband backhaul links using gigabit or carrier-grade Ethernet [38]. Effective interoperability between 5G and the smart grid is not only feasible, but also important

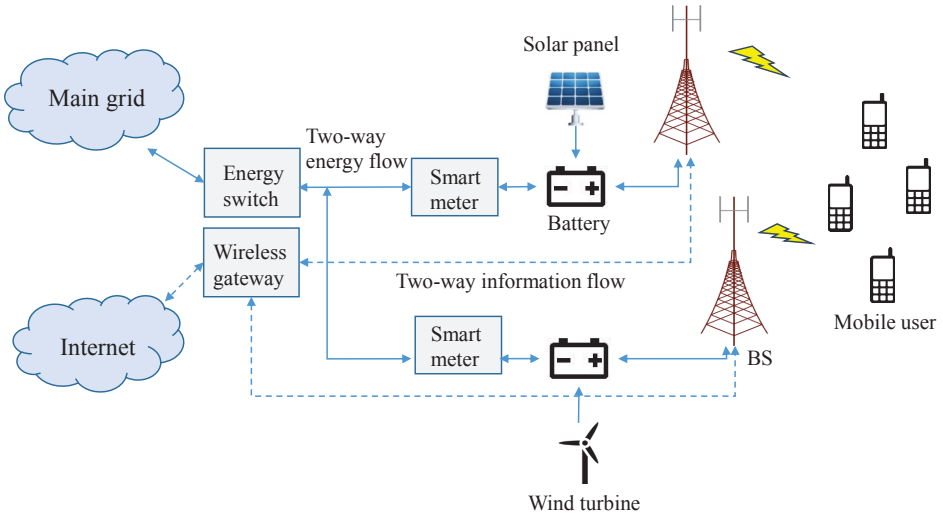

Figure 1.3: A new interoperable framework of 5G and smart grid. Two BSs with local renewable energy harvesting devices and batteries perform two-way energy trading with the main grid.

to both 5G and the smart grid.

A number of new functionalities become possible under this new interoperable framework.

Two-way energy trading: Cellular BSs, as an integral part of the grid, can purchase energy off the grid in shortage of renewable energy, and sell energy back to the grid when renewable energy is in abundance [36]. The abundant renewable energy can be redistributed through the smart grid for environmental benefits, as well as financial gains of 5G. This helps balance energy load and relieve pressure on the grid, and hence improve the reliability of the grid.

Dynamic energy pricing: As a result of intermittent renewable energy and two-way energy trading, energy prices are expected to exhibit strong dynamics in smart grid. The dynamic pricing is important to regulate the energy demands, and encourage users such as 5G networks to consume energy wisely and efficiently. The prices of both selling and

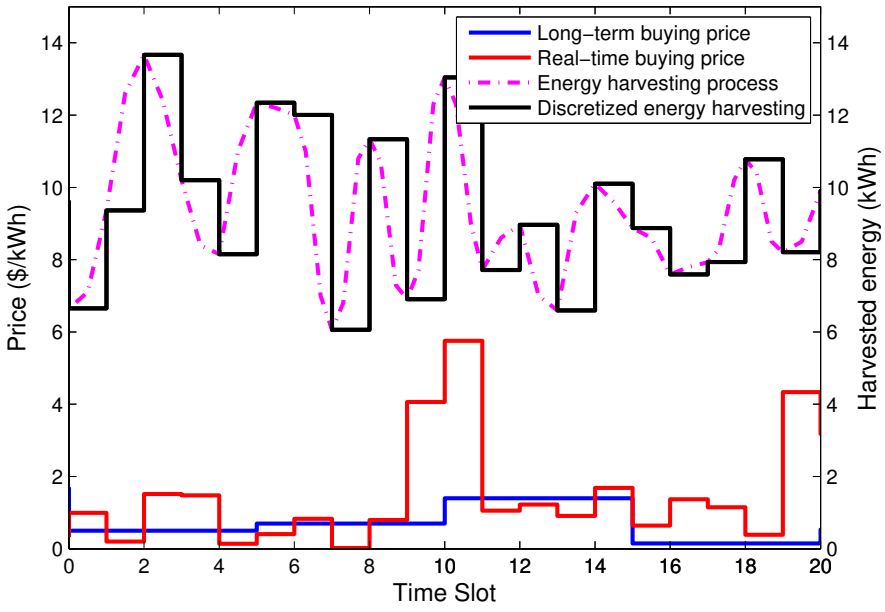

Figure 1.4: Multiple timescales of energy pricing and harvesting in the interoperable framework of future 5G and smart grid.

buying energy, fluctuate along the time to reflect the real-time energy demand and supply availability.

Multi-timescale energy planning: The interoperability of 5G and smart grid needs to be supported over multiple different timescales, i.e., for grid-energy pricing, energy harvesting and wireless transmission, as shown in Fig. 1.4. The different timescales are due to the physical properties of wireless channels and energy harvesting, the time-varying demand and supply across smart grid, and the marketing strategies of electricity utility companies.

- The wireless timescale depends on the channel coherence time of typically tens of milliseconds. The BSs update transmission schedules based on this interval to keep up with changing wireless channels.

- The smart-grid energy pricing timescales are regulated by the electricity utility com-

panies, depending on the demand and supply, and marketing strategies. Different business models and contractual arrangements can be made. Long-term pricing, lasting for up to days or months, reflects medium-to-long-term demand and supply, and changes in fuel market. On the other hand, short-term pricing reflects real-time changes in demand and supply. It can apply the wireless timescale, since wireless transmissions drive the changes.

- Energy harvesting is typically a slowly-changing continuous process, under current low energy transfer rate. Nevertheless, harvested energy is buffered in battery and the time instants transmitter attempts to use battery are discrete. To capture the real-time changes of energy consumption in wireless transmissions, it is reasonable to discretize energy harvesting based on the wireless timescale.

Taking these different timescales into account, a foresighted plan of energy usage in advance will be of significance to reduce the operational cost of 5G networks.

Other new interoperable functionalities between 5G and smart grid include energy- and spectrum-efficient wireless transmission, energy redistribution, wireless energy transfer, grid management and control monitoring [39].

In this thesis, we focus on two scenarios in 5G cellular networks: smart-grid powered multiple-input multiple-output (MIMO) downlink communications, and smart-grid powered coordinated multi-point (CoMP) communications.

MIMO

MIMO refers to the use of multiple transmit and receive antennas to exploit multipath propagation, thereby multiplying the capacity of a radio link and improving the communication quality. MIMO can make full use of space resources, realize multiple transmission and multiple reception through multiple antennas, and multiply the channel capacity of

the system without increasing the antenna transmission power or spectrum resources. MIMO has played an essential part in wireless communication standards, including IEEE 802.11n (Wi-Fi), WiMAX (4G), and Long Term Evolution (LTE 4G).

MIMO can be divided into three main categories: precoding, spatial multiplexing, and diversity coding.

Precoding narrowly refers to multi-stream beamforming. More generally, it refers to all spatial processing that occurs at the transmitter. In single-stream beamforming, the same signals are transmitted from each transmit antenna with proper phase and gain weighting to maximize the signal power at the receiver input. Beamforming can increase the gain of the received signals by making signals transmitted from different antennas add up constructively, and reduce the multipath fading effect. Nevertheless, conventional beams are primarily characterized by multipath propagation in cellular networks. The transmit beamforming could not maximize the signal level at all receive antennas at the same time, when the receiver has multiple antennas. It is usually beneficial to precode with multiple streams. It is worth noting that precoding needs a-priori knowledge of channel state information (CSI) at both the transmitter and the receiver.

Spatial multiplexing demands MIMO antenna configuration. In spatial multiplexing, the high-rate signal is divided into multiple low-rate streams, and each stream is emitted from a different transmit antenna in the same frequency channel [40, 41]. With accurate CSI known a priori, the receiver can separate the streams into almost parallel channels, only if the arrived signals have sufficiently different spatial signatures. Spatial multiplexing is particularly useful to increase channel capacity at higher signal-to-noise ratios. It can also be used to simultaneously transmit signals to multiple receivers, which is known as multi-user MIMO. In this case, the transmitter needs CSI [42]. Good separability is allowed for the scheduling of receivers with different spatial signatures. Spatial multiplexing can be implemented without CSI at the transmitter; and can be combined with

precoding with full knowledge of CSI.

In diversity coding, a single stream is transmitted and encoded using the technique called space-time coding. The signals are transmitted from each transmit antenna with either full or near orthogonal coding. Signal diversity is enhanced by diversity coding exploiting independent fading in multiple antenna links. Diversity coding can be used without CSI at the transmitter; no beamforming or array gain is produced since there is no channel information. When certain channel information is available at the transmitter, diversity encoding and spatial multiplexing can be jointly applied.

Benefiting from technological advances in the smart grid era, next-generation MIMO communication systems are expected to be powered by RES integrated in the distribution grid, thus realizing the vision of green communications. However, penetration of renewables introduces variabilities in the traditional power system, making RES benefits achievable only after appropriately mitigating their inherently high variability, which challenges existing resource allocation strategies.

CoMP

Currently, the wireless industry is facing the growing demand for data traffic in cellular networks. The performance of point-to-point communication solutions is rapidly approaching the limits of fundamental information theory. In order to meet this growing demand, we can increase network coverage and capacity by deploying heterogeneous networks (HetNets), which consist of small base stations and macro ones [43]. CoMP is an effective management mechanism for intercell interference in HetNets [44]. In CoMP systems, BSs are partitioned into multiple clusters, and BSs in the same cluster serve the users by emitting coordinated beamforming [45–47]. BSs communicate with each other through the backhaul link to limit intercell interference and take full advantage of the benefits of distributed multi-antenna systems, leading to the increase of network

throughput.

CoMP can effectively eliminate co-channel interference between cells by sharing some necessary information between BSs. According to whether users' information is shared between BSs, CoMP can be classified into two categories: joint processing/transmission (JP/JT) and coordinated scheduling/beamforming (CS/CB).

- JP/JT: BSs in the same cluster share channel information and users' information at the same time, and perform joint pre-processing on users' data to reduce the interference between BSs. In this way, BSs within the entire cluster serve one or more users simultaneously.

- CS/CB: BSs in the same cluster can properly allocate the resources of systems by cooperation, and try to avoid the conflicts between the resources used by cell edge users in time and frequency. In this way, BSs within the cluster only need to share channel information, and each serves its respective users.

Green CoMP communication pursue energy efficient transmission and economical and environmentally friendly operation mode of BSs. It is a crucial means to achieve EE and resource optimization. Combining smart grid technology to optimize the resource allocation of green CoMP communication is a new method to improve the performance of wireless communications.

1.2 Previous Work

1.2.1 EH-powered WSN communications

Some recent works have been conducted in EH powered wireless links [48–57], but none of them addresses the three challenges of QoS provision, energy efficiency, and computational complexity, altogether. The works [48–55] were all focused on delay-tolerant traffic, thus

cannot provide QoS to delay-intolerant applications in practical systems. In [48, 49], the optimal schedules were generated to maximize the delay-tolerant throughput of an EH powered wireless link with negligible circuit power in time-invariant channels. In [50], a directional water-filling approach was proposed to maximize the throughput in time-varying channels. In [51], an "on-off" transmit schedule was developed to maximize the throughput of delay-tolerant traffic over a static point-to-point channel with non-ideal circuit power consumption. Later, extensions to time-varying channels were carried out in [52, 53]. Asymptotically optimal resource allocation was developed to maximize the throughput of delay-tolerant traffic for EH point-to-point link, where symbols could be transmitted through several parallel independent streams in [54]. In [55], a game theoretic approach was proposed to distribute the EH power of a relay among multiple source-destination pairs, which improved the trade-off between the outage of delay-tolerant traffic and system complexity for wireless cooperative networks.

In a different context from our research, there are recent works focused on energy efficient transmissions of delay-sensitive traffic in systems with persistent power supply, such as [58, 59]. In [58], a "string tautening" algorithm was proposed to produce the most energy-efficient schedule for delay-limited traffic, where the circuit power was assumed to be negligible. Given the persistent and sufficient power supply, the optimal schedule was generated by tautening a string between the static staircase curves of the data amount that can be transmitted by any instant and that must be transmitted by then. In [59], the algorithm was extended to the case of non-negligible circuit power. However, it is non-trivial to extend these string tautening algorithms to EH systems, where unreliable and insufficient power supply can stop the data being transmitted before deadline (as is never experienced with persistent power supplies). Transmissions powered by EH also undergo dependence among the data amount transmitted across the schedule. Every instant a transmit rate is decided, the remaining (insufficient) energy for the rest of the

schedule can change, and so do the data that can be transmitted at future instants. None of the existing string tautening algorithms can deal with the dependence. More works also include [60–63], which assumed persistent power supplies and cannot apply to EH powered systems.

1.2.2 Smart-grid powered MIMO downlink communications

Assuming that transmitters are powered by harvesting RES, [64–67] investigated optimal resource allocation strategies to maximize the total throughput of broadcast channels. Without considering energy storage units in a simplified smart-grid model, recent works pursued energy-efficient resource allocation for coordinated downlink transmissions in cellular networks [37, 68, 69]. Building on practical smart-grid models, our recent works in [70, 71] developed energy management and transmit-beamforming designs to minimize the energy transaction cost subject to user quality-of-service (QoS) guarantees of coordinated cellular downlinks. However, none of these works addressed the impact of smart-grid capabilities on the fundamentally achievable rate limits for the broadcast (downlink) channels in cellular networks.

Since MIMO techniques are well-documented boosters of spectrum efficiency, we are particularly interested in optimal resource allocation for smart-grid powered MIMO downlink transmissions to approach the fundamental rate limits in future cellular networks. In this context, assuming that the random RES generation lies in a deterministic uncertainty region, *offline* robust rate-maximizing resource management over a finite time horizon was pursued in [72]. However, the approach in [72] is applicable only if future information of energy prices is perfectly known, and the scheduling time horizon is fairly small. Its computational complexity will become prohibitively high as the scheduling horizon increases.

1.2.3 Smart-grid powered CoMP communications

A few recent works have considered the smart-grid powered CoMP transmissions [37, 69–71]. Assuming that the energy harvested from RES is accurately available *a priori* through e.g., forecasting, [69] and [37] considered the energy-efficient resource allocation for RES-powered CoMP downlinks. Building on realistic models, our recent work dealt with robust energy management and transmit-beamforming designs that minimize the worst-case energy transaction cost for the CoMP downlink with RES and DSM [70]. Leveraging novel stochastic optimization tools [73–75], we further developed an efficient approach to obtain a feasible and asymptotically optimal online control scheme for smart-grid powered CoMP systems, without knowing the distributions of involved random variables [71].

A salient assumption in [37, 69–71] is that all involved resource allocation tasks are performed in a single time scale. However, RES and wireless channel dynamics typically evolve over different time scales in practice. Development of two-scale control schemes is then well motivated for CoMP systems with RES. In related contexts, a few stochastic optimization based two-scale control schemes were recently proposed and analyzed in [76–79]. Extending the traditional Lyapunov optimization approach [73–75], [76] introduced a two-scale control algorithm that makes distributed routing and server management decisions to reduce power cost for large-scale data centers. Based on a similar approach, [77] developed a so-called MultiGreen algorithm for data centers, which allows cloud service providers to make energy transactions at two time scales for minimum operational cost. As far as wireless communications are concerned, [78] performed joint precoder assignment, user association, and channel resource scheduling for HetNets with non-ideal backhaul; while [79] introduced a two-timescale approach for network selection and subchannel allocation for integrated cellular and Wi-Fi networks with an emphasis on using predictive future information. Note that, neither [78] nor [79] considers the diversity of energy prices in fast/slow-timescale energy markets, and the energy leakage effects in

the energy management task.

1.3 Contributions of the Thesis

The main contributions of this thesis can be summarized as follows.

1.3.1 A new dynamic string tautening algorithm for WSN links

- In Chapter 2 [1], we consider the new scenario of EH powered transmission of data packets with strict deadlines, where the new challenge of unreliable power supply is imposed .
- A new DST algorithm is developed to generate the optimal transmit schedule in a computationally efficient, graphical manner by recursively updating the energy constraint curve on-the-go. The visualization of DST algorithm is illustrated in Fig. 2.1.
- A well-structured on-line scheme is proposed based on DST algorithm in Section 2.5, which follows the optimal rules that we develop, and produces the transmit schedule in real-time without a-priori knowledge on the data or energy arrivals.

1.3.2 A novel stochastic subgradient based online control approach for MIMO downlinks

- In Chapter 3 [2][1], targeting a 'sweet spot' of spectrum and cost efficiency, we formulate the stochastic online resource allocation task for a smart-grid powered MIMO

[1]Note that the content of Chapter 3 has been published in [2], of which the author of this thesis is the 3rd author listed on the paper. The work presented in this chapter, and in [2], was done collaboratively and the author of this thesis contributed to all parts. In particular the main technical contributions individually made by this thesis author were the derivation of the conditions to ensure feasibility of the

downlink as an infinite horizon optimization problem in (3.6), which maximizes the time-average (weighted) throughput, subject to a time-average energy cost budget.

- Adopting the so-termed "virtual queue" relaxation techniques in [71, 73, 74], we decouple the optimization variables across the infinite time horizon, and reformulate the problem as a state-independent stochastic programming. Then leveraging the dual relaxation and stochastic approximation methods, we develop a novel online control algorithm in Section 3.3.

- Different from [71, 73], and [74], where only one virtual queue, or, multiple independent queues are accounted for, the considered energy cost budget and battery energy level (two virtual queues) are actually correlated under the designed problem structure (as shown in (3.17)), which challenges the design of appropriate algorithm parameters and initializations to guarantee system feasibility.

- Facing this difficulty, we generalize the performance analysis in [71, 73], and [74] to derive additional conditions that ensure feasibility of the proposed algorithm (Lemmas 3-5 and Remark 1), and rigorously establish asymptotic optimality under the i.i.d. assumption for the random processes involved.

- Though the analytical claim relies on the i.i.d. assumption for the underlying random processes, extensive numerical tests are performed in Section 3.4, using both i.i.d. and non i.i.d. data to demonstrate that the proposed algorithm also works well when the underlying random process is highly correlated over time.

proposed algorithm, and performing all the simulations in [2]. Although the thesis author was only listed third in the author list in [2], the work in [2] is included in this thesis as the thesis author did make significant and important contributions, and the paper investigated energy management for smart-grid powered CoMP systems with RES, which is directly integral to the theme of this thesis.

1.3.3 A novel two-scale online control approach for CoMP systems

- In Chapter 4 [3], leveraging the ahead-of-time and real-time electricity markets, and building on our generalized system models in [70,71], a novel two-scale optimization framework is developed to facilitate the dynamic resource management for smart-grid powered CoMP systems with RES and channel dynamics at different time scales.

- While [71,76] and [77] do not account for battery degeneration (energy leakage), we integrate the modified Lyapunov optimization technique into the two-scale stochastic optimization approach to leverage the diversity of energy prices along with the energy leakage effects on the dynamic energy management task in Section 4.3.1.

- Using only past channel and energy-price realizations, a novel stochastic subgradient approach is developed in Section 4.3.3 to solve the ahead-of-time energy planning (sub-)problem, which is suitable for a general family of continuous distributions, and avoids constructing the histogram estimate which is computationally cumbersome, especially for high-dimensional vector of random optimization variables.

- Rigorous analysis is presented in Section 4.4 to justify the feasibility and quantify the optimality gap for the proposed two-scale online control algorithm.

1.3.4 Other non-trivial contributions

In addition to the main contributions, there are other non-trivial contributions listed as follows:

1. A new interoperable framework of 5G and smart grid is illustrated in Fig. 1.1, where BSs equipped with energy harvesting devices are connected to the smart grid

through smart meters. The BSs are also connected to the core network (i.e., the gateway and Internet) through broadband backhaul links using gigabit or carrier-grade Ethernet.

2. In Chapter 2, the original non-convex problem is reformulated into a convex program through a series of changes of variables, as shown in (2.4).

3. Lemmas 1 and 2 show the two key findings that determine the pattern of the optimal transmit rate for EH powered WSN links.

4. Figs. 2.2 and 2.3 validate the optimality of our proposed algorithms from the perspectives of packet drop rate and total energy consumption, and also reveal that the circuit power consumption can have significant impact on the optimal transmit schedules.

5. Fig. 2.4 shows that the proposed off-line and on-line algorithms, i.e., Algorithms 1 and 2, only require about 3.7% and 1.6% of the CPU time that the standard CVX toolbox requires for large T values, respectively.

6. In Chapter 3, to construct a tractable problem, the BC capacity region can be alternatively characterized by the capacity regions of a set of "dual" multi-access channels (MACs) by using the information-theoretic uplink-downlink duality, as shown in (3.7).

7. Fig. 3.2 shows that ALGs 1 and 2 incur about 3.0% and 13.3% smaller throughputs than the proposed SGOC algorithm.

8. Fig. 3.6 shows that the transmission-related power follows the opposite trend to the fluctuation of energy purchase price.

9. In Chapter 4, derived from the feasibility requirement of the proposed algorithm, the maximum and minimum values of the queue perturbation parameter Γ and weight parameter V are given in (4.16)-(4.18).

10. In Chapter 4, we derive Proposition 2 which asserts that the proposed TS-OC algorithm converges to a region with a upper-bounded optimality gap. The optimality gap between the TS-OC and the offline optimal scheduling first decreases and then increases with the growth of the battery capacity, as depicted in Fig. 4.4.

11. Fig. 4.3 shows that the time-average transaction costs of ALGs 1 and 2 are about 71% and 31% larger than the proposed TS-OC algorithm, respectively.

12. Fig. 4.6 reveals that with a smaller storage efficiency, the TS-OC algorithm tends to maintain a lower energy level to reduce average energy loss, and (dis)charge the battery less frequently.

1.4 Organization of the Thesis

In Chapter 2, a new "dynamic string tautening" algorithm is proposed for data transmission on EH-powered WSN links. The proposed algorithm generates the most energy-efficient offline schedule for delay-limited traffic of transmitters with non-negligible circuit power. The algorithm is based on two key findings that we derive through judicious convex formulation and resultant optimality conditions, specifies a set of simple but optimal rules, and generates the optimal schedule with a low complexity of $\mathcal{O}(N^2)$ in the worst case. The proposed algorithm is also extended to on-line scenarios, where the transmit schedule is generated on-the-fly. Simulations show that the proposed algorithm requires substantially lower average complexity by almost two orders of magnitude to retain optimality than general convex solvers. The effective transmit region, specified by the trade-off

of the data arrival rate and the energy harvesting rate, is substantially larger using our algorithm than using other existing alternatives. Significantly more data or less energy can be supported in the proposed algorithm.

In Chapter 3, an infinite time-horizon resource allocation problem is formulated to maximize the time-average downlink throughput for smart-grid powered MIMO, subject to a time-average energy cost budget. By using the advanced time decoupling technique, a novel stochastic subgradient based online control (SGOC) approach is developed for the resultant smart-grid powered communication system. It is established analytically that even without a-priori knowledge of the independently and identically distributed (i.i.d.) processes involved such as channel coefficients, renewables and electricity prices, the proposed online control algorithm is still able to yield a feasible and asymptotically optimal solution. Numerical results further demonstrate that the proposed algorithm also works well in non i.i.d. scenarios, where the underlying randomness is highly correlated over time.

In Chapter 4, a novel two-scale stochastic control framework is put forth for smart-grid powered CoMP systems. Considering RES, dynamic pricing, two-way energy trading facilities and imperfect energy storage devices, the energy management task is formulated as an infinite horizon optimization problem minimizing the time-averaged energy transaction cost, subject to the users' QoS requirements. Leveraging the Lyapunov optimization approach as well as the stochastic subgradient method, a two-scale online control (TS-OC) approach is developed for the resultant smart- grid powered CoMP systems. Using only historical data, the proposed TS-OC makes online control decisions at two timescales, and features a provably feasible and asymptotically near-optimal solution. Numerical tests further corroborate the theoretical analysis, and demonstrate the merits of the proposed approach.

Chapter 2

Provisioning quality-of-service to EH-powered WSN communications

2.1 Introduction

Energy harvesting (EH) is a process of capturing and converting ambient energy (e.g., solar, wind and thermal energy) into usable electrical energy [80]. In wireless communication systems, environmental EH is a critical component to build self-sustainable networks, such as wireless sensor networks in remote human-unfriendly environments [29]. On the other hand, Quality-of-Service (QoS), such as delay and packet error rate, is crucial to many wireless applications [29, 81]. Many sensory data are delay intolerant, especially in bushfire or flood monitoring, and security/safety surveillance applications.

In this chapter, we propose a new Dynamic String Tautening (DST) algorithm, which jointly addresses the three critical challenges altogether and generates the most energy-efficient off-line schedule for delay-limited traffic of transmitters with non-negligible circuit power. While [48–55] aimed to maximize the throughput of delay-tolerant traffic under the assumption that data were always available, here we consider the EH powered trans-

mission of delay-sensitive packets that arrive in bursts and need to be delivered before strict deadlines. Our algorithm is based on two key findings that we derive through judicious convex formulation and resultant optimality conditions. The findings are visualized and interpreted as a set of rules which guide us to generate the optimal schedule in a computationally efficient, graphical manner by tautening a transmit string in a recursively updated solution region. The optimal transmit schedule here can be produced with a low computational complexity (which is $\mathcal{O}(N^2)$ in the worst case, where N is the number of instants within a schedule).

Given the optimality and reduced complexity of the algorithm, we further extend it to on-line scenarios, where the transmit schedule is generated on-the-fly. Simulation results show that our proposed algorithm requires substantially lower average complexity (i.e., less energy) to retain optimality than the standard convex programming methods, reducing the CPU running time by almost two orders of magnitude. As a result, the effective transmit region, specified by the data arrival rate and the EH rate, is substantially larger using our algorithm than using general convex solvers. In other words, significantly more data or less energy can be supported in the proposed algorithm.

In our earlier work [5], the transmit schedule was optimized for delay-limited traffic of EH powered links with negligible circuit power. The new algorithm proposed in this chapter is substantially different, because the consideration of non-ideal circuit power consumption results in a different optimization problem and hence the distinct structure of the optimal schedule. When compared to the proposed algorithm, a significant loss of data and energy efficiency could occur when the schedule generated in [5] is applied in the case of non-ideal circuit power consumption (as will be shown in Section 3.4). In [82], we gave a brief introduction on the concept of the new algorithm without providing technical details. In this chapter, the full technical details are provided, and the optimality is rigorously proved. Moreover, this chapter also extends the algorithm to generate an on-

line transmit schedule on-the-fly.

The rest of the chapter is organized as follows. In Section 2.2, the system model is described. In Section 2.3, the convex optimization problem is formulated and the two key insightful findings are derived. In Section 2.4, the proposed DST algorithm is elaborated on, which produces the optimal off-line schedule for delay-sensitive bursty data. In Section 2.5, the proposed algorithm is extended to practical on-line scenarios. In Section 2.6, simulations are carried out to validate the optimality of our algorithm and its superiority of reduced complexity, followed by conclusions in Section 2.7.

2.2 System Model

Consider a time-invariant wireless link, where the transmitter is powered by EH. Let $E_{\max}$ denote the capacity of the rechargeable battery at the transmitter. The channel coefficient of the wireless link is denoted by h, and the transmit rate of the link is r. The additive white Gaussian noise (AWGN) is assumed to have unit variance at the receiver.

Our discussion is focused on a time period $[0, T]$, over which there are $(N+1)$ time instants: $0 = t_0 < t_1 < t_2 < \cdots < t_N = T$. We refer to the interval between two consecutive time instants as an *epoch*; the duration of the ith epoch is $L_i = t_i - t_{i-1}$, $i = 1, \cdots, N$.

At each time instant $t_i\,(i = 0, 1, \cdots, N)$, new energy is harvested, or new bursty data are collected, or strict deadlines of the collected data are reached at the transmitter. The amount of the harvested energy, the collected data, and the data whose deadlines are reached can be written respectively as sequences $\{E_0, E_1, E_2, \cdots, E_{N-1}, 0\}$, $\{A_0, A_1, A_2, \cdots, A_{N-1}, 0\}$, and $\{0, D_1, D_2, \cdots, D_{N-1}, D_N\}$, corresponding to the time instants $\{t_0, t_1, t_2, \cdots, t_{N-1}, t_N\}$. $E_i \geq 0$ is the energy harvested at t_i; $A_i \geq 0$ is the number of packets collected at t_i; $D_i \geq 0$ is the number of packets that must be transmitted

by t_i. E_0 and A_0 are the initial energy level and the initial number of packets at the transmitter. Note that we consider the optimal schedule for the general case where the packets can have different delay requirements, i.e., the packets are of different traffic types or for different applications. Whenever new packets arrive, the transmitter may need to re-shuffle the packets in the buffer to ensure that the packets with more stringent deadlines are placed head-of-line. For the special case that all the packets have the same delay requirements, such reshuffling becomes unnecessary and the data queue simply operates in a first-in-first-out manner.

We set $E_N = A_N = 0$, as any energy harvested or data collected at t_N cannot be dealt with during the current time period of $[0, T]$ and will be used to initialize the next time period. Also, it is clear that $\sum_{i=0}^{N-1} A_i = \sum_{i=1}^{N} D_i$. In other words, the total number of packets required to deliver is equal to that of arrived packets.

2.3 Convex Formulation and Resultant Optimality Conditions

In this section, we mathematically characterize the optimal transmit schedule under the ideal (impractical) assumption that the arrival processes of data and energy are known a priori to the transmitter. The variables l_i and r_i $(i = 1, \cdots, N)$ are to be optimized, where $l_i \in [0, L_i]$ is the duration that the transmitter is on during epoch i and r_i is the transmit rate associated with l_i.

The way of our interpreting the optimal schedule is new. It involves formulating the convex optimization problem and rigorously proving that the optimal solution can be directly constructed based on the resultant optimality conditions. This lays foundation to a new simple and efficient on-line scheduling algorithm in practical scenarios where the data arrivals and energy collections are unknown a priori, as will be described in Sections

2.4 and 2.5.

First, the total power P_{total} consumed by the transmitter can be given by [51, 60]:

$$P_{total} = \begin{cases} \frac{P}{\eta} + \rho, & P > 0, \\ \beta, & P = 0, \end{cases} \tag{2.1}$$

where ρ denotes the circuit power consumption when the transmitter is transmitting (i.e., in an "on" mode), β the circuit power consumption when the transmitter is idle (i.e., in an "off" mode) and η the efficiency of the RF chain at the transmitter. For specificity, the transmit power P is given by

$$P(r) = \frac{1}{|h|^2}(e^r - 1), \tag{2.2}$$

where r is the instantaneous data rate of the wireless link.[1] We assume $\rho > 0$ and $\beta = 0$ without loss of generality, since $\rho \gg \beta$ in practical systems [60]. We also assume $\eta = 1$, as η is just a scaling factor.

Given that $P(r)$ is convex, it was proved that the transmit rate over the "on" period l_i of each epoch i, r_i, should remain unchanged in the optimal schedule [51]. The problem of interest becomes to find the optimal pairs of (r_i, l_i), $i = 1, \cdots, N$, to minimize the total energy consumed to deliver data packets by their deadlines. The problem can be formulated as

$$\begin{aligned} \min_{\boldsymbol{r},\boldsymbol{l}} \quad & \sum_{i=1}^{N} \{[P(r_i) + \rho] l_i\} \\ \text{s.t.} \quad & r_i \geq 0, \quad 0 \leq l_i \leq L_i, \ \ \forall i; \\ & (\mathbf{C1}): \ \sum_{i=1}^{n} r_i l_i \leq \sum_{i=0}^{n-1} A_i; \\ & (\mathbf{C2}): \ \sum_{i=1}^{n} r_i l_i \geq \sum_{i=1}^{n} D_i; \\ & (\mathbf{C3}): \ \sum_{i=1}^{n} \{[P(r_i) + \rho] l_i\} \leq \sum_{i=0}^{n-1} E_i; \\ & (n = 1, \cdots, N), \end{aligned} \tag{2.3}$$

[1] The proposed approach applies to any other convex power functions.

where $\boldsymbol{r} := \{r_1, r_2, \ldots, r_N\}$ collects the transmit rates during the "on" periods of the epochs, and $\boldsymbol{l} := \{l_1, l_2, \ldots, l_N\}$ collects the durations of the "on" periods of the epochs.

Here, (**C1**) presents the data causality constraints: the number of packets $\sum_{i=1}^{n}(r_i l_i)$ transmitted up to any time t_n cannot exceed the number of available packets $\sum_{i=0}^{n-1} A_i$ at the transmitter's buffer. (**C2**) presents the deadline constraints: $\sum_{i=1}^{n}(r_i l_i)$ must be no less than the data required to be transmitted to meet their deadlines, i.e., $\sum_{i=1}^{n} D_i$. (**C3**) presents the energy causality constraints: the total amount of energy $\sum_{i=1}^{n}\{[P(r_i)+\rho]l_i\}$ consumed up to any time t_n must be no greater than $\sum_{i=0}^{n-1} E_i$ that has been harvested and accumulated in the battery so far.

Clearly, (2.3) is not convex or concave, because neither of $r_i l_i$ and $P(r_i)l_i$ is convex or concave with respect to (r_i, l_i). Yet, it can be reformulated into a convex program through a series of changes of variables. Define $\Phi_i := r_i l_i$ and $\boldsymbol{\Phi} := \{\Phi_1, \Phi_2, \ldots, \Phi_N\}$. We can rewrite (2.3) into

$$\begin{aligned}
\min_{\boldsymbol{\Phi},\boldsymbol{l}} \quad & \sum_{i=1}^{N}\{[P(\frac{\Phi_i}{l_i})+\rho]l_i\} \\
\text{s.t.} \quad & \Phi_i \geq 0, \quad 0 \leq l_i \leq L_i, \ \ \forall i, \\
& \sum_{i=1}^{n}\Phi_i \leq \sum_{i=0}^{n-1} A_i, \\
& \sum_{i=1}^{n}\Phi_i \geq \sum_{i=1}^{n} D_i, \\
& \sum_{i=1}^{n}\{[P(\frac{\Phi_i}{l_i})+\rho]l_i\} \leq \sum_{i=0}^{n-1} E_i; \\
& (n = 1, \cdots, N).
\end{aligned} \tag{2.4}$$

where we have $P(\frac{\Phi_i}{l_i})l_i = 0$ if $l_i = 0$. For any convex $P(r_i)$, $P(\frac{\Phi_i}{l_i})l_i$ is called its perspective, and is a convex function of (Φ_i, l_i) [83]. As a result, (2.4) is a convex problem.

Let $\boldsymbol{\Lambda} := \{\lambda_n^c, \lambda_n^d, \mu_n^c, n = 1, \ldots, N\}$ where λ_n^c, λ_n^d, and μ_n^c are the Lagrange multipliers associated with the data causality, deadline and energy causality constraints, respectively.

The Lagrangian of (2.4) is given by

$$\begin{aligned} L(\boldsymbol{r},\boldsymbol{l},\boldsymbol{\Lambda}) &= \sum_{i=1}^{N}\{[P(\frac{\Phi_i}{l_i})+\rho]l_i\} + \sum_{n=1}^{N}\lambda_n^c(\sum_{i=1}^{n}\Phi_i - \sum_{i=0}^{n-1}A_i) \\ &\quad + \sum_{n=1}^{N}\lambda_n^d(\sum_{i=1}^{n}D_i - \sum_{i=1}^{n}\Phi_i) \\ &\quad + \sum_{n=1}^{N}\mu_n^c\{\sum_{i=1}^{n}\{[P(\frac{\Phi_i}{l_i})+\rho]l_i\} - \sum_{i=0}^{n-1}E_i\} \\ &= C(\boldsymbol{\Lambda}) + \sum_{i=1}^{N}\{\{[P(\frac{\Phi_i}{l_i})+\rho]l_i\}(1+\sum_{n=i}^{N}\mu_n^c) \\ &\quad - \Phi_i(\sum_{n=i}^{N}\lambda_n^d - \sum_{n=i}^{N}\lambda_n^c)\}, \end{aligned}$$

where $C(\boldsymbol{\Lambda}) := -\sum_{n=1}^{N}\lambda_n^c(\sum_{i=0}^{n-1}A_i) + \sum_{n=1}^{N}\lambda_n^d\times\ (\sum_{i=1}^{n}D_i) - \sum_{n=1}^{N}\mu_n^c(\sum_{i=0}^{n-1}E_i)$ for notation simplicity.

Let $(\boldsymbol{\Phi^*},\boldsymbol{l^*})$ denote the optimal solution for (2.4), and $\boldsymbol{\Lambda^*}$ the optimal Lagrange multiplier vector for its dual problem. Also define per epoch i:

$$w_i := \sum_{n=i}^{N}[(\lambda_n^d)^* - (\lambda_n^c)^*]/[1+\sum_{n=i}^{N}(\mu_n^c)^*]. \tag{2.5}$$

Then the sufficient and necessary Karush-Kuhn-Tucker (KKT) optimality conditions for (2.4) dictate that [84]: $\forall i$,

$$(\Phi_i^*, l_i^*) = \arg\min_{\Phi_i\geq 0,\ 0\leq l_i\leq L_i}\{[P(\frac{\Phi_i}{l_i})+\rho]l_i - w_i\Phi_i\}; \tag{2.6}$$

and the non-negative $(\lambda_n^c)^*$, $(\lambda_n^d)^*$ and $(\mu_n^c)^*$ satisfy the complementary slackness conditions: $\forall n$,

$$\begin{cases} (\lambda_n^c)^* = 0, \ \text{ if } \sum_{i=1}^{n}\Phi_i^* < \sum_{i=0}^{n-1}A_i; \\ \sum_{i=1}^{n}\Phi_i^* = \sum_{i=0}^{n-1}A_i, \ \text{ if } (\lambda_n^c)^* > 0; \end{cases} \tag{2.7}$$

$$\begin{cases} (\lambda_n^d)^* = 0, \quad \text{if } \sum_{i=1}^{n}\Phi_i^* > \sum_{i=1}^{n}D_i; \\ \sum_{i=1}^{n}\Phi_i^* = \sum_{i=1}^{n}D_i, \quad \text{if } (\lambda_n^d)^* > 0; \end{cases} \tag{2.8}$$

$$\begin{cases} (\mu_n^c)^* = 0, \quad \text{if } \sum_{i=1}^{n} \{[P(\frac{\Phi_i}{l_i}) + \rho] l_i\} < \sum_{i=0}^{n-1} E_i; \\ \sum_{i=1}^{n} \{[P(\frac{\Phi_i}{l_i}) + \rho] l_i\} = \sum_{i=0}^{n-1} E_i, \quad \text{if } (\mu_n^c)^* > 0. \end{cases} \tag{2.9}$$

For any i, we let $r_i^* = \frac{\Phi_i^*}{l_i^*}$ if $l_i^* > 0$, and allow r_i^* to take an arbitrary non-negative value if $l_i^* = 0$. It is obvious that $(\boldsymbol{r}^*, \boldsymbol{l}^*)$ is the optimal solution to (2.3).

From (2.6)–(2.9), we can establish the sufficient and necessary optimality conditions for (2.3), as given by

$$(r_i^*, l_i^*) = \arg \min_{r_i \geq 0,\ 0 \leq l_i \leq L_i} [P(r_i) + \rho - w_i r_i] l_i \tag{2.10}$$

$$\begin{cases} (\lambda_n^c)^* = 0, \quad \text{if } \sum_{i=1}^{n} (r_i l_i) < \sum_{i=0}^{n-1} A_i, \\ \sum_{i=1}^{n} (r_i l_i) = \sum_{i=0}^{n-1} A_i, \quad \text{if } (\lambda_n^c)^* > 0; \end{cases} \tag{2.11}$$

$$\begin{cases} (\lambda_n^d)^* = 0, \quad \text{if } \sum_{i=1}^{n} (r_i l_i) > \sum_{i=1}^{n} D_i, \\ \sum_{i=1}^{n} (r_i l_i) = \sum_{i=1}^{n} D_i, \quad \text{if } (\lambda_n^d)^* > 0; \end{cases} \tag{2.12}$$

$$\begin{cases} (\mu_n^c)^* = 0, \ \text{if } \sum_{i=1}^{n} \{[P(r_i) + \rho] l_i\} < \sum_{i=0}^{n-1} E_i, \\ \sum_{i=1}^{n} \{[P(r_i) + \rho] l_i\} = \sum_{i=0}^{n-1} E_i, \ \text{if } (\mu_n^c)^* > 0. \end{cases} \tag{2.13}$$

For any given $l_i > 0$, from (2.10) we can have the optimal transmit rate r_i^*, as given by

$$r_i^* = \arg \min_{r_i \geq 0} \ [P(r_i) + \rho - w_i r_i]. \tag{2.14}$$

As $P(r_i)$ is strictly convex and increasing, this is equivalent to: $P'(r_i^*) = w_i$, where $P'(\cdot)$ denotes the first derivative of function $P(\cdot)$.

Substituting $P'(r_i^*) = w_i$ into (2.10), we can have

$$l_i^* = \arg \min_{0 \leq l_i \leq L_i} \ [P(r_i^*) + \rho - P'(r_i^*) r_i^*] l_i, \tag{2.15}$$

which is the optimal duration of the "on" period per epoch i.

The followings are two key findings derived from (2.14) and (2.15).

Lemma 1. *The optimal schedule for (2.3) can only adopt one of the following three strategies per epoch i: (i) $l_i^* = 0$ (i.e., "off"), (ii) $r_i^* = r_{ee}$ and $l_i^* \leq L_i$ (i.e., "first-on-then-off" or "on-off" for short), or (iii) $r_i^* > r_{ee}$ and $l_i^* = L_i$ (i.e., "on"). Specifically, r_{ee} is the bits-per-Joule EE-maximizing rate, i.e.,*

$$r_{ee} = \arg\max_{r \geq 0} \frac{r}{P(r) + \rho}, \tag{2.16}$$

and can be efficiently obtained through a bisectional search [51], because $\frac{r}{P(r)+\rho}$ is (concave-over-linear) quasi-concave.

Proof. See Appendix A.0.1. □

Lemma 1 shows that any transmit rate $r_i < r_{ee}$ should not be adopted in the optimal schedule. In fact, since r_{ee} maximizes the bits-per-Joule EE, a transmission strategy with an $r_i < r_{ee}$ over an epoch is always dominated by an on-off transmission with r_{ee}, which can use less energy to deliver the same data amount. Only when the data deadlines are strict (i.e., no further delay is allowed) should we adopt an $r_i^* > r_{ee}$; in this case, the transmitter should be always on, i.e., $l_i^* = L_i$, over epoch i.

Let $P'^{-1}(\cdot)$ denote the inverse function of $P'(\cdot)$. If $l_i^* > 0$, we can obtain from (2.14) that

$$\begin{aligned} r_i^* &= \arg\min_{r_i \geq 0} \left[P(r_i) + \rho - w_i r_i\right] := P'^{-1}(w_i) \\ &= \log(|h|^2 w_i) \end{aligned} \tag{2.17}$$

which is an increasing function of w_i.

Given (2.17) and (2.11)–(2.13), we establish the following structure of the optimal transmit schedule, as stated in Lemma 2.

Lemma 2. *In the optimal schedule for* (2.3)*, the transmit rate r_i^* only changes at t_n on which the data causality, deadline or energy causality constraints are met with equality. Specifically, r_i^* increases after t_n with $\sum_{i=1}^{n}(r_i^* l_i^*) = \sum_{i=0}^{n-1} A_i$ or $\sum_{i=1}^{n}\{[P(r_i^*) + \rho] l_i^*\} = \sum_{i=0}^{n-1} E_i$, and decreases after t_n with $\sum_{i=1}^{n}(r_i^* l_i^*) = \sum_{i=1}^{n} D_i$.*

Proof. See Appendix A.0.2. □

Lemma 2 shows that the optimal transmit rate of the EH powered transmitter changes, if and only if the constraints take effect. Otherwise, the transmit rate should be maintained constant to minimize the energy consumption.

Note that this optimal off-line schedule could be obtained using standard convex programming methods. However, general convex solvers (e.g., the interior point methods) would require much higher complexity, which, in turn, compromises the optimality of the schedule by increasing power consumption on the circuit. Details will be provided in Section 2.6. In addition, no key findings would be observed to guide the design of practical on-line scheduling, if a standard convex programming solver is adopted.

2.4 Proposed Optimal Off-line Dynamic String Tautening Algorithm

In this section, we propose a new DST algorithm, which produces the optimal schedule for delay-sensitive data over EH powered wireless links, given the a-priori knowledge on E_i, A_i and D_i $(i = 0, \cdots, N)$. Based on the key results of the mathematical characterization in Section 2.3, the algorithm provides the energy consumption lower bound for EH powered wireless links. It will also be extended to play a key role in practical on-line operations where the a-priori knowledge is absent, as will be described in Section 2.5.

2.4.1 Visualization of Dynamic String Tautening

Fig. 2.1 illustrates our proposed DST process, where the data arrival curve $A_d(t)$ plots the amount of data generated for transmission and the deadline (minimum data departure) curve $D_{\min}(t)$ plots the amount of data reaching their deadlines. $A_d(t)$ and $D_{\min}(t)$ can

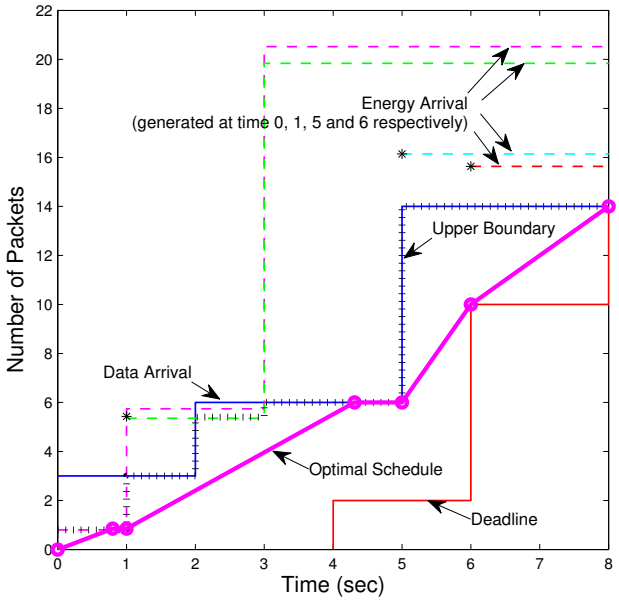

Figure 2.1: An illustrative example of the proposed DST method and the achieved optimal transmission schedule.

be written as

$$A_d(t) = \sum_{i=0}^{N-1} [A_i u(t - t_i)], \tag{2.18}$$

$$D_{\min}(t) = \sum_{i=1}^{N} [D_i u(t - t_i)], \tag{2.19}$$

where $0 \leq t \leq T$ and $u(t)$ is the unit-step function. $A_d(t)$ and $D_{\min}(t)$ are plotted in the very beginning and fixed, prior to the string tautening process, similar to the existing string tautening algorithm [61].

There are a series of energy curves, sequentially produced from left to right. Each curve plots the maximum amount of data that can be transmitted at future instants, given both the energy harvested and the data transmitted so far. The energy curves are plotted as follows.

At an instant t_τ where the transmit rate changes, a new energy curve starting from t_τ is generated tentatively by assuming that the transmitter remains "on" over all the

remaining unscheduled epochs, as given by

$$A_{e_\tau}(t) = \sum_{i=\tau}^{N-1} \Big[(r_{i+1}^e \sum_{n=\tau+1}^{i+1} L_n - r_i^e \sum_{n=\tau+1}^{i} L_n) u(t - t_i) \Big], \tag{2.20}$$

where $r_i^e > 0$ satisfies $\sum_{k=\tau+1}^{i} \{[P(r_i^e) + \rho] L_k\} = \sum_{k=\tau}^{i-1} e_k$, or $r_i^e = 0$, with e_τ being the residual energy in the battery by instant t_τ, and $e_k = E_k$ for $k = \tau + 1, \cdots, N$.

The $A_{e_\tau}(t)$ curve of (2.20) may not be exact, as the optimal transmit rate $r_{\tau+1}^*$ that is yet to be determined for the epoch beginning at t_τ may differ from $r_{\tau+1}^e$. The curve may need to be adjusted once the optimal transmit rate is determined; and in turn, it can affect the duration of the transmission with the optimal rate. Details will be provided later.

The $A_d(t)$, $D_{\min}(t)$, and $A_{e_\tau}(t)$ curves specify the (tentative) closed feasible solution region for the transmit rate. Specifically, the $A_d(t)$ and $A_{e_\tau}(t)$ curves provide the upper boundary of the region, and the $D_{\min}(t)$ curve provides the lower boundary, as shown in the figure.

We can generate the optimal data departure curve $D^*(t)$ whose slopes present the optimal transmit rates r_i^*, within the feasible solution region, yielding the following rules.

1. Connect the origin $(0, 0)$ and the rightmost joint of the $A_d(t)$ and $D_{\min}(t)$ curves with a string, and tauten the string tight so that it only bends at the corners.

2. Compare the slope of the lowest straight segment of the string to r_{ee}.

   (a) If the slope is no less than r_{ee}, set the right end of the segment to be the left end of a new string.

   (b) If the slope is less than r_{ee},

      i. shift the right end of the segment leftwards along the $A_d(t)$ or $A_{e_\tau}(t)$ curve, and tauten the segment until it intersects the $A_d(t)$ or $A_{e_\tau}(t)$ curve with the slope of r_{ee}. If the segment bends at a corner and becomes two segments,

repeat 2b-i) on the lower of the two segments, until the lower segment is unbent.

ii. Update the $A_{e_\tau}(t)$ curve for the case where the lowest unbent segment adopts the "on-off" mode (r_{ee} is adopted), and update the lowest segment accordingly (i.e., if the segment intersects the $A_{e_\tau}(t)$ curve, it needs to be updated to intersect the updated $A_{e_\tau}(t)$ curve).

iii. Set the corner right to the lowest unbent segment to be the left end of a new string.

3. Tauten the new string to the rightmost joint of the $A_d(t)$ and $D_{\min}(t)$ curves, and repeat 2) on the lowest straight segment of the new string.

Rules 1 and 3 are designed to satisfy Lemma 2, because a string tautening process (as described in the rules) can guarantee that the slope of the string increases after the string bends around a corner of the upper boundary of the feasible solution region, and decreases after bending around the corner of the lower boundary; refer to instants 5 and 6 in Fig. 2.1.

Rule 2a is based on both Lemma 1 (that $r_i^* \geq r_{ee}$) and Lemma 2 (that the optimal transmit rate keeps unchanged, until the data/energy causality constraint is met with equality and the rate increases; or the deadline constraint is met with equality and the rate decreases). The rule is optimal because it is able to meet the constraints in the most energy efficient way. For the epochs with $\Phi = r_i^* L_i \geq r_{ee} L_i$, any "on-off" strategy (r_i, l_i) with $r_i > r_i^*$ and $r_i l_i = \Phi$ would only increase the energy consumption, since

$$[P(r_i) + \rho] l_i = \Phi \frac{P(r_i) + \rho}{r_i} > \Phi \frac{P(r_i^*) + \rho}{r_i^*}, \tag{2.21}$$

where the inequality is due to the fact that $\frac{P(r)+\rho}{r}$ is strictly increasing when $r \geq r_{ee}$. The examples of implementing the rule are the epochs $[5, 6]$ and $[6, 8]$ in the figure.

Rule 2b is based on Lemma 1 that $r_i^* = r_{ee}$ with $l_i^* \leq L_i$ is the most energy efficient. The optimality of the rule lies in the fact that the energy cost for transmission of data amount $\Phi = r_i L_i$ over epochs is minimized by a transmission with $r_{ee} \geq r_i$ over an "on" period of $l_i^* = \Phi / r_{ee} < L_i$, as shown in

$$\begin{aligned}[P(r_{ee}) + \rho] l_i^* &= \frac{[P(r_{ee}) + \rho]\Phi}{r_{ee}} = \Phi \min_{r \geq 0} \frac{P(r) + \rho}{r} \\ &= \min_{r l_i = \Phi} [P(r) + \rho] l_i.\end{aligned} \tag{2.22}$$

The examples of implementing the rule are the epochs $[0, 1]$ and $[1, 5]$.

In this sense, Rule 2 generates the optimal transmit rate over the epochs where the rate does not change. Rule 3 extrapolates Rule 2 to generate such optimal rates across the transmission period $[0, T]$, rendering the optimality of the entire transmit schedule generated. Particularly, Rule 2b specifies that the left end of a new string to be tautened corresponds to the case where the transmitter is running out of either data or energy (i.e., the data or energy causality constraint is met with equality). No causality remains between the past and the current tautening processes. Tautening the new string using Rule 3 does not invalidate the optimality of the transmit schedules generated so far by Rule 2.

The reason for tentatively plotting the $A_{e_\tau}(t)$ curve as (2.20) also becomes clear. It is because the optimal transmit rate determined by Rule 2 may lift the tentative $A_{e_\tau}(t)$ curve due to the improved energy efficiency (as compared to r_i^e). The optimal transmit rate will not be invalidated by the lifted $A_{e_\tau}(t)$ curve, if the segment associated with the rate intersects with the $A_d(t)$ or $D_{\min}(t)$ curve. The optimal transmit rate will also remain valid, if the segment intersects with the tentative $A_{e_\tau}(t)$ curve, since the optimal transmit rate is r_{ee} in this case (as specified in Rule 2). However, the duration of the segment can increase to intersect the lifted $A_{e_\tau}(t)$ curve (or the $A_d(t)$ curve if the intersecting part of the $A_d(t)$ curve is between the tentative and lifted $A_{e_\tau}(t)$ curves). An example is given by epoch $[0, 1]$ in the figure, where l_1^* is slightly extended to intersect the lifted (pink) $A_{e_\tau}(t)$

curve.

Note that the upper boundary $A_d(t)$ and $A_{e_\tau}(t)$ curves may cross and become underneath the lower boundary $D_{\min}(t)$ curve during part of the transmission period. No transmissions will take place during that part of the period due to insufficient energy. The part of the period is an infeasible solution region. Note also that the rules can apply directly to the case where the transmitter has a maximum transmit power. In this case, the slope of the string is upper-bounded by a maximum transmit rate.

2.4.2 Dynamic String Tautening Algorithm

Algorithm 1 Proposed DST Algorithm

Input $\mathcal{A}$, $\mathcal{D}$, $\mathcal{E}$ and $\mathcal{T}$, set $n_{\text{offset}} = 0$, $r_i^* = l_i^* = 0$, $\forall i$.
while $n_{\text{offset}} < N$ **do**
    Calculate r_n^a, r_n^d and r_n^e, $n = n_{\text{offset}} + 1, \ldots, N$;
    $r^- = 0, r^+ = \infty, \tau^- = \tau^+ = 0$;
    $\tau = N, \tilde{r} = r_N^a = r_N^d$;
    for $n = n_{\text{offset}} + 1$ to N **do**
        if $r^+ \geq \min\{r_n^a, r_n^e\}$ **then**
            $r^+ = \min\{r_n^a, r_n^e\}$, $\tau^+ = n$;
        end if
        if $r^- \leq r_n^d$ **then**
            $r^- = r_n^d$, $\tau^- = n$;
        end if
        if $r^- \geq r^+$ **then**
            if $\tau^+ \geq \tau^-$ **then**
                $\tau = \tau^-, \tilde{r} = r^-$;
            else

17: $\tau = \tau^+, \tilde{r} = r^+$;

18: **end if**

19: break;

20: **end if**

21: **end for**

22: **for** $i = n_{\text{offset}} + 1$ to τ **do**

23: $r_i^* = \max\{r_{ee}, \tilde{r}\}$;

24: **end for**

25: **if** t_τ is the instant the data causality or deadline

26: constraint is met with equality **then**

27: find a feasible set of $\{l_i^*\}$ satisfying

28: $\sum_{i=n_{\text{offset}}+1}^{\tau} l_i^* = \sum_{i=n_{\text{offset}}+1}^{\tau} \frac{\tilde{r}L_i}{r_i^*}$

29: **else**

30: find a feasible set of $\{l_i^*\}$ satisfying

31: $\sum_{i=n_{\text{offset}}+1}^{\tau} l_i^* = \sum_{i=n_{\text{offset}}+1}^{\tau} \frac{[P(\tilde{r})+\rho]L_i}{P(r_i^*)+\rho}$

32: **end if**

33: update $(\mathcal{A}, \mathcal{D}, \mathcal{E}, \mathcal{T})$;

34: $n_{\text{offset}} = \tau$;

35: **end while**

Algorithm 1 summarizes the proposed off-line DST process in a structured way, which will play a key role in the practical on-line algorithm, as will be described in Section 2.5. Denote $\mathcal{A} := \{A_0, A_1, \cdots, 0\}$, $\mathcal{D} := \{0, D_1, \cdots, D_N\}$, $\mathcal{E} := \{E_0, E_1, \cdots, 0\}$, and $\mathcal{T} := \{t_0, t_1, \cdots, t_N\}$. n_{offset} denotes the left end of the series of strings to be tautened. It is initially set to zero, and updated through the WHILE loop of Steps 2 to 35.

Steps 3 to 33 describe the operations specified in Rules 1–3 in Section 2.4.1.

- In Steps 3 to 21, the number of epochs since n_{offset}, during which the optimal transmit

rate keeps unchanged, is identified by recursively updating and comparing r^+ (in Steps 7-9), the minimum of the rates determined by the upper boundary of the feasible region (i.e., r_n^a and r_n^e), and r^- (in Steps 10-12), the maximum of the rates determined by the lower boundary of the region (i.e., r_n^d), from $n = n_{\text{offset}} + 1$ until $r^- \geq r^+$ (in Steps 13-20). τ indicates the index of the time instant at which the string bends, i.e., the optimal transmit rate changes. In other words, Steps 3 to 21 determine every straight segment of the entire string generated by Rule 1 in every iteration. By iteratively running Steps 3 to 21, the string connecting $(0, 0)$ and the rightmost joint of the $A_d(t)$ and $D_{\min}(t)$ curves, which is specified in Rule 1, can be determined. As mentioned in (2.20), r_n^e satisfies $\sum_{i=n_{\text{offset}}+1}^{n}\{[P(r_n^e) + \rho]L_i\} = \sum_{i=n_{\text{offset}}}^{n-1} e_i$. It is unique and can be determined by a bisectional search per n, since $P(\cdot)$ is monotonically increasing. Likewise, r_n^a and r_n^d can be obtained by solving $\sum_{i=n_{\text{offset}}+1}^{n}(r_n^a L_i) = \sum_{i=n_{\text{offset}}}^{n-1} A_i$ and $\sum_{i=n_{\text{offset}}+1}^{n}(r_n^d L_i) = \sum_{i=n_{\text{offset}}+1}^{n} D_i$, respectively.

- Steps 22 to 24 adjust the transmit rate to be no less than r_{ee}.

- Steps 25 to 33 summarize the operations that decide the durations associated with the optimal transmit rates determined above, as specified in Rule 2. Particularly, Steps 30 and 31 describe the case where the tentative $A_{e_\tau}(t)$ curve needs to be lifted and subsequently the duration of a transmission with r_{ee} is to be extended, as discussed earlier in Section 2.4.1.

As noted earlier in Section 2.4.1, the solution region of the optimal transmit schedule may be infeasible. The data arrival and EH processes are independent by nature. It is then possible that the transmitter runs out of energy when there are still deadline-approaching data in the buffer, i.e., D_i is too large to be supported by the available energy harvested and accumulated so far. In this case, the upper boundary curve can cross and

go underneath the lower boundary $D_{\min}(t)$ curve, the problem becomes infeasible. No transmissions can be scheduled until new energy is harvested. Data with deadlines within the infeasible region are dropped.

The following theorem confirms the global optimality and efficiency of the proposed Algorithm 1.

Theorem 1. *Algorithm 1 can find the optimal transmission schedule for* (2.3) *when it is feasible.*

The theorem can be proved by first confirming the existence of a Lagrange multiplier vector $\mathbf{\Lambda}^*$, with which $\boldsymbol{r}^*$ and $\boldsymbol{l}^*$ satisfy the sufficient and necessary conditions (2.10)–(2.13), followed by showing that $(\boldsymbol{r^*}, \boldsymbol{l^*})$ ensures $l_i^* = L_i$ when $r_i^* > r_{ee}$ and $l_i^* \leq L_i$ when $r_i^* = r_{ee}$. In other words, $(\boldsymbol{r^*}, \boldsymbol{l^*})$ is a global optimum. A detailed proof of the theorem is provided in Appendix A.0.3.

We also confirm that Algorithm 1 has a complexity of $\mathcal{O}(N^2)$ in the worst case. In that case, the optimal transmit rate changes at every instant, i.e., N optimal rates are to be calculated. Besides, to confirm the rate change at any instant, all the future instants after that instant need to be evaluated. This is because r^- remains less than r^+ until the last instant at which r^- becomes equal to or larger than r^+. As a result, at every instant t_n $(n = 0, 1, \cdots, N-1)$, the algorithm evaluates the future $(N-n)$ instants. It calculates the three rates r_i^a, r_i^e and r_i^d, compares $\min\{r_i^a, r_i^e\}$ with r^+ and compares r_i^d with r^-, and updates r^+ and r^- (as described in Steps 3 to 21), from $i = n+1$ all the way through $i = N$. The calculation required is $3\sum_{n=0}^{N-1}(N-n) = \frac{3}{2}(N^2+N)$.

In fact, the complexity of Algorithm 1 is much lower than $\mathcal{O}(N^2)$ in most cases. This is because the optimal transmit rate may keep unchanged across a number of instants; in other words, fewer optimal transmit rates need to be calculated. It is also because it often does not require all the future instants to be evaluated to get $r^- \geq r^+$. Fewer instants are evaluated to calculate an optimal transmit rate.

In contrast, the standard convex solvers designed for generality, such as the interior point methods, typically require matrix operations, high-order multiplications and repeated iterations. They have a polynomial complexity higher than $\mathcal{O}(N^3)$ [84]. Corroborated by our simulations, the CPU time for Algorithm 1 is less than 3.7% of that with the standard CVX program [30], as will be shown in Section 2.6.

It is worth mentioning that our proposed algorithm can be readily extended to a general time-varying channel. In that case, the time-invariant channel coefficient h will be replaced by h_i $(i = 1, \cdots, N)$, where h_i is the channel coefficient per epoch i. The extension of our algorithm can be done by tautening the "water-level" w_i, defined in (2.5), in the same way as we did on r_i, since in the optimal schedule w_i only changes at the instants where the data/energy causality or the deadline constraint is met with equality, as proved in Appendix A.0.2. Based on a "water-level" based DST approach, the optimal w_i^* can be determined per epoch i. Given w_i^*, the optimal transmit rate r_i^* can then be determined using (2.17). It is clear that for the time-varying case, the water-filling type power allocation will be resulted; i.e., with the same water-level w_i^*, higher power (and rate) is allocated for epoch with better channel quality. Interested readers can refer to our conference paper [5] for such a generalization.

The emphasis of the chapter is on unreliable and insufficient power supply of EH systems, which is the dominant cause of compromised QoS. We have also pointed out that the EH ratio is typically low (e.g., 10%) in practice. For these reasons, we assume that the capacity of battery is large enough to accommodate the harvested energy; i.e., battery capacity induced energy overflow is not considered in our formulation to facilitate elaboration of main ideas. The impact of the finite battery capacity on the optimality of the proposed schedule will be tested through simulations in Section 2.6. It will be justified that a battery capacity of 1500 mJ (recall that the capacity of a typical AAA Alkaline battery is 2700 J) is sufficient to render negligible optimality loss for the proposed

approach.

2.5 On-line Extension of Dynamic String Tautening

We proceed to extend the proposed off-line DST algorithm to practical on-line applications where a-priori knowledge on data and energy arrivals is unavailable.

The extension is done as such that, at any time instant, we set the current instant as t_0, and set the future latest deadline instant of all the arrived data as t_N. The period between the two instants is T. We use (2.18), (2.19) and (2.20) to plot the future data causality and deadline curves, and the energy curve between t_0 and t_N. The transmit rates till the latest future instant can be optimized by conducting the proposed DST algorithm within the feasible solution region specified by the curves. Data will be transmitted with the optimal transmit rates, until a new arrival of data or energy.

At the instant of the new data/energy arrival, the data arrival, deadline, and energy curves will be updated by taking the instant as the initial instant. The optimal transmit rate will be recalculated for the instant and beyond. This process repeats, and automates the on-line transmit schedule generation, as summarized in Algorithm 2.

Of course, the on-line extension may not be optimal. This is because the transmit rates, optimized for a future period of T without a-priori data/energy arrival knowledge during the period, may violate Lemma 2 in the case where data or energy does arrive during the period and new schedules are generated. In the other cases, no data or energy arrives during the period. The schedule generated at the beginning of the period will remain optimal till the end of the period. In this sense, the on-line DST algorithm provides a structured way to schedule future transmissions in practice.

Algorithm 2 Proposed On-line Scheduling based on DST Algorithm

while The transmitter is powered on **do**
  if new data or energy arrives at the current instant **then**
    Set the current instant as t_0, and the instant of
    the future latest data deadline as t_N;
    Update $(\mathcal{A}, \mathcal{D}, \mathcal{E}, \mathcal{T})$;
    Run Algorithm 1 to update the transmit rates
    through t_N;
  end if
  Transmit the data with the updated transmit rates;
end while

2.6 Numerical Results

In this section, simulations are carried out to evaluate our proposed DST algorithms, where we set $\rho = 30$ mW (unless otherwise specified) and $|h|^2 = 20$ dB during $[0, T]$. The data arrival process and the EH process are modelled as two independent Poisson processes. The average data arrival rate is 1 packet/sec, unless otherwise specified. The average EH rate ranges from 40 to 400 mJ/sec. For illustration simplicity, we set all the packets with the same delay requirement (i.e., the maximum delay allowed). It is noteworthy that our algorithms are general and applicable to other stochastic processes of data arrival and EH.

For comparison purpose, we use the MATLAB CVX toolbox to solve (2.3) for off-line transmit schedules, and to replace Algorithm 1 in Algorithm 2 for on-line transmit schedule generation. The CVX toolbox is based on the standard convex optimization solver – the interior point methods [30]. It is effective and has been extensively used to solve optimization problems with convex structures. Particularly, the CVX toolbox can

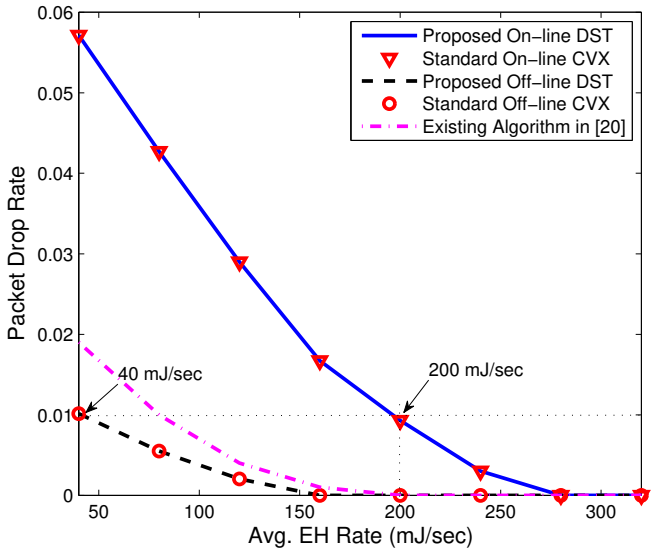

Figure 2.2: Packet drop rate versus EH rate, where we assume the transmitter has unlimited battery capacity, the deadline is 2.5 seconds for every packet and the data arrival rate is 0.6 packet/sec.

produce the exactly same optimal schedules as our proposed algorithms, in the case where the energy consumed to generate transmit schedules is negligible as compared to the rest of the energy consumed on the circuit, such as baseband processing and radio generation. However, in practice, the energy for schedule generation is non-negligible, especially in short-distance wireless sensor networks. Given the complexity of $\mathcal{O}(N^3)$, the standard interior point methods would consume more energy, drain the battery faster, and incur higher packet losses than our proposed algorithms which only have a complexity of lower than $\mathcal{O}(N^2)$.

Figs. 2.2 and 2.3 validate the optimality of our proposed algorithms from the perspectives of PDR and total energy consumption, where the energy required to generate the optimal schedules is assumed to be negligible. The packet drop is caused by the expiration of the deadlines of some packets which are unsent due to insufficient energy. The opti-

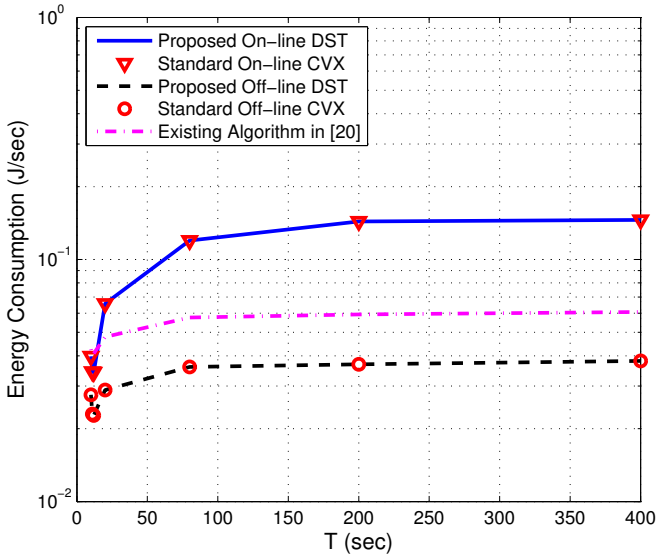

Figure 2.3: Comparison of average energy consumption for the proposed algorithms, the existing algorithm developed in [5], and the standard CVX toolbox, where we assume the transmitter has unlimited battery capacity, the deadline is 2 seconds for every packet, the data arrival rate is 0.6 packet/sec and the EH rate is 400 mJ/sec.

mality of the proposed algorithms is confirmed by comparing to the optimal results of the CVX toolbox, and revealing that the results of our algorithms coincide with those of the CVX toolbox. The PDR and energy consumption of the off-line energy-efficient transmit schedule optimized under the assumption of negligible circuit power consumption are also plotted, using the algorithm developed in [5].

In a sense, our proposed algorithm can minimize the infeasible region, by developing the most energy-efficient transmit schedules. In other words, it can minimize the number of packets dropped. This is because our algorithm can minimize the number of undelivered packets by the instant when the problem becomes infeasible. As a result, the energy requirement is minimized for the problem to become feasible again, which minimizes the duration of the infeasible region, as well as the packets dropped during the region.

As expected, the figures also show that on-line generation of transmit schedules can

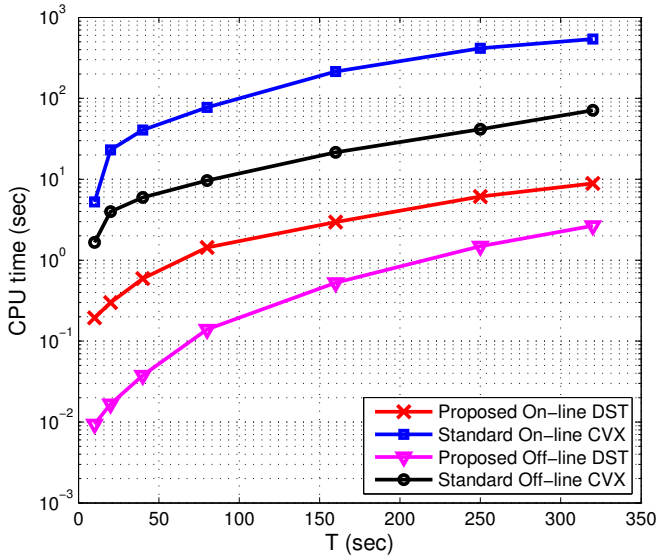

Figure 2.4: Comparison of average CPU time for the proposed off-line and on-line algorithms, with the CVX toolbox.

increase the PDR and the energy consumption, compared to the optimal schedules generated off-line. This is due to the unavailability of future knowledge on data and energy arrival in practice. As a result, the on-line transmit rates change more frequently than the optimal rates generated off-line. The energy consumption grows, as shown in Fig. 2.3. In turn, more packets are dropped, as shown in Fig. 2.2. In this sense, a higher EH rate is required for on-line algorithms to maintain a given PDR. Consider a PDR of 1%. The proposed on-line algorithm needs to increase the EH rate from 40 mJ/sec of the proposed off-line optimal scheme to 200 mJ/sec, as pointed out in Fig. 2.2.

Figs. 2.2 and 2.3 also reveal that the circuit power consumption can have significant impact on the optimal transmit schedules. It is shown that a significant loss of both the packet and energy would occur if the circuit power consumption is neglected, as in [5]. Our proposed algorithms, which take the circuit power consumption into account, are important, and have applications to practical circuits.

In practice, the energy consumed to generate transmit schedules is often non-negligible,

due to the complexity involved. Fig. 2.4 plots the average CPU time required for the proposed algorithms in comparison to the CVX toolbox, where T ranges from 10 to 320 seconds, and the EH rate is 400 mJ/sec. The average values are taken over the number of trials run on a computer. It is shown that the proposed off-line and on-line algorithms, i.e., Algorithms 1 and 2, only require about 3.7% and 1.6% of the CPU time that the standard CVX toolbox requires for large T values, respectively. This is because our algorithms are specialized and directly construct the optimal solution for (2.3) based on the optimality conditions. Therefore, they are much more computationally efficient than the CVX toolbox, which is general and is designed to solve any convex optimization problems.

As noted earlier, the proposed Algorithm 1 has a worst-case complexity of $\mathcal{O}(N^2)$, whereas the general CVX toolbox has a complexity of $\mathcal{O}(N^3)$. On the other hand, a much larger gap of complexity can be observed between Algorithm 1 and the CVX toolbox in Fig. 2.4. This confirms that Algorithm 1 has a significantly lower complexity in most cases than it has in the worst case, as discussed earlier in Section 2.4.2.

In light of Fig. 2.4, we proceed with a practical on-line scenario, where the energy for generating transmit schedules is non-negligible. Consider $\rho = \rho_1 + \rho_2$, where ρ_1 is the non-negligible energy consumption on schedule generation and ρ_2 is the rest of the energy consumed on the circuit. ρ_1 can differ between the proposed Algorithm 2 and the CVX program. We assume $\rho_1 = 15$ mW for Algorithm 2. The value of ρ_1 for the on-line CVX program depends on the ratio of the CPU time between the CVX program and Algorithm 2. The ratio can be obtained from Fig. 2.4. ρ_2 stays the same for both the approaches. We set $\rho_2 = 15$ mW.

Fig. 2.5 compares the PDR of the proposed Algorithm 2 and the on-line CVX program with the growth of deadline, where the transmitter is assumed to have unlimited battery. As expected, the PDR decreases, as the deadline increases. It also decreases, as the EH

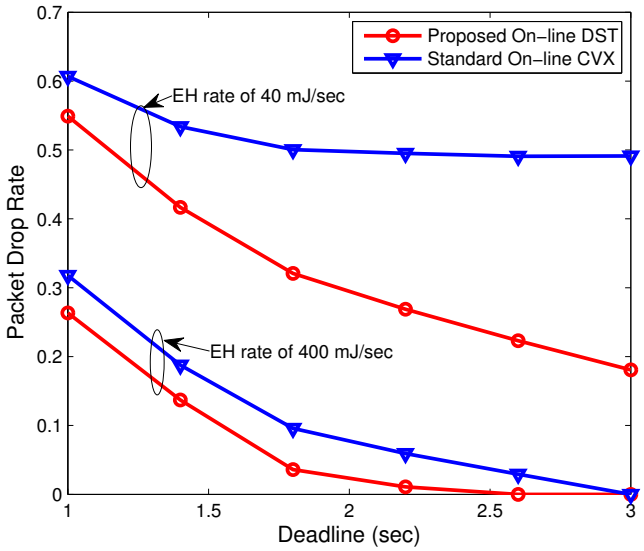

Figure 2.5: Packet drop rate of the proposed Algorithm 2 and the on-line CVX program versus delay requirement, where we assume the transmitter has unlimited battery capacity and the data arrival rate is 1 packet/sec.

rate increases. The reason for these is obvious, i.e., more available energy and/or looser data deadlines allow more packets to be delivered, hence reducing the PDR. In either case, we see that Algorithm 2 is better than the CVX program, given its superiority of substantially reduced energy requirement (as implied by Fig. 2.4).

As observed in Fig. 2.5, the reduced PDR of Algorithm 2 (compared to the CVX program) diminishes with the increasing deadline for large EH rates (e.g., 400 mJ/sec), while keeping growing for small EH rates (e.g., 40 mJ/sec). The reason for this is that the higher energy requirement of the CVX program makes the approach "saturate" at a smaller EH rate. In other words, the PDR stops decreasing further with the growth of deadline. It would not converge to zero, even without deadline (i.e., the deadline is infinite). The convergent/saturated PDR value can be easily obtained by first calculating the difference between the total energy harvested and the total energy consumed on the

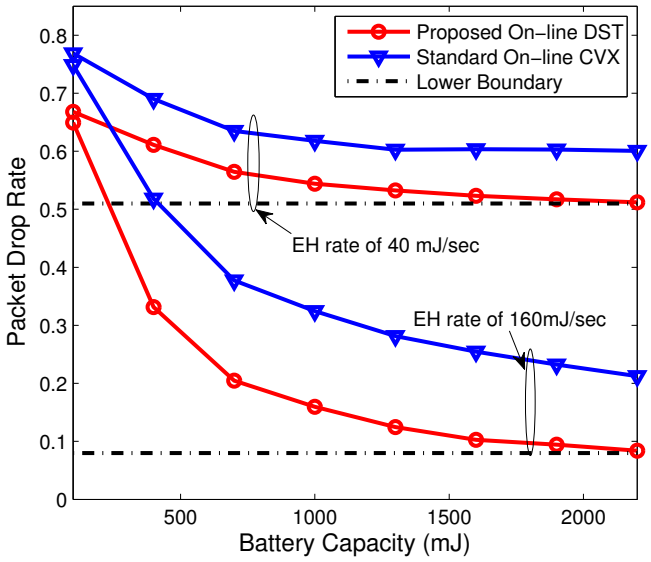

Figure 2.6: Packet drop rate of the proposed Algorithm 2 and the on-line CVX program versus battery capacity, where the data arrival rate is 1 packet/sec and the deadline requirement is 2.5 seconds.

circuit, and then the number of packets that can be supported by the energy difference using r_{ee}.

Given the substantially low energy requirement, our proposed Algorithm 2 tolerates much smaller EH rates before saturating. Our algorithm also has much lower convergent PDR values. As shown in Fig. 2.5, the CVX program saturates with a convergent PDR of about 50%, when the EH rate is 40 mJ/sec. Meanwhile, Algorithm 2 is unsaturated, and it exhibits the obvious tendency of continuously decreasing.

Fig. 2.6 compares the PDR of the proposed Algorithm 2 and the standard on-line CVX program with the growth of the limited battery at the transmitter. The battery overflows, if the energy harvested and accumulated exceeds the battery capacity. As expected, we see that the PDR starts by decreasing with the growth of battery capacity at the transmitter, and then becomes flat when the battery is large and little energy is overflown. We also see

that our proposed algorithm outperforms the standard CVX program with a consistent PDR reduction, across the entire spectrum of battery capacity, for a given EH rate. The consistent PDR reduction is due to the energy that our algorithm saves against the CVX program, and the saved energy is independent of the battery capacity.

The consistent PDR reduction is also enlarged when the EH rate increases; in other words, more energy can be saved with the increased EH rate. Specifically, the CVX program has bigger ρ and subsequently a smaller r_{ee} according to (2.16), compared to the proposed Algorithm 2. This increases the likelihood of transmitting data over an entire epoch with a less energy-efficient rate r_n^e or r_n^a, since the optimal rate is the largest of r_{ee} and those rates based on Lemma 1. The likelihood is further increased due to more and shorter epochs with the increased EH rate. The increased number of epochs, over which the energy is less efficiently utilized in the CVX program, results in the enlarged gap between Algorithm 2 and the CVX program. More energy is saved by the proposed Algorithm 2, and more packets can be sent using the saved energy under a larger EH rate.

Last but not least, we plot the trade-off between the data arrival rate and the EH rate in Fig. 2.7, where we set a fixed PDR of 10%. In addition to Algorithm 2 and the on-line CVX program, we also plot the proposed optimal off-line algorithm – Algorithm 1. In general, the proposed on-line algorithm, Algorithm 2, substantially surpasses the standard on-line CVX program. The effective on-line transmit region, which is the close region underneath every plotted curve, is significantly larger in Algorithm 2 than it is in the on-line CVX program. This is the result of the reduced complexity of Algorithm 2, and significantly more data or less energy can be supported in the proposed algorithm. The difference of sizes between the effective transmit regions of the two on-line approaches enlarges with the increased tightness of deadline.

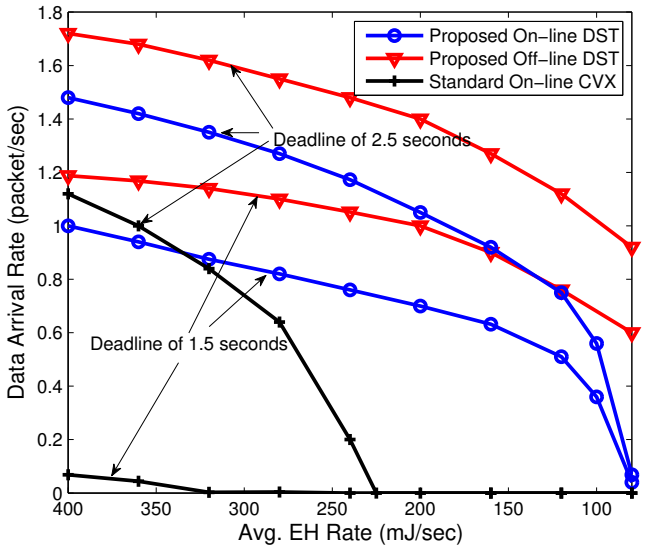

Figure 2.7: EH rate versus packet arrival rate, where we assume the transmitter has unlimited battery capacity, the deadline is 2.5 seconds for every packet.

2.7 Conclusions

In this chapter, we proposed the new DST algorithm to generate the optimal off-line transmit schedule for delay-limited traffic under non-negligible circuit power. Only consisting of a set of string tautening rules that we derived from the optimality conditions of the original problem, the proposed algorithm has a low complexity (i.e., $\mathcal{O}(N^2)$ in the worst case). We also extended the algorithm to generate energy-efficient transmit schedules on-the-fly. Simulation shows that our algorithm reduces the average complexity by almost two orders of magnitude, compared to general convex solvers. The effective transmit region can also be substantially enlarged by our algorithm. Significantly more data or less energy can be supported in the proposed algorithm. Building on this work, promising future directions include modeling more practical battery unit with finite capacity and energy leakage, accounting for charging/discharging loss, and developing low-complexity on-line schemes with analytical performance guarantees.

Chapter 3

Smart-grid powered MIMO downlink communications

3.1 Introduction

Downlink communications from the base station (BS) to mobile users in wireless cellular systems is usually analyzed as a Gaussian broadcast channel in information-theoretic approaches. Shannon's capacity for both single-input-single-output (SISO) and multi-input multi-output (MIMO) broadcast channels has been well addressed [85–87], when the transmitters (i.e., BSs) are powered by persistent energy sources of the conventional electricity grid. However, the current grid infrastructure is on the verge of a major paradigm shift, migrating from the aging grid to a "smart" one. The smart grid is envisioned with new features and capabilities, including e.g., high-penetration of renewable energy sources (RES), two-way energy trading, and demand-side management (DSM) [88–90].

While integration of smart-grid technologies into resource allocation clearly holds the key to fully exploiting the potential of future downlink communications [69], only a few works explore this direction.

In the present chapter, we develop a stochastic *online* resource allocation approach, which dynamically makes *instantaneous* decisions without a-priori knowledge of any statistics of the underlying random channel, renewables, and electricity price processes. To this end, the intended task is formulated as an infinite horizon optimization problem aiming to maximize the time-average (weighted) downlink throughput subject to a time-average energy cost budget. Targeting a low-complexity online solution, we adopt the relaxation techniques in [71, 73, 74] to decouple the decision variables across time. Then leveraging the stochastic dual-subgradient method, we develop a novel online control algorithm. To analyze the proposed scheme, we generalize the framework in [71, 73, 74] to characterize the two coupled "virtual" queues involved in our online control setting. It is then rigorously established that the proposed online control algorithm yields a feasible and asymptotically optimal resource allocation strategy for the original problem. Although the performance analysis is based on i.i.d. random processes, numerical results further demonstrate that the proposed algorithm also works well in non i.i.d. scenarios, where the underlying randomness is highly correlated over time.

The rest of the chapter is organized as follows. The system models are described in Section 3.2. The proposed dynamic resource allocation scheme is developed and analyzed in Section 3.3. Numerical results are provided in Section 3.4, followed by concluding remarks in Section 3.5.

3.2 System Models

Consider a MIMO downlink where a BS with N_t antennas communicates to K mobile users, each having N_r antennas; see Fig. 3.1. Powered by a smart microgrid, the BS is equipped with one or more energy harvesting devices (solar panels and/or wind turbines), and can perform two-way energy trading with the main grid upon energy surplus or deficit

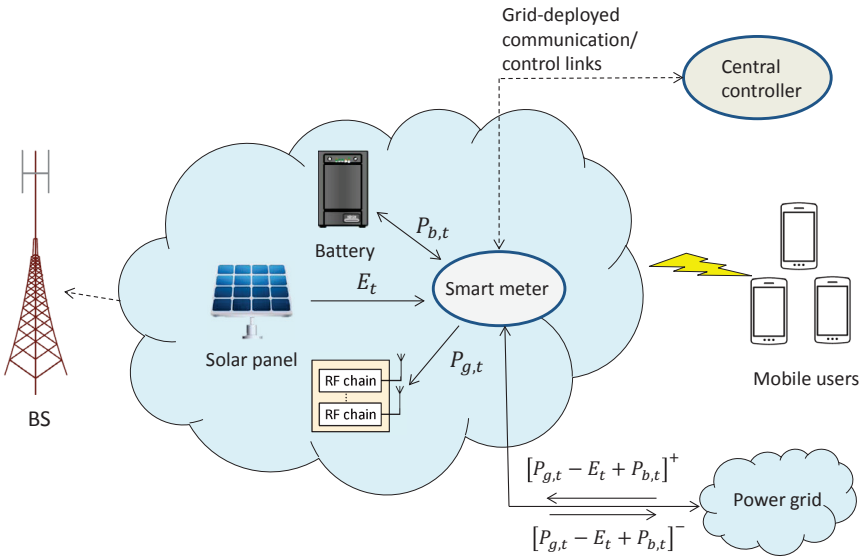

Figure 3.1: A smart-grid powered MIMO downlink system.

in the microgrid. In addition, with a goal of mitigating the high variability of RES, an energy storage device (i.e., battery) is considered in the BS, so the BS does not have to consume or sell all the harvested energy on the spot, but can save it for later use. A controller at the BS coordinates the energy trading as well as the allocation of communication resources. This central entity can collect both the channel state information (CSI) through the feedback links from the users, as well as the energy information (energy buying/selling prices) via the smart meter installed at the BS.

3.2.1 MIMO Downlink Channels

The downlink from the BS to the users constitutes a broadcast channel (BC). Assume slot-based transmissions from the BS to the users, and a quasi-static model for the wireless channels, where the channel coefficients remain invariant per slot but are allowed to vary across slots. This assumption is reasonable when the length of the slot is selected to be smaller than the coherence time of the wireless channels. Suppose also a slowly time-

varying setup so that the slot length is sufficiently large to accommodate the Shannon capacity-achieving encoding schemes. For convenience, the slot duration is normalized to unity; thus, the terms "energy" and "power" will be used interchangeably throughout the chapter. Notice that our algorithm could also be extended to a two time scale scheduling approach, where the battery can be operated in the slow scale, while the remaining decision variables in the fast time scale [76].

Consider a (possibly infinite) scheduling horizon consisting of T slots, indexed by the set $\mathcal{T} := \{0, \ldots, T-1\}$. Per slot t, let $\boldsymbol{H}_{k,t} \in \mathbb{C}^{N_r \times N_t}$ denote the channel coefficient matrix from the BS to user $k = 1, \ldots, K$, and $\mathcal{H}_t := \{\boldsymbol{H}_{1,t}, \ldots, \boldsymbol{H}_{K,t}\}$. For simplicity, we assume that $\mathcal{H}_t$ evolves according to an independent and identically distributed (i.i.d.) random process. Note that the proposed algorithm in the sequel can be applied without any modification to non-i.i.d. scenarios as well. Yet, performance guarantees in the non-i.i.d. case must be obtained by applying the more sophisticated delayed Lyapunov drift techniques in [91].

Let $\boldsymbol{x}(t) \in \mathbb{C}^{N_t \times 1}$ denote the transmitted vector signal, which is the sum of the signal independently transmitted to individual users: $\boldsymbol{x}(t) = \sum_{k=1}^{K} \boldsymbol{x}_k(t)$. The received complex-baseband signal at user k is then

$$\boldsymbol{y}_k(t) = \boldsymbol{H}_{k,t}\boldsymbol{x}(t) + \boldsymbol{z}_k(t) \tag{3.1}$$

where $\boldsymbol{z}_k(t)$ is additive complex-Gaussian noise with zero mean and covariance matrix $\boldsymbol{I}$ (the identity matrix of size N_r).

The capacity of the MIMO BC can be achieved by dirty paper coding (DPC) [92]. With DPC, users are sequentially encoded such that each user sees no interference from previously encoded users. For the DPC codeword $\boldsymbol{x}_k(t)$, the transmit covariance matrix of user k is $\boldsymbol{\Gamma}_{k,t} := \mathbb{E}[\boldsymbol{x}_k(t)\boldsymbol{x}_k^{\dagger}(t)]$. With $P_{x,t}$ denoting the transmit-power budget at the BS per slot t, it holds that $\sum_{k=1}^{K} \mathrm{tr}(\boldsymbol{\Gamma}_{k,t}) \leq P_{x,t}$. The BC capacity region per slot t is then

given by

$$\mathcal{C}_{\mathrm{BC}}(P_{x,t};\mathcal{H}_t) = Co\left(\bigcup_{\pi}\mathcal{R}_{\pi}(P_{x,t};\mathcal{H}_t)\right) \tag{3.2}$$

where $Co(\cdot)$ denotes the convex hull, the union is over all permutations π of $\{1,2,\ldots,K\}$, and

$$\mathcal{R}_{\pi}(P_{x,t};\mathcal{H}_t) = \bigcup_{\{\boldsymbol{\Gamma}_{k,t}:\,\sum_{k=1}^{K}\mathrm{tr}(\boldsymbol{\Gamma}_{k,t})\le P_{x,t}\}} \Bigg\{(r_1,\ldots,r_K): \\ r_{\pi(k)} \le \log\frac{\left|\boldsymbol{I}+\sum_{u=1}^{k}\boldsymbol{H}_{\pi(u),t}\boldsymbol{\Gamma}_{\pi(u),t}\boldsymbol{H}_{\pi(u),t}^{\dagger}\right|}{\left|\boldsymbol{I}+\sum_{u=1}^{k-1}\boldsymbol{H}_{\pi(u),t}\boldsymbol{\Gamma}_{\pi(u),t}\boldsymbol{H}_{\pi(u),t}^{\dagger}\right|},\ \forall k\Bigg\}.$$

Here r_k denotes the achievable transmission rate for user $k=1,\ldots,K$, and $|\cdot|$ signifies the determinant operator.

3.2.2 Smart Grid Operations

While Section 3.2.1 shows the communication model for MIMO downlink channels, in what follows, we introduce the operation model for smart grid. The smart-grid powered BS can harvest RES and store the energy in the battery for future use. Let E_t denote the (random) energy harvested at the beginning of slot t at the BS, with $E_t \le E^{\max}$, $\forall t$.

Let C_0 denote the initial energy, and C_t the state of charge (SoC) in the battery at the beginning of slot t. The battery is assumed to have a finite capacity $C^{\max}$. Furthermore, for reliability purposes, it may be required to ensure that a minimum energy level $C^{\min}$ is maintained at all times[1]; hence, we have $C^{\min} \le C_t \le C^{\max}$, $\forall t \in \mathcal{T}$. Let $P_{b,t}$ denote the power delivered to or drawn from the battery at slot t, which amounts to either charging ($P_{b,t} > 0$) or discharging ($P_{b,t} < 0$). Hence, the stored energy obeys the dynamic equation

$$C_{t+1} = C_t + P_{b,t}, \quad \forall t. \tag{3.3}$$

[1]Battery will become unreliable with high depth-of-discharge (DoD) – percentage of maximum charge removed during a discharge cycle; hence, a minimum level $C^{\min}$ is to avoid high DoD. Such a level could be also required to support the BS operation in the event of a grid outage.

The amount of power (dis-)charged is also bounded by

$$P_b^{\min} \leq P_{b,t} \leq P_b^{\max} \tag{3.4}$$

where $P_b^{\min} < 0$, and $P_b^{\max} > 0$.

Per slot t, the total energy consumption $P_{g,t}$ at the BS includes the transmission-related power $P_{x,t}$, and the rest that is due to other components such as air conditioning, data processor, and circuits, which can be collectively modeled as a constant power, $P_c > 0$ [37]; namely,

$$P_{g,t} = P_c + P_{x,t}/\xi$$

where $\xi > 0$ denotes the power amplifier efficiency. Without loss of generality, we normalize the constant to $\xi = 1$; and further assume that $P_{g,t}$ is bounded by $P_g^{\max}$.

When the renewable harvested energy is insufficient, the main grid can supply the needed $P_{g,t}$ to the BS. With a two-way energy trading facility, the BS can also sell its surplus energy to the grid at a fair price in order to reduce operational costs. Given the required energy $P_{g,t}$, the harvested energy E_t, and the battery charging energy $P_{b,t}$, the shortage energy that needs to be purchased from the grid for the BS is $[P_{g,t} - E_t + P_{b,t}]^+$; or, the surplus energy (when the harvested energy is abundant) that can be sold to the grid is $[P_{g,t} - E_t + P_{b,t}]^-$, where $[a]^+ := \max\{a, 0\}$, and $[a]^- := \max\{-a, 0\}$. Both the shortage and surplus energies are non-negative, and we have at most one of them be positive at any time t.

Suppose that the energy can be purchased from the grid at price α_t, while the energy is sold to the grid at price β_t per slot t. Assume that the prices are bounded; i.e., $\alpha_t \in [\alpha_{\min}, \alpha_{\max}]$, $\beta_t \in [\beta_{\min}, \beta_{\max}]$, $\forall t$. Note that we shall always set $\alpha_t > \beta_t$, $\forall t$, to avoid meaningless buy-and-sell activities of the BS for profit. Per slot t, the transaction cost for the BS is given by

$$G(P_{g,t}, P_{b,t}) = \alpha_t [P_{g,t} - E_t + P_{b,t}]^+ - \beta_t [P_{g,t} - E_t + P_{b,t}]^-. \tag{3.5}$$

Again for simplicity, we assume that the random variables (E_t, α_t, β_t) are generated according to an i.i.d. random process, while generalization to non-i.i.d. scenarios can be addressed using the techniques in [91].

3.3 Dynamic Resource Allocation Algorithm

Based on the models of Section 3.2, we formulate and optimize in this section, the allocation of resources for the smart-grid powered broadcasting operation. Let w_k denote the priority weight for user $k = 1, \ldots, K$, $\mathbf{\Gamma}_t := \{\mathbf{\Gamma}_{1,t}, \ldots, \mathbf{\Gamma}_{K,t}\}$, and $G^{\max}$ the maximum allowable power cost at the BS. Over the scheduling horizon $\mathcal{T}$, the central controller at the BS determines the optimal transmit covariance matrices $\{\mathbf{\Gamma}_t, \forall t\}$, transmit-power $\{P_{x,t}, \forall t\}$, and battery charging energy $\{P_{b,t}, \forall t\}$, in order to maximize the average (weighted) total throughput $\lim_{T\to\infty} \frac{1}{T} \sum_{k=1}^{K} [w_k \sum_{t=0}^{T-1} (r_k^B(\mathbf{\Gamma}_t))]$, subject to an average energy cost constraint. For notational brevity, we introduce the auxiliary variables $P_t := P_{g,t} + P_{b,t}$, and formulate the problem as

$$\max_{\{\mathbf{\Gamma}_t, C_t, P_t, P_{x,t}, P_{b,t}\}} \quad \lim_{T\to\infty} \frac{1}{T} \sum_{k=1}^{K} [w_k \sum_{t=0}^{T-1} (r_k^B(\mathbf{\Gamma}_t))] \tag{3.6a}$$

$$\text{s. t.} \quad \lim_{T\to\infty} \frac{1}{T} \sum_{t=0}^{T-1} G(P_t) \leq G^{\max} \tag{3.6b}$$

$$P_t = P_{x,t} + P_{b,t} + P_c \tag{3.6c}$$

$$0 \leq P_c + P_{x,t} \leq P_g^{\max} \tag{3.6d}$$

$$P_b^{\min} \leq P_{b,t} \leq P_b^{\max} \tag{3.6e}$$

$$C_{t+1} = C_t + P_{b,t} \tag{3.6f}$$

$$C^{\min} \leq C_t \leq C^{\max} \tag{3.6g}$$

$$\boldsymbol{r}^B(\mathbf{\Gamma}_t) \in \mathcal{C}_{\text{BC}}(P_{x,t}; \mathcal{H}_t), \ \forall t. \tag{3.6h}$$

Here, (3.6b) is the average energy cost constraint, (3.6d) is the maximum power consumption constraint for BSs, and (3.6e)-(3.6g) are the constraints related to battery operations.

3.3.1 Reformulation and Relaxation

For the tractability of (3.6), in this subsection, the problem is reformulated and relaxed to a convex sum-power allocation problem for a point-to-point link.

With $\psi_t := (\alpha_t - \beta_t)/2$ and $\phi_t := (\alpha_t + \beta_t)/2$, it follows readily from (3.5) that

$$G(P_t) = \psi^t |P_t - E_t| + \phi_t (P_t - E_t).$$

Since $\alpha_t > \beta_t > 0$, we have $\phi_t > \psi_t > 0$ which clearly implies that $G(P_t)$ is a convex function of P_t.

Now let us convexify the rate functions $r_k^B(\boldsymbol{\Gamma}_t)$. By the information-theoretic uplink-downlink duality [93, 94], the BC capacity region $\mathcal{C}_{\rm BC}(P_{x,t}; \mathcal{H}_t)$ can be alternatively characterized by the capacity regions of a set of "dual" multi-access channels (MACs). In the dual MAC, the received signal is

$$\boldsymbol{y}(t) = \sum_{k=1}^{K} \boldsymbol{H}_{k,t}^{\dagger} \boldsymbol{x}_k(t) + \boldsymbol{z}(t)$$

where $\boldsymbol{x}_k(t)$ is the signal transmitted by user k, and $\boldsymbol{z}(t)$ is additive complex-Gaussian with zero mean and covariance matrix $\boldsymbol{I}$ (the identity matrix of size N_t). Let $\boldsymbol{Q}_k := \mathbb{E}[\boldsymbol{x}_k \boldsymbol{x}_k^{\dagger}] \succeq \boldsymbol{0}$ denote the transmit covariance matrix of user k, and let $\boldsymbol{p} := [P_1, \ldots, P_K]^{\top}$ collect the transmit-power budgets of all users. For a given $\boldsymbol{p}$, the MAC capacity region is

$$\mathcal{C}_{\rm MAC}(\boldsymbol{p}; \mathcal{H}_t^{\dagger}) = \bigcup_{\{\boldsymbol{Q}_k:\, {\rm tr}(\boldsymbol{Q}_k) \le P_k,\, \forall k\}} \Big\{ (r_1, \ldots, r_K) : \sum_{k \in \mathcal{S}} r_k \le \log \Big| \boldsymbol{I} + \sum_{k \in \mathcal{S}} \boldsymbol{H}_{k,t}^{\dagger} \boldsymbol{Q}_k \boldsymbol{H}_{k,t} \Big|,\ \forall \mathcal{S} \subseteq \{1, \ldots, K\} \Big\}.$$

The uplink-downlink duality dictates that the BC capacity region (3.2) equals the union of these MAC capacity regions corresponding to all power vectors $\boldsymbol{p}$ satisfying $\sum_{k=1}^{K} P_k \leq P_{x,t}$; that is,

$$\mathcal{C}_{\mathrm{BC}}(\boldsymbol{p}; \mathcal{H}_t) = \bigcup_{\{\boldsymbol{p}: \sum_{k=1}^{K} P_k \leq P_{x,t}\}} \mathcal{C}_{\mathrm{MAC}}(\boldsymbol{p}; \mathcal{H}_t^{\dagger}). \tag{3.7}$$

Using the definition

$$R_t(P_{x,t}) := \max_{\boldsymbol{r}^B(\boldsymbol{\Gamma}_t) \in \mathcal{C}_{\mathrm{BC}}(P_{x,t}; \mathcal{H}_t)} \sum_{k=1}^{K} w_k r_k^B(\boldsymbol{\Gamma}_t)$$

[67, Lemma 1] has established the following result.

Lemma 3. *The function $R_t(P_{x,t})$ can be alternatively obtained by the optimal value of the problem:*

$$\begin{aligned} \max_{\boldsymbol{Q}_k \succeq \boldsymbol{0}} \quad & \sum_{k=1}^{K} (w_{\pi(k)} - w_{\pi(k+1)}) \log \left| \boldsymbol{I} + \sum_{u=1}^{k} \boldsymbol{H}_{\pi(u),t}^{\dagger} \boldsymbol{Q}_{\pi(u)} \boldsymbol{H}_{\pi(u),t} \right| \\ \text{s. t.} \quad & \sum_{k=1}^{K} \mathrm{tr}(\boldsymbol{Q}_k) = P_{x,t} \end{aligned} \tag{3.8}$$

where π is the permutation of user indices $\{1, \ldots, K\}$ such that $w_{\pi(1)} \geq \cdots \geq w_{\pi(K)}$, and $w_{\pi(K+1)} = 0$. In addition, $R_t(P_{x,t})$ is a strictly concave and increasing function of $P_{x,t}$.

Using $R_t(P_{x,t})$ and expressing the variables $\{P_{b,t}\}$ in terms of $\{P_t, P_{x,t}\}$, the optimal broadcasting problem can be converted into the optimal sum-power allocation for an

equivalent "point-to-point" link without any optimality loss, as follows

$$\max_{\{C_t,P_t,P_{x,t}\}} \quad \lim_{T\to\infty}\frac{1}{T}\sum_{t=0}^{T-1}[R_t(P_{x,t})] \tag{3.9a}$$

$$\text{s. t.} \quad \lim_{T\to\infty}\frac{1}{T}\sum_{t=0}^{T-1}G(P_t)\leq G^{\max} \tag{3.9b}$$

$$0\leq P_{x,t}\leq P_g^{\max}-P_c \tag{3.9c}$$

$$P_b^{\min}\leq P_t-P_{x,t}-P_c\leq P_b^{\max} \tag{3.9d}$$

$$C_{t+1}=C_t+P_t-P_{x,t}-P_c \tag{3.9e}$$

$$C^{\min}\leq C_t\leq C^{\max},\ \forall t. \tag{3.9f}$$

The convexity of constraint (3.9b) has been clarified, and constraints (3.9c)-(3.9f) are linear. As $R_t(P_{x,t})$ is a concave function of $P_{x,t}$ per Lemma 3, problem (3.9) is a convex program. Note that here we implement a nested optimization procedure. Namely, we first solve (3.9) to find the optimal $\{C_t^*, P_t^*, P_{x,t}^*, P_{b,t}^*\}$. Given $P_{x,t}^*$ per slot, we then solve the convex optimization (3.8) to obtain the optimal "virtual" uplink covariance matrices $\boldsymbol{Q}_k(P_{x,t}^*)$, $\forall k$, and subsequently, the desired downlink covariance matrices $\boldsymbol{\Gamma}_{k,t}^*$ from $\boldsymbol{Q}_k(P_{x,t}^*)$ via uplink-downlink duality. Let R^* denote the value of the objective in (3.6) under an optimal control policy.

Although (3.9) becomes convex after judicious reformulation, it is still difficult to solve since we aim to maximize the average total throughput over an infinite time horizon. In particular, the battery energy level relations in (3.6f) couple the optimization variables over the infinite time horizon, which renders the problem intractable for traditional solvers such as dynamic programming.

By recognizing that (3.6f) can be viewed as an energy queue recursion, we next apply the time decoupling technique to turn (3.9) into a tractable form [73, 74]. For the queue of C_t, the arrival and departure are P_t and $P_{x,t}+P_c$, respectively, per slot t. Over the infinite time horizon, the time-averaging rates of arrival and departure are given

by $\lim_{T\to\infty}\frac{1}{T}\sum_{t=0}^{T-1}P_t$ and $P_c+\lim_{T\to\infty}\frac{1}{T}\sum_{t=0}^{T-1}P_{x,t}$, respectively. Define the following expected values:

$$\mathbb{E}[R_t(P_{x,t})]:=\lim_{T\to\infty}\frac{1}{T}\sum_{t=0}^{T-1}R_t(P_{x,t})$$

$$\mathbb{E}[G(P_t)]:=\lim_{T\to\infty}\frac{1}{T}\sum_{t=0}^{T-1}G(P_t)$$

$$\mathbb{E}[P_t]:=\lim_{T\to\infty}\frac{1}{T}\sum_{t=0}^{T-1}P_t,\quad \mathbb{E}[P_{x,t}]:=\lim_{T\to\infty}\frac{1}{T}\sum_{t=0}^{T-1}P_{x,t}$$

where the expectations are taken over all sources of randomness. These expectations exist due to the stationarity of $\{\mathcal{H}_t,E_t,\alpha_t,\beta_t\}$.

Now simply remove the variables $\{C_t\}$ and consider the following problem

$$\begin{aligned}\tilde{R}^*:=&\max_{\{P_t,P_{x,t}\}}\mathbb{E}[R_t(P_{x,t})]\\ \text{s. t.}\quad&\mathbb{E}[G(P_t)]\le G^{\max},\quad \mathbb{E}[P_t]=P_c+\mathbb{E}[P_{x,t}]\\ &(4.23\text{c})-(3.9\text{d}).\end{aligned}\tag{3.10}$$

It can be shown that (3.10) is a relaxed version of (3.9). Specifically, any feasible solution of (3.9) also satisfies the constraints in (3.10). To see this, consider any policy that satisfies (3.9e) and (3.9f). Then summing equations in (3.9e) over all $t\in\mathcal{T}$ yields: $C_T-C_0=\sum_{t=0}^{T-1}[P_t-P_c-P_{x,t}]$. Since both C^T and C^0 are bounded due to (3.9f), dividing both sides by T and taking limits as $T\to\infty$, yields $\mathbb{E}[P_t]=P_c+\mathbb{E}[P_{x,t}]$. It is then clear that any feasible policy for (3.9) is also feasible for (3.10). As a result, the optimal value of (3.10) is not less than that of (3.9); that is, $\tilde{R}^*\ge R^*$.

Note that the time coupling constraint (3.9e) has been relaxed in problem (3.10), which then becomes easier to solve. It can be shown that the optimal solution to (3.10) can be achieved by a stationary control policy that chooses control actions $\{P_t,P_{x,t}\}$ every slot purely as a function (possibly randomized) of the current $\{\mathcal{H}_t,E_t,\alpha_t,\beta_t\}$ [91]. We next develop a stochastic dual subgradient solver for (3.10), which under proper initialization

can provide an asymptotically optimal solution to the original resource allocation problem (3.6).

3.3.2 Dual Subgradient Approach

Let $\mathcal{F}_t$ denote the set of $\{P_t, P_{x,t}\}$ satisfying constraints (3.9c)–(3.9d) per t, and $\boldsymbol{\lambda} := \{\lambda_1, \lambda_2\}$ collect the Lagrange multipliers associated with the two average constraints. With the convenient notation $\boldsymbol{X}_t := \{P_t, P_{x,t}\}$ and $\boldsymbol{X} := \{\boldsymbol{X}_t, \forall t\}$, the partial Lagrangian function of (3.10) is

$$\begin{aligned} L(\boldsymbol{X}, \boldsymbol{\lambda}) :=& \mathbb{E}[R_t(P_{x,t})] - \lambda_1(\mathbb{E}[G(P_t)] - G^{\max}) \\ & - \lambda_2(\mathbb{E}[P_t] - P_c - \mathbb{E}[P_{x,t}]) \end{aligned} \tag{3.11}$$

while the Lagrange dual function is given by

$$D(\boldsymbol{\lambda}) := \max_{\{\boldsymbol{X}^t \in \mathcal{F}^t\}_t} L(\boldsymbol{X}, \boldsymbol{\lambda}) \tag{3.12}$$

and the dual problem of (3.10) is: $\min_{\lambda_1 \geq 0, \lambda_2} D(\boldsymbol{\lambda})$.

For the dual problem, we can resort to a standard subgradient method to obtain the optimal $\boldsymbol{\lambda}^*$. This amounts to running the iterations

$$\begin{aligned} \lambda_1(j+1) &= [\lambda_1(j) - \mu g_{\lambda_1}(j)]^+ \\ \lambda_2(j+1) &= \lambda_2(j) - \mu g_{\lambda_2}(j) \end{aligned} \tag{3.13}$$

where j is the iteration index, and $\mu > 0$ is an appropriate stepsize. The subgradient $\boldsymbol{g}(j) := [g_{\lambda_1}(j), g_{\lambda_2}(j)]$ can be then expressed as

$$\begin{aligned} g_{\lambda_1}(j) &= G^{\max} - \mathbb{E}[G(P_t(j))] \\ g_{\lambda_2}(j) &= P_c + \mathbb{E}[P_{x,t}(j)] - \mathbb{E}[P_t(j)] \end{aligned} \tag{3.14}$$

where $P_t(j)$ and $P_{x,t}(j)$ are given by

$$\begin{aligned} \{P_t(j), P_{x,t}(j)\} \in \arg & \max_{\{P_t, P_{x,t}\} \in \mathcal{F}_t} [R_t(P_{x,t}) \\ & -\lambda_1(j) G(P_t) - \lambda_2(j)(P_t - P_c - P_{x,t})]. \end{aligned} \tag{3.15}$$

By the concavity of $R_t(P_{x,t})$, convexity of $G(P_t)$, and the nonnegativity of $\lambda_1(j)$, the objective function here is concave. Since $\mathcal{F}^t$ is a convex set, the maximization problem in (3.15) is a convex program. By Lemma 3, the problem can be transformed into (3.16), which can be efficiently solved by the Matlab CVX solver in polynomial time. With $\{P_t(\boldsymbol{\lambda}(j)), \boldsymbol{Q}_k^*(\boldsymbol{\lambda}(j)), \forall k\}$ denoting the optimal solution of (3.16), one can subsequently determine $P_t(j) = P_t(\boldsymbol{\lambda}(j))$, and $P_{x,t}(j) = \sum_{k=1}^K \mathrm{tr}(\boldsymbol{Q}_k^*(\boldsymbol{\lambda}(j)))$.

$$\max_{\boldsymbol{Q}_k \succeq 0, P_t \geq 0} \sum_{k=1}^{K} (w_{\pi(k)} - w_{\pi(k+1)}) \log \left| \boldsymbol{I} + \sum_{u=1}^{k} \boldsymbol{H}_{\pi(u),t}^{\dagger} \boldsymbol{Q}_{\pi(u)} \boldsymbol{H}_{\pi(u),t} \right| + \lambda_2(j) \sum_{k=1}^{K} \mathrm{tr}(\boldsymbol{Q}_k)$$
$$- \lambda_2(j) P_t - \lambda_1(j) G(P_t)$$
$$\text{s. t.} \quad 0 \leq \sum_{k=1}^{K} \mathrm{tr}(\boldsymbol{Q}_k) \leq P_g^{\max} - P_c, \quad P_b^{\min} \leq P_t - \sum_{k=1}^{K} \mathrm{tr}(\boldsymbol{Q}_k) - P_c \leq P_b^{\max}$$

When a constant stepsize μ is adopted, the subgradient iterations (3.13) are guaranteed to converge to a neighborhood of the optimal $\boldsymbol{\lambda}^*$ for the dual problem from any initial point $\boldsymbol{\lambda}(0)$. The size of the neighborhood is proportional to the stepsize μ. In fact, if we adopt a sequence of non-summable diminishing stepsizes satisfying $\lim_{j\to\infty} \mu(j) = 0$ and $\sum_{j=0}^{\infty} \mu(j) = \infty$, then the iterations (3.13) converge to the exact $\boldsymbol{\lambda}^*$ as $j \to \infty$ [95]. Since (3.10) is convex, the duality gap is zero, and convergence to $\boldsymbol{\lambda}^*$ will also yield the optimal solution $\{P_t^*, P_{x,t}^*, \forall t\}$ to the primal problem (3.10).

3.3.3 Online Control Algorithm

A challenge associated with the subgradient iterations (3.13) is computing $\mathbb{E}[P_t(j)]$, $\mathbb{E}[P_{x,t}(j)]$, and $\mathbb{E}[G(P_t(j))]$ per iterate. This amounts to performing (high-dimensional) integration over unknown joint distribution functions; or approximately computing the corresponding time-averages over an infinite time horizon. Clearly, such a requirement is impractical. To bypass this impasse, we will rely on a stochastic subgradient approach. Specifically,

dropping $\mathbb{E}$ from (3.13), we propose the following iteration

$$\begin{aligned}\hat{\lambda}_1^{t+1} &= [\hat{\lambda}_1^t - \mu(G^{\max} - G(P_t(\hat{\boldsymbol{\lambda}}^t)))]^+ \\ \hat{\lambda}_2^{t+1} &= \hat{\lambda}_2^t - \mu(P_c + P_{x,t}(\hat{\boldsymbol{\lambda}}^t) - P_t(\hat{\boldsymbol{\lambda}}^t))\end{aligned} \tag{3.16}$$

where $\{\hat{\lambda}_1^t, \hat{\lambda}_2^t\}$ are stochastic estimates of those in (3.13), and $P_t(\hat{\boldsymbol{\lambda}}^t)$, $P_{x,t}(\hat{\boldsymbol{\lambda}}^t)$ are obtained by solving (3.15) with $\boldsymbol{\lambda}(j)$ replaced by $\hat{\boldsymbol{\lambda}}^t$.

Note that t denotes both iteration and slot indices. In other words, the update (3.16) is an *online* approximation algorithm based on the *instantaneous* decisions $\{P_t(\hat{\boldsymbol{\lambda}}^t), P_{x,t}(\hat{\boldsymbol{\lambda}}^t)\}$ per slot t. This stochastic approach is made possible due to the decoupling of optimization variables across time in (3.10). Convergence of online iterations (3.16) to the optimal $\boldsymbol{\lambda}^*$ can be established in different senses; see [91] and [96–98].

Based on the stochastic iterations (3.16), we will develop next a stochastic subgradient based online control (SGOC) algorithm for the original problem (3.6). The algorithm is implemented at the BS as follows.

SGOC: Initialize with a proper $\hat{\boldsymbol{\lambda}}^0 := \{\hat{\lambda}_1^0, \hat{\lambda}_2^0\}$. At every time slot t, observe $\hat{\boldsymbol{\lambda}}^t$, $\mathcal{H}_t$, E_t, α_t, β_t, and then do:

- **Real-time energy management**: Obtain $\{P_t(\hat{\boldsymbol{\lambda}}^t), P_{x,t}(\hat{\boldsymbol{\lambda}}^t)\}$ by solving (3.15). Perform energy transaction with the main grid; that is, buy the energy amount $[P_t(\hat{\boldsymbol{\lambda}}^t) - E_t]^+$ with price α_t upon energy deficit, or, sell the energy amount $[P_t(\hat{\boldsymbol{\lambda}}^t) - E_t]^-$ with price β_t upon energy surplus. Charge (or discharge) the battery with the amount $P_{b,t} = P_t(\hat{\boldsymbol{\lambda}}^t) - P_{x,t}(\hat{\boldsymbol{\lambda}}^t) - P_c$.

- **Real-time broadcast schedule**: Given the transmit-power $P_{x,t}(\hat{\boldsymbol{\lambda}}^t)$ at the BS, solve the convex problem (3.8) to obtain the optimal "dual" MAC transmit-covariance matrices $\{\boldsymbol{Q}_k(P_{x,t}(\hat{\boldsymbol{\lambda}}^t)), \forall k\}$. With π being the permutation of user indices $\{1, \ldots, K\}$

such that $w_{\pi(1)} \geq \cdots \geq w_{\pi(K)}$, define for $k = 1, \ldots, K$,

$$\boldsymbol{A}_k := \boldsymbol{I} + \boldsymbol{H}_{\pi(k)} \left(\sum_{u=1}^{k-1} \boldsymbol{\Gamma}_{\pi(u),t-1} \right) \boldsymbol{H}_{\pi(k)}^{\dagger},$$

$$\boldsymbol{B}_k := \boldsymbol{I} + \sum_{u=k+1}^{K} \left(\boldsymbol{H}_{\pi(u)}^{\dagger} \boldsymbol{Q}_{\pi(u)}(P_{x,t}(\hat{\boldsymbol{\lambda}}^t)) \boldsymbol{H}_{\pi(u)} \right).$$

Using $\boldsymbol{A}_k$ and $\boldsymbol{B}_k$, find the optimal transmit covariance matrices: $k = 1, \ldots, K$,

$$\boldsymbol{\Gamma}_{\pi(k),t} = \boldsymbol{B}_k^{-\frac{1}{2}} \boldsymbol{F}_k \boldsymbol{G}_k^{\dagger} \boldsymbol{A}_k^{\frac{1}{2}} \boldsymbol{Q}_{\pi(k)}(P_{x,t}(\hat{\boldsymbol{\lambda}}^t)) \boldsymbol{A}_k^{\frac{1}{2}} \boldsymbol{G}_k \boldsymbol{F}_k^{\dagger} \boldsymbol{B}_k^{-\frac{1}{2}}$$

where the matrices $\boldsymbol{F}_k$ and $\boldsymbol{G}_k$ could be obtained by singular value decomposition (SVD) of the effective channel $\boldsymbol{H}_{\pi(k)}$: $\boldsymbol{B}_k^{-\frac{1}{2}} \boldsymbol{H}_{\pi(k)}^{\dagger} \boldsymbol{A}_k^{-\frac{1}{2}} = \boldsymbol{F}_k \boldsymbol{S} \boldsymbol{G}_k^{\dagger}$ with a square and diagonal matrix $\boldsymbol{S}$ [94].[2] Perform MIMO broadcast with the transmit covariance matrix $\boldsymbol{\Gamma}_{k,t}$ per user k.

- **Lagrange multipliers updates**: With $P_t(\hat{\boldsymbol{\lambda}}^t)$, $P_{x,t}(\hat{\boldsymbol{\lambda}}^t)$ available, update Lagrange multipliers $\hat{\boldsymbol{\lambda}}^{t+1}$ via (3.16).

3.3.4 Performance Guarantees

Next, we will rigorously establish that the proposed algorithm asymptotically yields a feasible and optimal solution of (3.6) under proper initialization of $\hat{\boldsymbol{\lambda}}^0$. To this end, we first establish the asymptotic optimality of the proposed SGOC algorithm in the following sense.

Lemma 4. *If $\{\mathcal{H}_t, E_t, \alpha_t, \beta_t\}$ are i.i.d. over slots, then the time-averaging throughput under the proposed SGOC algorithm satisfies*

$$\lim_{T \to \infty} \frac{1}{T} \sum_{t=0}^{T-1} \mathbb{E}[R_t(P_{x,t}(\hat{\boldsymbol{\lambda}}^t))] \geq R^* - \mu M$$

[2]Note that $\boldsymbol{\Gamma}_{\pi(1),t} = \boldsymbol{B}_1^{-\frac{1}{2}} \boldsymbol{F}_1 \boldsymbol{G}_1^{\dagger} \boldsymbol{Q}_{\pi(1)}(P_{x,t}(\hat{\boldsymbol{\lambda}}^t)) \boldsymbol{G}_1 \boldsymbol{F}_1^{\dagger} \boldsymbol{B}_1^{-\frac{1}{2}}$, which only requires knowledge of $\boldsymbol{Q}_k(P_{x,t}(\hat{\boldsymbol{\lambda}}^t))$, $\forall k$. When calculating $\boldsymbol{\Gamma}_{\pi(k),t}$, $k > 1$, we need $\boldsymbol{A}_k$ whose calculation requires knowledge of previously obtained $\{\boldsymbol{\Gamma}_{\pi(u),t}\}_{u=1}^{k-1}$. In such a sequential way, all $\boldsymbol{\Gamma}_{k,t}$ can be determined.

where the constant is given by

$$M := \frac{1}{2}\Big[(\max\{P_b^{\max}, -P_b^{\min}\})^2 + (G^{\max})^2 + (\max\{\alpha^{\max}(P_g^{\max} + P_b^{\max}), \beta^{\max}(E^{\max} - P_b^{\min})\})^2\Big] \tag{3.17}$$

and R^* is the optimal value of (3.9), or, equivalently, (3.6), under any feasible control algorithm, even if that relies on knowing future random realizations.

Proof. See Appendix A.0.4. □

Lemma 4 asserts that the proposed SGOC algorithm converges to a region with optimality gap smaller than μM, which vanishes as the stepsize $\mu \to 0$. The proof mimics the lines of the Lyapunov optimization technique in e.g., [91]. Yet, slightly different from [91], here the Lagrange dual theory is utilized to simplify the arguments.

We have shown that the SGOC iteration can achieve a near-optimal objective value for (3.9). However, since the proposed algorithm is based on a solver for the relaxed (3.10), it is not guaranteed that the resultant dynamic control policy is a feasible one for (3.9). In the sequel, we will establish that the SGOC in fact can yield a feasible policy for (3.9), when it is properly initialized.

Since $R_t(P_{x,t})$ is strictly concave and increasing per Lemma 3, it has left and right derivatives at any $P_{x,t}$, and the left derivative is no less than the right one. Let $R_t'(P_{x,t})$ be the left (or right) derivative of $R_t(P_{x,t})$. Clearly, $R_t'(P_{x,t}) \geq 0$ is strictly decreasing in $P_{x,t}$. Let $R'(0) := \max\{R_t'(0), \forall t\}$, and assume $R'(0) < \infty$ (this holds when $\boldsymbol{H}_{k,t}$, $\forall k, t$, have bounded maximum eigenvalues). We can show that:

Lemma 5. *The BS transmit-powers $P_{x,t}$ under the SGOC algorithm satisfy: $P_{x,t}(\hat{\boldsymbol{\lambda}}^t) = 0$, if $\hat{\lambda}_1^t > \frac{R_t'(0)}{\beta_t}$. In addition, the battery (dis-)charging amounts $P_{b,t}$ under the SGOC obey: i) $P_{b,t}(\hat{\boldsymbol{\lambda}}^t) = P_b^{\min}$, if $\hat{\lambda}_2^t > -\hat{\lambda}_1^t \beta_t$; and ii) $P_{b,t}(\hat{\boldsymbol{\lambda}}^t) = P_b^{\max}$, if $\hat{\lambda}_2^t < -\hat{\lambda}_1^t \alpha_t$.*

Proof. See Appendix A.0.5. □

Lemma 5 reveals partial characteristics of the dynamic SGOC policy. Such a structure can be justified by the economic interpretation of the Lagrange multipliers. Specifically, $\hat{\lambda}_1^t$ and $\hat{\lambda}_2^t$ can be viewed as the stochastic instantaneous power and charging prices, respectively. When the power price $\hat{\lambda}_1^t$ is high, zero transmit-power is adopted at the BS, i.e., $P_{x,t}(\hat{\boldsymbol{\lambda}}^t) = 0$. For high charging prices $\hat{\lambda}_2^t > -\hat{\lambda}_1^t \beta_t$, the SGOC dictates the full discharge $P_{b,t}(\hat{\boldsymbol{\lambda}}^t) = P_b^{\min}$. Conversely, the battery units can afford full charge if the charging price is low; i.e., $\hat{\lambda}_2^t < -\hat{\lambda}_1^t \alpha_t$. Note that here, whether the charging price $\hat{\lambda}_2^t$ is high or low, depends also on the power price $\hat{\lambda}_1^t$.

Based on the structure revealed by Lemma 5, we can first establish the following lemma.

Lemma 6. *If* $\alpha^{\max}(P_c + P_b^{\max}) \leq G^{\max}$*, then the SGOC guarantees:* $0 \leq \hat{\lambda}_1^t \leq \frac{R'(0)}{\beta^{\min}} + \max\{0, \mu(\alpha^{\max}(P_g^{\max} + P_b^{\max}) - G^{\max})\}$*,* $\forall t$*.*

Proof. See Appendix A.0.6. □

Note that $\alpha^{\max}(P_c + P_b^{\max}) \leq G^{\max}$ is in fact a mild condition, which implies that the BS has a (minimum) power budget to support its normal operation and full battery charge at any time. Use short-hand notation $\delta_{\lambda_1} := \max\{0, \alpha^{\max}(P_g^{\max} + P_b^{\max}) - G^{\max}\}$. Leveraging the bounds in Lemma 6 and the structure in Lemma 5, we can subsequently establish that:

Lemma 7. *If the stepsize satisfies* $\mu \geq \underline{\mu}$*, where*

$$\underline{\mu} := \frac{\alpha^{\max} R'(0)}{\beta^{\min}(C^{\max} - C^{\min} + P_b^{\min} - P_b^{\max} - \delta_{\lambda_1})} \tag{3.18}$$

then the SGOC guarantees the Lagrange multiplier $\hat{\lambda}_2^t \in [-\alpha^{\max}(\frac{R'(0)}{\beta^{\min}} + \mu\delta_{\lambda_1}) + \mu P_b^{\min}, \mu C^{\max} - \mu C^{\min} - \alpha^{\max}(\frac{R'(0)}{\beta^{\min}} + \mu\delta_{\lambda_1}) + \mu P_b^{\min}]$*,* $\forall t$*.*

Proof. See Appendix A.0.7. □

Consider now the linear mapping

$$C_t = \frac{\hat{\lambda}_2^t}{\mu} + \frac{\alpha^{\max} R'(0)}{\mu \beta^{\min}} + \alpha^{\max} \delta_{\lambda_1} + C^{\min} - P_b^{\min}. \tag{3.19}$$

It can be readily inferred from Lemma 7 that $C^{\min} \leq C_t \leq C^{\max}$ holds, $\forall t$; i.e, (3.9f) is always satisfied under the SGOC. With the battery (dis-)charging dynamics (3.9e) naturally performed, it follows that the proposed SGOC scheme yields a feasible dynamic control policy for the problem (3.9).

Remark 1. *From (3.19), the Lagrange multiplier $\hat{\lambda}_2^t$ can be regarded as a scaled version of the "perturbed" energy queue-size C_t (i.e., $\hat{\lambda}_2^t$ equals C_t after subtracting a constant $(\alpha^{\max}/\mu\beta^{\min})R'(0) + \alpha^{\max}\delta_{\lambda_1} + C^{\min} - P_b^{\min}$, and then multiplying by a scalar μ). Hence, $\hat{\lambda}_2^t$ can be treated as a "virtual" queue, and likewise for $\hat{\lambda}_1^t$. Different from [71] and [73], where the "virtual" queues evolve independently, the evolution of $\hat{\lambda}_2^t$ in (3.16) clearly depends on the value of $\hat{\lambda}_1^t$, and vice-versa; e.g., $\{P_t(\hat{\boldsymbol{\lambda}}^t), P_{x,t}(\hat{\boldsymbol{\lambda}}^t)\}$ are actually functions of $\hat{\boldsymbol{\lambda}}^t := \{\hat{\lambda}_1^t, \hat{\lambda}_2^t\}$, and $P_{b,t}(\hat{\boldsymbol{\lambda}}^t)$ is characterized by the joint relationship among $\hat{\lambda}_1^t, \hat{\lambda}_2^t, \alpha_t, \beta_t$. This is different from a simple threshold-based (dis-)charging profile in [71, Lemma 2] and [73, Lemma 2]. In this sense, the coupling of the "virtual" queues complicates the analysis, and the performance analysis framework in [71, 73] is generalized here to derive additional conditions that ensure feasibility of the proposed algorithm. Specifically, by exploiting the revealed characteristics of our SGOC policy, we first establish bounds for $\hat{\lambda}_1^t$ in Lemma 6. Capitalizing on the specific coupling of the two "queues," we further establish a lower bound on the stepsize $\underline{\mu}$ to ensure the bounds for $\hat{\lambda}_2^t$ in Lemma 7.*

Based on Lemmas 4, 6 and 7, we arrive at the main result.

Theorem 2. *If we set $\hat{\lambda}_1^0 \in [0, \frac{R'(0)}{\beta^{\min}} + \mu\delta_{\lambda_1}]$, and $\hat{\lambda}_2^0 = \mu C_0 - \mu C^{\min} + \mu P_b^{\min} - \alpha^{\max}(\frac{R'(0)}{\beta^{\min}} + \mu\delta_{\lambda_1})$, and select a stepsize $\mu \geq \underline{\mu}$, then the proposed SGOC yields a feasible dynamic*

control scheme for (3.9)*, which is asymptotically optimal in the sense that*

$$\lim_{T\to\infty}\frac{1}{T}\sum_{t=0}^{T-1}\mathbb{E}[R_t(P_{x,t}(\hat{\boldsymbol{\lambda}}^t))]\geq R^*-\mu M$$

where M *and* $\underline{\mu}$ *are given by (3.17) and (3.18), respectively.*

Remark 2. *Choosing* $\mu=\underline{\mu}$*, the minimum optimality gap (regret) between the SGOC, and the offline scheduling is clearly given by* $\underline{\mu}M$*. The asymptotically optimal solution can be attained if the power purchase prices* α_t *are very small, or, the battery capacities* $C^{\max}$ *are large enough, so that* $\underline{\mu}\to 0$*. This makes sense intuitively because when the BS battery has large capacity, the upper bound in (3.9f) is loose. In this case, with proper initialization, the SGOC using any* μ *will be feasible for (3.9), or, (3.6).*

3.4 Numerical Results

In this section, simulations are presented to evaluate our proposed dynamic approach, and justify the analytical claims of Section 3.3.

The considered MIMO downlink has a BS with $N_t=2$ antennas, communicating to $K=10$ mobile users equipped with $N_r=2$ antennas each. The system bandwidth is 1 MHz, and each element in channel coefficient matrix $\boldsymbol{H}_{k,t}$, $\forall k,t$, is a zero-mean complex-Gaussian random variable with unit variance. The duration of a time slot is set to be 1 second. The default parameters are listed in Table 3.1. The energy purchase price α_t is uniformly distributed within [0.1, 1] and the selling price is set as $\beta=r\alpha$ with $r=0.9$. Samples of the harvested energy E_t are generated from a Weibull distributed wind speed using the wind-speed-to-wind-power mapping. An autoregressive model is adopted to capture the possible spatio-temporal correlations as in [99]. Although all the random quantities are assumed i.i.d. in our performance analysis, here the renewable generations are actually generated from the non i.i.d. process in order to better simulate the real-world traces. Finally, the stepsize is chosen as $\mu=\underline{\mu}$ [cf. Theorem 1] by default.

Table 3.1: Parameter Values for the MIMO network. All units are kWh.

Maximum electricity cost $G^{\max}$	15
Maximum energy consumption of BSs $P_g^{\max}$	50
Minimum charging amount of battery $P_b^{\min}$	-5
Maximum charging amount of battery $P_b^{\max}$	5
Minimum energy level of battery $C^{\min}$	0
Maximum energy level of battery $C^{\max}$	50
Initial energy level of battery C_0	0

The proposed SGOC algorithm is compared with two baseline schemes to benchmark its performance. ALG 1 is a "greedy" scheme that maximizes the instantaneous throughput per time slot without leveraging the battery. Specifically, the instantaneous decisions $\{P_t, P_{x,t}\}$ are obtained by solving the convex problem (3.9) per slot t without (dis-)charging, i.e., $P_{b,t} = 0$. The instantaneous throughput maximization and lack of a storage device make ALG 1 myopic, and vulnerable to future high purchase prices. ALG 2 is similar to the proposed one in the sense that it uses the stochastic dual subgradient to iteratively approximate the primal solution. Yet, neither renewable energy nor battery is taken into account, and only one-way trading mechanism is adopted between the BS and grid market implying that all consumed energy are bought from grid with no energy sold in the energy surplus case.

Fig. 3.2 compares the average throughputs of the proposed algorithm and ALGs 1-2 over time slots. It is observed that within 300 time slots, the proposed approach converges to the largest throughput, while ALGs 1-2 incur about 3.0% and 13.3% smaller throughputs. Intuitively speaking, this is because the proposed algorithm intelligently leverages the renewable energy and energy storage device to hedge against future losses, which cannot be fully exploited by ALGs 1-2.

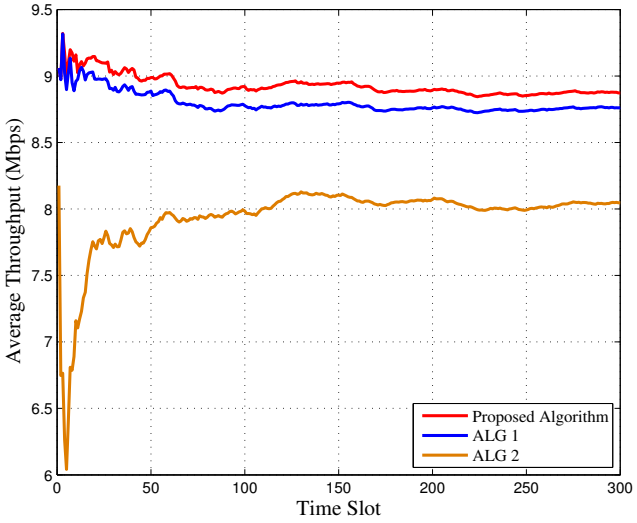

Figure 3.2: Comparison of average throughput.

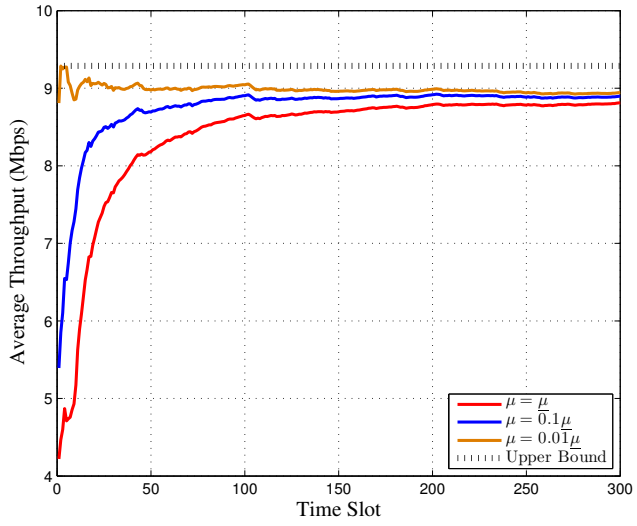

Figure 3.3: Average throughput versus stepsize μ.

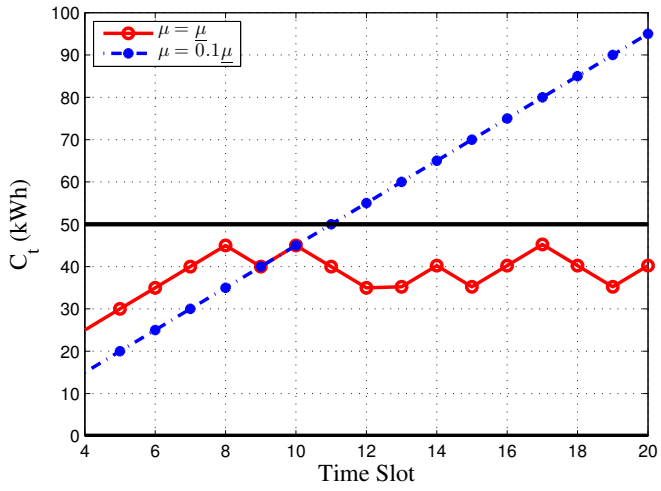

Figure 3.4: The battery state-of-charge C_t versus stepsize μ, where $P_g^{\max} = 10$ kWh.

Fig. 3.3 validates the impact of the stepsize μ on the average throughput of the proposed algorithm. The average throughput is compared under different $\mu = \{0.01\underline{\mu}, 0.1\underline{\mu}, \underline{\mu}\}$. The dotted upper bound is obtained in the case where $P_{x,t} = P_g^{\max} - P_c$ for all time slots t without considering the maximum budget $G^{\max}$. It is shown that the proposed algorithm always converges to a value lower than the upper bound with different stepsize μ. However, it approaches the upper bound with a smaller stepsize. Specifically, when $\mu = 0.01\underline{\mu}$, the proposed algorithm obtains an average throughput only 3.2% lower than the upper bound, which is consistent with Lemma 4 in a way that the optimality gap is proportional to the stepsize μ.

However, as stated in Lemma 7, the value of stepsize μ can significantly affect feasibility of the proposed online scheme. Fig. 3.4 illustrates the evolution of battery SoC C_t with different $\mu = \{0.1\underline{\mu}, \underline{\mu}\}$. It reveals that C_t is always within the prescribed bounds (i.e., $C^{\min} \leq C_t \leq C^{\max}$) when $\mu = \underline{\mu}$. In contrast, if a smaller stepsize $\mu = 0.1\underline{\mu}$ is chosen, C_t will violate its physical upper bound frequently.

In Fig. 3.5, $-\hat{\lambda}_1^t \alpha_t$, $-\hat{\lambda}_1^t \beta_t$, $\hat{\lambda}_2^t$ as well as $P_{b,t}$ are jointly depicted to demonstrate the

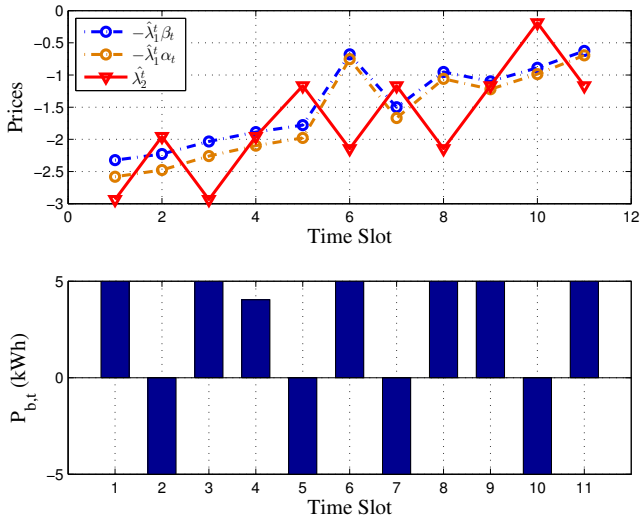

Figure 3.5: SGOC based schedule of battery power $P_{b,t}$, where $P_g^{\max} = 10$ kWh.

(dis-)charging rules revealed by Lemma 5. It can be seen that the SGOC dictates the full discharge $P_{b,t} = P_b^{\min}$ when $\hat{\lambda}_2^t > -\hat{\lambda}_1^t \beta_t$ at $t = 2, 5, 7, 10$, while the battery is fully charged $P_{b,t} = P_b^{\max}$ when $\hat{\lambda}_2^t < -\hat{\lambda}_1^t \alpha_t$ at $t = 1, 3, 6, 8, 11$. In addition, when $\hat{\lambda}_2^t \in [-\hat{\lambda}_1^t \alpha_t, -\hat{\lambda}_1^t \beta_t]$ at $t = 4, 9$, $P_{b,t}$ can only been obtained by solving (16) numerically. Note that the insightful online policy are also applicable for the slots after $t = 11$, and it can be further observed that the Lagrange multiplier $\hat{\lambda}_2^t$ is in fact an affine mapping of the real-time battery SoC C_t [cf. 21].

Fig. 3.6 depicts the optimal power schedule $P_{x,t}$ of the proposed SGOC over time, and the fluctuation of energy purchase prices α_t is also plotted to illustrate the resultant online policy. It can be clearly observed that the power consumption highly depends on the instantaneous energy purchase price α_t. Specifically, the proposed scheme tends to consume more power when α_t is lower (e.g., $t = 2, 12, 24$), and tends to consume less power when α_t is higher (e.g., $t = 3, 14, 15$). In other words, the proposed method allows purchasing more energy from the smart-grid when energy purchase price α_t is lower for economic concern. Fig. 3.6 shows that the transmission-related power $P_{x,t}$ follows the

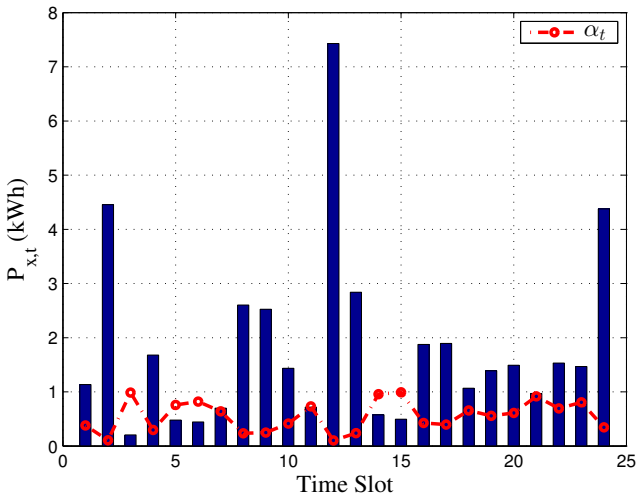

Figure 3.6: SGOC based schedule of transmission-related power $P_{x,t}$.

opposite trend to the price fluctuation.

The average throughputs of the SGOC and ALGs 1-2 are compared with respect to the growth of $G^{\max}$ in Fig. 3.7. Clearly, the throughputs of all three algorithms increase as $G^{\max}$ or $P_g^{\max}$ increases since larger energy cost or looser maximum energy consumption limit will allow more energy purchases from the smart grid and larger energy consumption, leading to the increase of average throughputs. In both cases, we observe that the proposed algorithm performs better than ALGs 1-2. For instance, when $G^{\max} = 10$ and $P_g^{\max} = 50$ kWh, the proposed scheme has 5.0% and 24.3% gains in average throughput over ALGs 1 and 2, respectively. Besides, it turns out that the average throughput of the SGOC approaches the upper bounds when $G^{\max}$ is large or $P_g^{\max}$ is small. Intuitively speaking, with a limited $P_{g,t}$, a large $G^{\max}$ becomes redundant so that the SGOC could always allocate maximal transmission power to increase throughput. We can see that the proposed algorithm converges faster than ALGs 1-2 with a given $P_g^{\max}$, which also means it expects a smaller budget in order to "saturate."

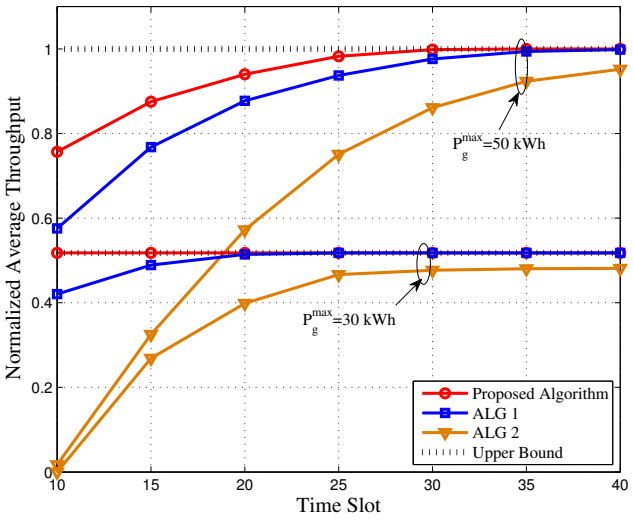

Figure 3.7: Average throughput versus $G^{\max}$.

3.5 Conclusions

In this chapter, real-time resource allocation was developed for smart-grid powered MIMO downlink transmissions. Taking into account the time variations of channels, harvested renewables and electricity prices, a stochastic optimization problem was formulated to maximize the expected throughput while satisfying the energy cost constraints. Relying on the stochastic subgradient method, an online algorithm was developed to obtain feasible decisions 'on-the-fly' by relaxing the time-coupling storage and budget dynamics. It was proven that the novel approach yields feasible and asymptotically optimal resource schedules without knowing any statistics of the underlying stochastic processes. Simulations further corroborated the merits of the proposed scheme in non i.i.d. cases, where the underlying randomness is highly correlated over time. In the guidance of present work, interesting future works include modeling more practical storage units with energy leakage, considering the power network structures, and pursuing the two-timescale energy management and wireless resource allocation mechanism.

Chapter 4

Smart-grid powered CoMP communications

4.1 Introduction

Interference is a major obstacle in wireless communication systems due to their broadcast nature, and becomes more severe in next-generation spectrum- and energy-constrained cellular networks with smaller cells and more flexible frequency reuse [100]. With ever increasing demand for energy-efficient transmissions, coordinated multi-point processing (CoMP) has been proposed as a promising paradigm for efficient inter-cell interference management in heterogeneous networks (HetNets) [101]. In CoMP systems, base stations (BSs) are partitioned into clusters, where BSs per cluster perform coordinated beamforming to serve the users [102–104]. The BSs in the same cluster share channel information and users' information at the same time, and perform joint pre-processing on users' data to reduce the interference between BSs. As the number of BSs in HetNets increases, their electricity consumption constitutes a major part of their operational expenditure, and contributes a considerable portion to the global *carbon footprint* [105]. Fortunately,

emerging characteristics of smart grids offer ample opportunities to achieve both energy-efficient and environmentally-friendly communication solutions. Such characteristics include high penetration of renewable energy sources (RES), two-way energy trading, and dynamic pricing based demand-side management (DSM) [89, 90, 106]. In this context, energy-efficient "green" communication solutions have been proposed for their economic and ecological merits [102–105]. Driven by the need of sustainable "green communications," manufacturers and network operators such as Ericsson, Huawei, Vodafone and China Mobile have started developing "green" BSs that can be jointly supplied by the persistent power sources from the main electric grid as well as from harvested renewable energy sources (e.g., solar and wind) [107, 108]. It is expected that renewable powered BSs will be widely deployed to support future-generation cellular systems.

In the present chapter, we develop a two-scale online control (TS-OC) approach for smart-grid powered CoMP systems considering RES, dynamic pricing, two-way energy trading facilities and imperfect energy storage devices. Suppose that the RES harvesting occurs at the BSs over a slow timescale relative to the coherence time of wireless channels. The proposed scheme performs an ahead-of-time (e.g., 15-minute ahead, or, hour-ahead) energy planning upon RES arrivals, while deciding real-time energy balancing and transmit-beamforming schedules per channel coherence time slot. Specifically, the TS-OC determines the amount of energy to trade (purchase or sell) with the ahead-of-time wholesale market based on RES generation, as the basic energy supply for all the time slots within a RES harvesting interval. On the other hand, it decides the amount of energy to trade with the real-time market, energy charging to (or discharging from) the batteries, as well as the coordinated transmit-beamformers to guarantee the users' quality of service (QoS) per time slot. Generalizing the Lyapunov optimization techniques in [76–79, 109], we propose a synergetic framework to design and analyze such a two-scale dynamic management scheme to minimize the long-term time-averaged energy transac-

tion cost of the CoMP transmissions, without knowing the distributions of the random channel, RES, and energy price processes.

The rest of the chapter is organized as follows. The system models are described in Section 4.2. The proposed dynamic resource management scheme is developed in Section 4.3. Performance analysis is the subject of Section 4.4. Numerical tests are provided in Section 4.5, followed by concluding remarks in Section 4.6.

4.2 System Models

Consider a cluster-based CoMP downlink setup, where a set $\mathcal{I} := \{1, \ldots, I\}$ of distributed BSs (e.g., macro/micro/pico BSs) is selected to serve a set $\mathcal{K} := \{1, \ldots, K\}$ of mobile users, as in e.g., [70, 71]. Each BS is equipped with $M \geq 1$ transmit antennas, whereas each user has a single receive antenna. Suppose that through the smart-grid infrastructure conventional power generation is available, but each BS can also harvest RES (through e.g., solar panels and/or wind turbines), and it has an energy storage device (i.e., battery) to save the harvested energy. Relying on a two-way energy trading facility, the BS can also buy energy from or sell energy to the main grid at dynamically changing market prices. For the CoMP cluster, there is a low-latency backhaul network connecting the set of BSs to a central controller [103], which coordinates energy trading as well as cooperative communication. This central entity can collect both communication data (transmit messages, channel state information) from each BS through the cellular backhaul links, as well as the energy information (energy purchase/selling prices, energy queue sizes) via smart meters installed at BSs, and the grid-deployed communication/control links connecting them.[1]

[1]Perfect channel state information will be assumed hereafter, but the proposed formulation can readily account for the channel estimation errors to robustify the beamforming design; see e.g., [70, 71]. In addition, generalizations are possible to incorporate imperfect energy queue information based on the Lyapunov optimization framework in [77]. Although their detailed study falls outside the present work's

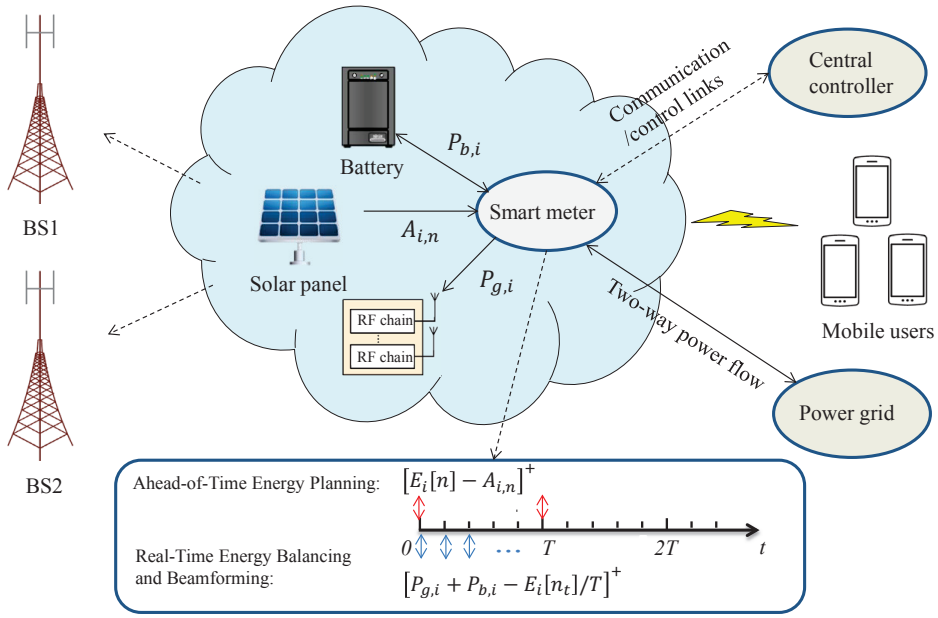

Figure 4.1: A smart grid powered CoMP system. Two BSs with local renewable energy harvesting and storage devices implement two-way energy trading with the main grid.

As the RES and wireless channel dynamics emerge typically at different time scales in practice, we propose a two-scale control mechanism. As shown in Fig. 4.1, time is divided in slots of length smaller than the coherence time of the wireless channels. For convenience, the slot duration is normalized to unity; thus, the terms "energy" and "power" can be used interchangeably. On the other hand, we define the (virtual) "coarse-grained" time intervals in accordance with the slow RES harvesting scale, with each coarse-grained interval consisting of T time slots.

4.2.1 Ahead-of-Time Energy Planning

At the beginning of each "coarse-grained" interval, namely at time $t = nT$, $n = 1, 2, \ldots$, let $A_{i,n}$ denote the RES amount collected per BS $i \in \mathcal{I}$, and $\boldsymbol{A}_n := [A_{1,n}, \ldots, A_{I,n}]'$. With $\boldsymbol{A}_n$ available, an energy planner at the central unity decides the energy amounts $E_i[n]$, $\forall i$,

scope, such imperfections are not expected to substantially affect the effectiveness of the proposed scheme.

to be used in the next T slots per BS i. With a two-way energy trading facility, the BSs then either purchase energy from the main grid according to their shortage, or sell their surplus energy to the grid at a fair price in order to reduce operational costs. Specifically, following the decision, BS i contributes its RES amount $A_{i,n}$ to the main grid and requests the grid to supply an average energy amount of $E_i[n]/T$ per slot $t = nT, \ldots, (n+1)T-1$.

RES is assumed harvested for free after deployment. Given the requested energy $E_i[n]$ and the harvested energy $A_{i,n}$, the shortage energy that is purchased from the grid for BS i is clearly $[E_i[n] - A_{i,n}]^+$; or, the surplus energy that is sold to the grid is $[A_{i,n} - E_i[n]]^+$, where $[a]^+ := \max\{a, 0\}$. Depending on the difference $(E_i[n] - A_{i,n})$, the BS i either buys electricity from the grid with the ahead-of-time (i.e., long-term) price α_n^{lt}, or sells electricity to the grid with price β_n^{lt} for profit (the latter leads to a negative cost). Notwithstanding, we shall always set $\alpha_n^{\text{lt}} > \beta_n^{\text{lt}}$ to avoid meaningless buy-and-sell activities of the BSs for profit. The transaction cost with BS i for such an energy planning is therefore given by

$$G^{\text{lt}}(E_i[n]) := \alpha_n^{\text{lt}}[E_i[n] - A_{i,n}]^+ - \beta_n^{\text{lt}}[A_{i,n} - E_i[n]]^+. \tag{4.1}$$

For conciseness, we concatenate into a single random vector all the random variables evolving at this slow timescale; i.e., $\boldsymbol{\xi}_n^{\text{lt}} := \{\alpha_n^{\text{lt}}, \beta_n^{\text{lt}}, \mathbf{A}_n, \forall n\}$.

4.2.2 CoMP Downlink Transmissions

Per slot t, let $\mathbf{h}_{ik,t} \in \mathbb{C}^M$ denote the vector channel from BS i to user k, $\forall i \in \mathcal{I}$, $\forall k \in \mathcal{K}$; let $\mathbf{h}_{k,t} := [\mathbf{h}'_{1k,t}, \ldots, \mathbf{h}'_{Ik,t}]'$ collect the channel vectors from all BSs to user k, and $\mathbf{H}_t := [\mathbf{h}_{1,t}. \ldots, \mathbf{h}_{K,t}]$. With linear transmit beamforming performed across BSs, the vector signal transmitted to user k is: $\mathbf{q}_k(t) = \mathbf{w}_k(t)s_k(t)$, $\forall k$, where $s_k(t)$ denotes the information-bearing scalar symbol with unit-energy, and $\mathbf{w}_k(t) \in \mathbb{C}^{MI}$ denotes the beamforming vector

across the BSs serving user k. The received vector at slot t for user k is therefore

$$y_k(t) = \mathbf{h}_{k,t}^H \mathbf{q}_k(t) + \sum_{l \neq k} \mathbf{h}_{k,t}^H \mathbf{q}_l(t) + n_k(t) \tag{4.2}$$

where $\mathbf{h}_{k,t}^H \mathbf{q}_k(t)$ is the desired signal of user k, $\sum_{l \neq k} \mathbf{h}_{k,t}^H \mathbf{q}_l(t)$ is the inter-user interference from the same cluster, and $n_k(t)$ denotes additive noise, which may also include the downlink interference from other BSs outside user k's cluster. It is assumed that $n_k(t)$ is a circularly symmetric complex Gaussian (CSCG) random variable with zero mean and variance σ_k^2.

The signal-to-interference-plus-noise ratio (SINR) at user k can be expressed as

$$\mathrm{SINR}_k(\{\mathbf{w}_k(t)\}) = \frac{|\mathbf{h}_{k,t}^H \mathbf{w}_k(t)|^2}{\sum_{l \neq k}(|\mathbf{h}_{k,t}^H \mathbf{w}_l(t)|^2) + \sigma_k^2} \ . \tag{4.3}$$

The transmit power at each BS i clearly is given by

$$P_{x,i}(t) = \sum_{k \in \mathcal{K}} \mathbf{w}_k^H(t) \mathbf{B}_i \mathbf{w}_k(t) \tag{4.4}$$

where the matrix

$$\mathbf{B}_i := \mathrm{diag}\left(\underbrace{0, \ldots, 0}_{(i-1)M}, \underbrace{1, \ldots, 1}_{M}, \underbrace{0, \ldots, 0}_{(I-i)M} \right) \in \mathbb{R}^{MI \times MI}$$

selects the corresponding rows out of $\{\mathbf{w}_k(t)\}_{k \in \mathcal{K}}$ to form the i-th BS's transmit-beamforming vector of size $M \times 1$.

To guarantee QoS per slot user k, it is required that the central controller selects a set of $\{\mathbf{w}_k(t)\}$ satisfying [cf. (4.3)]

$$\mathrm{SINR}_k(\{\mathbf{w}_k(t)\}) \geq \gamma_k, \quad \forall k \tag{4.5}$$

where γ_k denotes the target SINR value per user k.

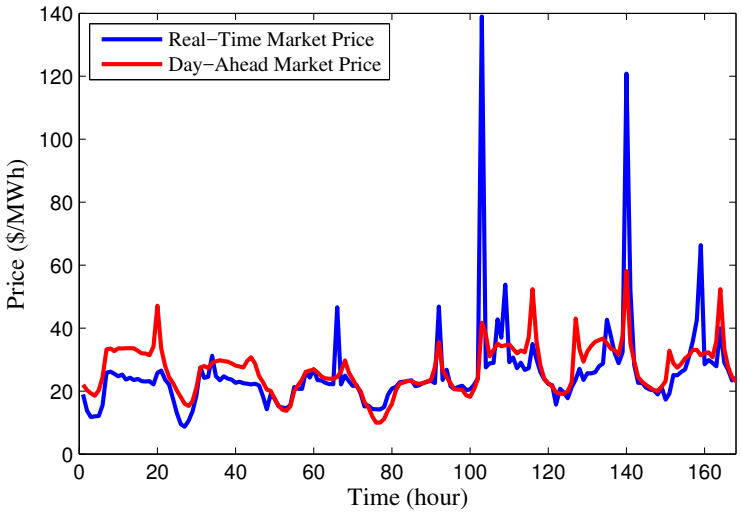

Figure 4.2: Hourly price trend for day-ahead and real-time electricity markets during Oct. 01-07, 2015 [6].

4.2.3 Real-Time Energy Balancing

For the i-th BS, the total energy consumption $P_{g,i}(t)$ per slot t includes the transmission-related power $P_{x,i}(t)$, and the rest that is due to other components such as air conditioning, data processor, and circuits, which can be generally modeled as a constant power, $P_c > 0$ [37]. We further suppose that $P_{g,i}(t)$ is bounded by $P_g^{\max}$. Namely,

$$P_{g,i}(t) = P_c + \sum_{k\in\mathcal{K}} \mathbf{w}_k^H(t)\mathbf{B}_i\mathbf{w}_k(t) \le P_g^{\max}, \quad \forall i. \tag{4.6}$$

Per slot t, the energy supply available from the ahead-of-time planning may not exactly meet the actual demand at BS i. Hence, the BS i is also allowed to perform real-time energy trading with the main grid to balance its supply with demand. Let $P_i(t)$ denote the real-time energy amount that is purchased from ($P_i(t) > 0$) or sold to ($P_i(t) < 0$) the grid by BS i. Let α_t^{rt} and β_t^{rt} ($\alpha_t^{\mathrm{rt}} > \beta_t^{\mathrm{rt}}$) denote the real-time energy purchase and selling prices, respectively. Then the real-time energy transaction cost for BS i is

$$G^{\mathrm{rt}}(P_i(t)) := \alpha_t^{\mathrm{rt}}[P_i(t)]^+ - \beta_t^{\mathrm{rt}}[-P_i(t)]^+. \tag{4.7}$$

Fig. 4.2 depicts the day-ahead and real-time energy prices in the Pennsylvania-Jersey-Maryland (PJM) wholesale market [6]. In practice, the average purchase price in the real-time market tends to be no lower than that in the day-ahead market; that is, $\mathbb{E}\{\alpha_t^{\rm rt}\} \geq \mathbb{E}\{\alpha_n^{\rm lt}\}$; similarly, we have $\mathbb{E}\{\beta_t^{\rm rt}\} \leq \mathbb{E}\{\beta_n^{\rm lt}\}$. Again, we use a random vector $\boldsymbol{\xi}_t^{\rm rt} := \{\alpha_t^{\rm rt}, \beta_t^{\rm rt}, \mathbf{H}_t, \forall t\}$ to collect all random variables evolving at the fast timescale.

4.2.4 Energy Storage with Degeneration

As energy consumption will become a major concern of the future large-scale cellular networks, uninterrupted power supply type storage units can be installed at the BSs to prevent power outages, and provide opportunities to optimize the BSs' electricity bills. Different from the ideal battery models in [37,69–71,77], we consider here a practical battery with degeneration (i.e., energy leakage over time even in the absence of discharging) as in [109].

For the battery of the i-th BS, let $C_i(0)$ denote the initial amount of stored energy, and $C_i(t)$ its state of charge (SoC) at the beginning of time slot t. The battery is assumed to have a finite capacity $C^{\max}$. Furthermore, for reliability purposes, it might be required to ensure that a minimum energy level $C^{\min}$ is maintained at all times. Let $P_{b,i}(t)$ denote the energy delivered to or drawn from the battery at slot t, which amounts to either charging ($P_{b,i}(t) > 0$) or discharging ($P_{b,i}(t) < 0$). The stored energy then obeys the dynamic equation

$$C_i(t+1) = \eta C_i(t) + P_{b,i}(t),\ C^{\min} \leq C_i(t) \leq C^{\max},\ \forall i \tag{4.8}$$

where $\eta \in (0, 1]$ denotes the storage efficiency (e.g., $\eta = 0.9$ means that 10% of the stored energy will be "leaked" over a slot, even in the absence of discharging).

The amount of power (dis)charged is also assumed bounded by

$$P_b^{\min} \leq P_{b,i}(t) \leq P_b^{\max}, \quad \forall i \tag{4.9}$$

where $P_b^{\min} < 0$ and $P_b^{\max} > 0$ are introduced by physical constraints.

With $n_t := \lfloor \frac{t}{T} \rfloor$ and consideration of $P_{b,i}(t)$, we have the following demand-and-supply balance equation per slot t:

$$P_c + \sum_{k \in \mathcal{K}} \mathbf{w}_k^H(t) \mathbf{B}_i \mathbf{w}_k(t) + P_{b,i}(t) = \frac{E_i[n_t]}{T} + P_i(t), \ \forall i. \tag{4.10}$$

4.3 Dynamic Resource Management Scheme

Note that the harvested RES amounts $\{\boldsymbol{A}_n, \forall n\}$, the ahead-of-time prices $\{\alpha_n^{\mathrm{lt}}, \beta_n^{\mathrm{lt}}, \forall n\}$, the real-time prices $\{\alpha_t^{\mathrm{rt}}, \beta_t^{\mathrm{rt}}, \forall t\}$, and the wireless channel matrices $\{\mathbf{H}_t, \forall t\}$ are all random. The smart-grid powered CoMP downlink to be controlled is a stochastic system. The goal is to design an online resource management scheme that chooses the ahead-of-time energy-trading amounts $\{E_i[n], \forall i\}$ at every $t = nT$, as well as the real-time energy-trading amounts $\{P_i(t), \forall i\}$, battery (dis)charging amounts $\{P_{b,i}(t), \forall i\}$, and the CoMP beamforming vectors $\{\mathbf{w}_k(t), \forall k\}$ per slot t, so as to minimize the expected total energy transaction cost, without knowing the distributions of the aforementioned random processes.

According to (4.1) and (4.7), define the energy transaction cost for BS i per slot t as:

$$\Phi_i(t) := \frac{1}{T} G^{\mathrm{lt}}(E_i[n_t]) + G^{\mathrm{rt}}(P_i(t)). \tag{4.11}$$

Let $\mathcal{X} := \{E_i[n], \forall i, n; P_i(t), P_{b,i}(t), C_i(t), \forall i, t; \mathbf{w}_k(t), \forall k, t\}$. The problem of interest is to find

$$\begin{aligned} \Phi^{opt} := \min_{\mathcal{X}} \ \lim_{N \to \infty} \frac{1}{NT} \sum_{t=0}^{NT-1} \sum_{i \in \mathcal{I}} \mathbb{E}\{\Phi_i(t)\} \\ \text{subject to} \quad (4.5), (4.6), (4.8), (4.9), (4.10), \quad \forall t \end{aligned} \tag{4.12}$$

where the expectations of $\Phi_i(t)$ are taken over all sources of randomness. Note that here the constraints (4.5), (4.6), (4.8), (4.9), and (4.10) are implicitly required to hold for every realization of the underlying random states $\boldsymbol{\xi}_t^{\mathrm{rt}}$ and $\boldsymbol{\xi}_n^{\mathrm{lt}}$.

4.3.1 Two-Scale Online Control Algorithm

(4.12) is a stochastic optimization task. We next generalize and integrate the Lyapunov optimization techniques in [76–79, 109] to develop a TS-OC algorithm, which will be proven feasible, and asymptotically near-optimal for (4.12). To start, assume the following two relatively mild conditions for the system parameters:

$$P_b^{\max} \geq (1-\eta)C^{\min} \tag{4.13}$$

$$C^{\max} - C^{\min} \geq \frac{1-\eta^T}{1-\eta}(P_b^{\max} - P_b^{\min}). \tag{4.14}$$

Condition (4.13) simply implies that the energy leakage of the battery can be compensated by the charging. Condition (4.14) requires that the allowable SoC range is large enough to accommodate the largest possible charging/discharging over T time slots of each coarse-grained interval. This then makes the system "controllable" by our two-scale mechanism.

Our algorithm depends on two parameters, namely a "queue perturbation" parameter Γ, and a weight parameter V. Define $\bar{\alpha} := \max\{\alpha_t^{\mathrm{rt}}, \forall t\}$ and $\underline{\beta} := \min\{\beta_t^{\mathrm{rt}}, \forall t\}$. Derived from the feasibility requirement of the proposed algorithm (see the proof of Proposition 1 in the sequel), any pair (Γ, V) that satisfies the following conditions can be used:

$$\Gamma^{\min} \leq \Gamma \leq \Gamma^{\max}, \quad 0 < V \leq V^{\max} \tag{4.15}$$

where

$$\Gamma^{\min} := \max_{\tau=1,\ldots,T} \left\{ \frac{1}{\eta^\tau}\left(\frac{1-\eta^\tau}{1-\eta}P_b^{\max} - C^{\max}\right) - V\underline{\beta} \right\} \tag{4.16}$$

$$\Gamma^{\max} := \min_{\tau=1,\ldots,T} \left\{ \frac{1}{\eta^\tau}\left(\frac{1-\eta^\tau}{1-\eta}P_b^{\min} - C^{\min}\right) - V\bar{\alpha} \right\} \tag{4.17}$$

$$V^{\max} := \min_{\tau=1,\ldots,T} \left\{ \frac{C^{\max} - C^{\min} - \frac{1-\eta^\tau}{1-\eta}(P_b^{\max} - P_b^{\min})}{\eta^\tau(\bar{\alpha} - \underline{\beta})} \right\}. \tag{4.18}$$

Note that the interval for V in (4.15) is well defined under condition (4.14), and the interval for Γ is valid when $V \leq V^{\max}$.

We now present the proposed TS-OC algorithm:

- **Initialization**: Select Γ and V, and introduce a virtual queue $Q_i(0) := C_i(0) + \Gamma$, $\forall i$.

- **Ahead-of-time energy planning**: Per interval $\tau = nT$, observe a realization $\boldsymbol{\xi}_n^{\mathrm{lt}}$, and determine the energy amounts $\{E_i^*[n], \forall i\}$ by solving

$$\min_{\{E_i^*[n]\}} \sum_{i\in\mathcal{I}} \Bigg\{ V\Big[G^{\mathrm{lt}}(E_i[n]) + \sum_{t=\tau}^{\tau+T-1} \mathbb{E}\{G^{\mathrm{rt}}(P_i(t))\}\Big] + \sum_{t=\tau}^{\tau+T-1} Q_i(\tau)\mathbb{E}\{P_{b,i}(t)\} \Bigg\}$$
$$\text{s. t. } (4.5), (4.6), (4.9), (4.10), \quad \forall t = \tau, \ldots, \tau+T-1 \tag{4.19}$$

  where expectations are taken over $\boldsymbol{\xi}_t^{\mathrm{rt}}$. Then the BSs trade energy with the main grid based on $\{E_i^*[n], \forall i\}$, and request the grid to supply an average amount $E_i^*[n]/T$ per slot $t = \tau, \ldots, \tau+T-1$.

- **Energy balancing and beamforming schedule**: At every slot $t \in [nT, (n+1)T-1]$, observe a realization $\boldsymbol{\xi}_t^{\mathrm{rt}}$, and decide $\{P_i^*(t), P_{b,i}^*(t), \forall i; \mathbf{w}_k^*(t), \forall k\}$ by solving the following problem given $E_i[n] = E_i^*[n]$

$$\min_{\{P_i^*(t), P_{b,i}^*(t), \mathbf{w}_k^*(t)\}} \sum_{i\in\mathcal{I}} \big\{ VG^{\mathrm{rt}}(P_i(t)) + Q_i(nT)P_{b,i}(t) \big\}$$
$$\text{s. t.} \quad (4.5), (4.6), (4.9), (4.10). \tag{4.20}$$

  The BSs perform real-time energy trading with the main grid based on $\{P_i^*(t), \forall i\}$, and coordinated beamforming based on $\{\mathbf{w}_k^*(t), \forall k\}$.

- **Queue updates**: Per slot t, charge (or discharge) the battery based on $\{P_{b,i}^*(t)\}$, so that the stored energy $C_i(t+1) = \eta C_i(t) + P_{b,i}^*(t)$, $\forall i$; and update the virtual queues $Q_i(t) := C_i(t) + \Gamma, \forall i$.

Remark 3. *Note that we use queue sizes $Q_i(\tau)$ instead of $Q_i(t)$ in problems (4.19) and (4.20); see also [76, 77]. Recall that the main design principle in Lyapunov optimization is to choose control actions that minimize $\sum_t \sum_i \mathbb{E}\left[V\Phi_i(t) + Q_i(t)P_{b,i}(t)\right]$. For the ahead-of-time energy planning, this requires a-priori knowledge of the future queue backlogs $Q_i(t)$ over slots $[\tau+1, \ldots, \tau+T-1]$ at time $\tau = nT$. It is impractical to assume that this information is available. For this reason, we simply approximate future queue backlog values as the current value at $\tau = nT$, i.e., $Q_i(t) \approx Q_i(\tau)$, $\forall t = \tau+1, \ldots, \tau+T-1$, in (4.19). To ensure that the real-time energy balancing and beamforming schedule solves the same problem as the ahead-of-time energy planning, we also use $Q_i(nT)$ in (4.20) although the real-time battery state of charge $Q_i(t)$ is available at slot t. Rigorous analysis shows that the performance penalty incurred by such an approximation does not affect the asymptotic optimality of the proposed stochastic control scheme. On the other hand, using $Q_i(t)$ in real-time energy balancing can be also suggested in practice. While our feasibility analysis affords such a modification, deriving the optimality gap is left for future research.*

Next, we develop efficient solvers of (4.19) and (4.20) to obtain the TS-OC algorithm.

4.3.2 Real-Time Energy Balancing and Beamforming

It is easy to argue that the objective (4.20) is convex. Indeed, with $\alpha_t^{\mathrm{rt}} > \beta_t^{\mathrm{rt}}$, the transaction cost with $P_i(t)$ can be alternatively written as

$$G^{\mathrm{rt}}(P_i(t)) = \max\{\alpha_t^{\mathrm{rt}} P_i(t),\ \beta_t^{\mathrm{rt}} P_i(t)\} \tag{4.21}$$

which is clearly convex [84]; and so is the objective in (4.20).

The SINR constraints in (4.5) can be actually rewritten into a convex form. Observe that an arbitrary phase rotation can be added to the beamforming vectors $\boldsymbol{w}_k(t)$ without affecting the SINRs. Hence, we can choose a phase so that $\boldsymbol{h}_{k,t}^H \boldsymbol{w}_k(t)$ is real and nonnegative. Then by proper rearrangement, the SINR constraints become convex second-order

cone (SOC) constraints [110]; that is,

$$\sqrt{\sum_{l\neq k}|\boldsymbol{h}_{k,t}^H\boldsymbol{w}_l(t)|^2+\sigma_k^2}\leq\frac{1}{\sqrt{\gamma_k}}\mathrm{Re}\{\boldsymbol{h}_{k,t}^H\boldsymbol{w}_k(t)\},$$

$$\mathrm{Im}\{\boldsymbol{h}_{k,t}^H\boldsymbol{w}_k(t)\}=0,\quad\forall k.$$

We can then rewrite the problem (4.20) as

$$\begin{aligned}\min\ &\sum_{i\in\mathcal{I}}\Big\{VG^{\mathrm{rt}}(P_c+\sum_{k\in\mathcal{K}}\mathbf{w}_k^H(t)\mathbf{B}_i\mathbf{w}_k(t)+P_{b,i}(t)-\frac{E_i^*[n_t]}{T})\\&\qquad+Q_i(n_tT)P_{b,i}(t)\}\Big\}\\\text{s. t. }&\sqrt{\sum_{l\neq k}|\boldsymbol{h}_{k,t}^H\boldsymbol{w}_l(t)|^2+\sigma_k^2}\leq\frac{1}{\sqrt{\gamma_k}}\mathrm{Re}\{\boldsymbol{h}_{k,t}^H\boldsymbol{w}_k(t)\},\\&\mathrm{Im}\{\boldsymbol{h}_{k,t}^H\boldsymbol{w}_k(t)\}=0,\ \forall k\\&P_b^{\min}\leq P_{b,i}(t)\leq P_b^{\max},\ \forall i\\&P_c+\sum_{k\in\mathcal{K}}\mathbf{w}_k^H(t)\mathbf{B}_i\mathbf{w}_k(t)\leq P_g^{\max},\ \forall i.\end{aligned}\tag{4.22}$$

As $G^{\mathrm{rt}}(\cdot)$ is convex and increasing, it is easy to see that $G^{\mathrm{rt}}(P_c+\sum_k\mathbf{w}_k^H(t)\mathbf{B}_i\mathbf{w}_k(t)+P_{b,i}(t)-E_i^*[n_t]/T)$ is jointly convex in $(P_{b,i}(t),\{\mathbf{w}_k(t)\})$ [84, Sec. 3.2.4]. It then readily follows that (4.22) is a convex optimization problem, which can be solved via off-the-shelf solvers.

4.3.3 Ahead-of-Time Energy Planning

To solve (4.19), the probability distribution function (pdf) of the random state $\boldsymbol{\xi}_t^{\mathrm{rt}}$ must be known across slots $t=nT,\ldots,(n+1)T-1$. However, this pdf is seldom available in practice. Suppose that $\boldsymbol{\xi}_t^{\mathrm{rt}}$ is independent and identically distributed (i.i.d.) over time slots, and takes values from a finite state space. It was proposed in [76] to obtain an empirical pdf of $\boldsymbol{\xi}_t^{\mathrm{rt}}$ from past realizations over a large window comprising L intervals. This estimate becomes accurate as L grows sufficiently large; then it can be used to

evaluate the expectations in (4.19). Based on such an empirical pdf, an approximate solution for (4.19) could be obtained.

Different from [76], here we propose a stochastic gradient approach to solve (4.19). Suppose that $\boldsymbol{\xi}_t^{\rm rt}$ is i.i.d. across time slots (but not necessarily with a finite support). For stationary $\boldsymbol{\xi}_t^{\rm rt}$, we can remove the index t from all optimization variables, and rewrite (4.19) as (with short-hand notation $Q_i[n] := Q_i(nT)$)

$$\min \sum_{i\in\mathcal{I}} \Big\{ VG^{\rm lt}(E_i[n]) + T\mathbb{E}\left[VG^{\rm rt}(P_i(\boldsymbol{\xi}_t^{\rm rt})) + Q_i[n]P_{b,i}(\boldsymbol{\xi}_t^{\rm rt})\right]\Big\}$$

$$\text{s. t. } \sqrt{\sum_{l\neq k} |\boldsymbol{h}_k^H \boldsymbol{w}_l(\boldsymbol{\xi}_t^{\rm rt})|^2 + \sigma_k^2} \leq \frac{1}{\sqrt{\gamma_k}} \mathrm{Re}\{\boldsymbol{h}_k^H \boldsymbol{w}_k(\boldsymbol{\xi}_t^{\rm rt})\},$$

$$\mathrm{Im}\{\boldsymbol{h}_k^H \boldsymbol{w}_k(\boldsymbol{\xi}_t^{\rm rt})\} = 0,\ \forall k, \boldsymbol{\xi}_t^{\rm rt} \tag{4.23a}$$

$$P_b^{\min} \leq P_{b,i}(\boldsymbol{\xi}_t^{\rm rt}) \leq P_b^{\max},\ \forall i, \boldsymbol{\xi}_t^{\rm rt} \tag{4.23b}$$

$$P_c + \sum_{k\in\mathcal{K}} \mathbf{w}_k^H(\boldsymbol{\xi}_t^{\rm rt}) \mathbf{B}_i \mathbf{w}_k(\boldsymbol{\xi}_t^{\rm rt}) \leq P_g^{\max},\ \forall i, \boldsymbol{\xi}_t^{\rm rt} \tag{4.23c}$$

$$P_c + \sum_{k\in\mathcal{K}} \mathbf{w}_k^H(\boldsymbol{\xi}_t^{\rm rt}) \mathbf{B}_i \mathbf{w}_k(\boldsymbol{\xi}_t^{\rm rt}) + P_{b,i}(\boldsymbol{\xi}_t^{\rm rt}) = \frac{E_i[n]}{T} + P_i(\boldsymbol{\xi}_t^{\rm rt}), \forall i, \boldsymbol{\xi}_t^{\rm rt}. \tag{4.23d}$$

Note that this form explicitly indicates the dependence of the decision variables $\{P_i, P_{b,i}, \mathbf{w}_k\}$ on the realization of $\boldsymbol{\xi}_t^{\rm rt}$.

Since the energy planning problem (4.19) only determines the optimal ahead-of-time energy purchase $E_i^*[n]$, we can then eliminate the variable P_i and write (4.23) as an unconstrained optimization problem with respect to the variable $E_i^*[n]$, namely

$$\min_{\{E_i[n]\}} \sum_{i\in\mathcal{I}} \Big[VG^{\rm lt}(E_i[n]) + T\bar{G}^{\rm rt}(\{E_i[n]\})\Big] \tag{4.24}$$

where we define

$$\bar{G}^{\rm rt}(\{E_i[n]\}) := \min_{\{P_i, P_{b,i}, \mathbf{w}_k\}} \sum_{i\in\mathcal{I}} \mathbb{E}\Big\{ V\Psi^{\rm rt}(E_i[n], P_{b,i}(\boldsymbol{\xi}_t^{\rm rt}), \{\mathbf{w}_k(\boldsymbol{\xi}_t^{\rm rt})\})$$
$$+ Q_i[n]P_{b,i}(\boldsymbol{\xi}_t^{\rm rt})\Big\} \text{ s. t. (4.23a), (4.23b), (4.23c)} \tag{4.25}$$

with the compact notation $\Psi^{\rm rt}(E_i, P_{b,i}, \{\mathbf{w}_k\}) := G^{\rm rt}(P_c + \sum_{k\in\mathcal{K}} \mathbf{w}_k^H \mathbf{B}_i \mathbf{w}_k + P_{b,i} - \frac{E_i}{T})$. Since $\mathbb{E}[V\Psi^{\rm rt}(E_i[n], P_{b,i}(\boldsymbol{\xi}_t^{\rm rt}), \{\mathbf{w}_k(\boldsymbol{\xi}_t^{\rm rt})\}) + Q_i[n]P_{b,i}(\boldsymbol{\xi}_t^{\rm rt})]$ is jointly convex in $(E_i, P_{b,i}, \{\mathbf{w}_k\})$ [cf.

(4.22)], then the minimization over $(P_{b,i}, \{\mathbf{w}_k\})$ is within a convex set; thus, (4.23a)-(4.23c) is still convex with respect to $E_i[n]$ [84, Sec. 3.2.5]. In addition, due to $\alpha_n^{\mathrm{lt}} > \beta_n^{\mathrm{lt}}$, we can alternatively write $G^{\mathrm{lt}}(E_i[n]) = \max\{\alpha_n^{\mathrm{lt}}(E_i[n] - A_{i,n}), \beta_n^{\mathrm{lt}}(E_i[n] - A_{i,n})\}$, which is in the family of convex functions. Hence, (4.24) is generally a nonsmooth and unconstrained convex problem with respect to $\{E_i[n]\}$, which can be solved using the stochastic subgradient iteration described next.

The subgradient of $G^{\mathrm{lt}}(E_i[n])$ can be first written as

$$\partial G^{\mathrm{lt}}(E_i[n]) = \begin{cases} \alpha_n^{\mathrm{lt}}, & \text{if } E_i[n] > A_{i,n} \\ \beta_n^{\mathrm{lt}}, & \text{if } E_i[n] < A_{i,n} \\ \text{any } x \in [\beta_n^{\mathrm{lt}}, \alpha_n^{\mathrm{lt}}], & \text{if } E_i[n] = A_{i,n}. \end{cases}$$

With $\{P_{b,i}^E(\boldsymbol{\xi}_t^{\mathrm{rt}}), \mathbf{w}_k^E(\boldsymbol{\xi}_t^{\mathrm{rt}})\}$ denoting the optimal solution for the problem in (4.25), the partial subgradient of $\bar{G}^{\mathrm{rt}}(\{E_i[n]\})$ with respect to $E_i[n]$ is $\partial_i \bar{G}^{\mathrm{rt}}(\{E_i[n]\}) = V\mathbb{E}\{\partial\Psi^{\mathrm{rt}}(E_i[n], P_{b,i}^E(\boldsymbol{\xi}_t^{\mathrm{rt}}), \{\mathbf{w}_k^E(\boldsymbol{\xi}_t^{\mathrm{rt}})\})\}$, where

$$\partial\Psi^{\mathrm{rt}}(E_i[n], P_{b,i}^E(\boldsymbol{\xi}_t^{\mathrm{rt}}), \{\mathbf{w}_k^E(\boldsymbol{\xi}_t^{\mathrm{rt}})\}) = \begin{cases} \frac{-\beta_t^{\mathrm{rt}}}{T}, & \text{if } \frac{E_i[n]}{T} > \Delta \\ \frac{-\alpha_t^{\mathrm{rt}}}{T}, & \text{if } \frac{E_i[n]}{T} < \Delta \\ x \in [\frac{-\alpha_t^{\mathrm{rt}}}{T}, \frac{-\beta_t^{\mathrm{rt}}}{T}], & \text{else} \end{cases}$$

with $\Delta := P_c + \sum_k \mathbf{w}_k^{E\,H}(\boldsymbol{\xi}_t^{\mathrm{rt}})\mathbf{B}_i\mathbf{w}_k^E(\boldsymbol{\xi}_t^{\mathrm{rt}}) + P_{b,i}^E(\boldsymbol{\xi}_t^{\mathrm{rt}})$.

Defining $\bar{g}_i(E_i) := V\partial G^{\mathrm{lt}}(E_i) + T\partial_i\bar{G}^{\mathrm{rt}}(\{E_i\})$, a standard sub-gradient descent iteration can be employed to find the optimal $E_i^*[n]$ for (4.24), as

$$E_i^{(j+1)}[n] = [E_i^{(j)}[n] - \mu^{(j)}\bar{g}_i(E_i^{(j)}[n])]^+, \quad \forall i \tag{4.26}$$

where j denotes iteration index, and $\{\mu^{(j)}\}$ is the sequence of stepsizes.

Implementing (4.26) essentially requires performing (high-dimensional) integration over the unknown multivariate distribution function of $\boldsymbol{\xi}_t^{\mathrm{rt}}$ present in $\bar{g}_i$ through $\bar{G}^{\mathrm{rt}}$ in

(4.25). To circumvent this impasse, a stochastic subgradient approach is devised based on the past realizations $\{\boldsymbol{\xi}_\tau^{\rm rt}, \tau = 0, 1, \ldots, nT-1\}$. Per iteration j, we randomly draw a realization $\boldsymbol{\xi}_\tau^{\rm rt}$ from past realizations, and run the following iteration

$$E_i^{(j+1)}[n] = [E_i^{(j)}[n] - \mu^{(j)} g_i(E_i^{(j)}[n])]^+, \quad \forall i \tag{4.27}$$

where $g_i(E_i^{(j)}[n]) := V(\partial G^{\rm lt}(E_i^{(j)}[n]) + T\partial\Psi^{\rm rt}(E_i^{(j)}[n], P_{b,i}^E(\boldsymbol{\xi}_\tau^{\rm rt}), \{\mathbf{w}_k^E(\boldsymbol{\xi}_\tau^{\rm rt})\}))$ with $\{P_{b,i}^E(\boldsymbol{\xi}_\tau^{\rm rt}), \mathbf{w}_k^E(\boldsymbol{\xi}_\tau^{\rm rt})\}$ obtained by solving a convex problem (4.25) with $E_i[n] = E_i^{(j)}[n]$.

As $g_i(E_i^{(j)}[n])$ is indeed an unbiased random realization of $\bar{g}_i(E_i^{(j)}[n]) = \mathbb{E}\{g_i(E_i^{(j)}[n])\}$ [111], if we adopt a sequence of non-summable diminishing stepsizes satisfying $\lim_{j\to\infty} \mu^{(j)} = 0$ and $\sum_{j=0}^{\infty} \mu^{(j)} = \infty$, the iteration (4.27) asymptotically converges to the optimal $\{E_i^*[n], \forall i\}$ as $j \to \infty$ [95].

Compared with [76], the proposed stochastic subgradient method is particularly tailored for our setting, which does not require the random vector $\boldsymbol{\xi}_t^{\rm rt}$ to have discrete and finite support. In addition, as the former essentially belongs to the class of statistical learning based approaches [112], the proposed stochastic method avoids constructing a histogram for learning the underlying multivariate distribution and requires a considerably smaller number of samples to obtain an accurate estimate of $E_i^*[n]$.

Remark 4. *The computational complexity of the proposed algorithm is fairly low. Specifically, for solving the real-time energy balancing and beamforming problem* (4.22) *per slot* t*, the off-the-shelf interior-point solver incurs a worst-case complexity* $\mathcal{O}(I^{3.5}K^{3.5})$ *to obtain the decisions* $\{P_{b,i}^*(t), \forall i; \mathbf{w}_k^*(t), \forall k\}$ *[30]; for solving the ahead-of-time energy planning problem* (4.25) *every* T *slots, the stochastic subgradient approach needs* $\mathcal{O}(1/\epsilon^2)$ *iterations to obtain an* ϵ*-optimal solution, while the per iteration complexity is in the order of* $\mathcal{O}(I^{3.5}K^{3.5})$*. And updating* $E_i^{(j)}[n]$ *in (27) requires only linear complexity* $\mathcal{O}(I)$*.*

4.4 Performance Analysis

In this section, we show that the TS-OC can yield a feasible and asymptotically (near-)optimal solution for problem (4.12).

4.4.1 Feasibility Guarantee

Note that in problems (4.19) and (4.20), $\{C_i(t)\}$ are removed from the set of optimization variables and the constraints in (4.8) are ignored. While the battery dynamics $C_i(t+1) = \eta C_i(t) + P_{b,i}(t)$ are accounted for by the TS-OC algorithm (in the step of "Queue updates"), it is not clear whether the resultant $C_i(t) \in [C^{\min}, C^{\max}]$, $\forall i, t$. Yet, we will show that by selecting a pair (Γ, V) in (4.15), we can guarantee that $C^{\min} \leq C_i(t) \leq C^{\max}$, $\forall i, t$; meaning, the online control policy produced by the TS-OC is a feasible one for the original problem (4.12), under the conditions (4.13)–(4.14).

To this end, we first show the following lemma.

Lemma 8. *If* $\bar{\alpha} := \max\{\alpha_t^{\mathrm{rt}}, \forall t\}$ *and* $\underline{\beta} := \min\{\beta_t^{\mathrm{rt}}, \forall t\}$*, the battery (dis)charging amounts* $P_{b,i}^*(t)$ *obtained from the TS-OC algorithm satisfy: i)* $P_{b,i}^*(t) = P_b^{\min}$*, if* $C_i(n_t T) > -V\underline{\beta} - \Gamma$*; and ii)* $P_{b,i}^*(t) = P_b^{\max}$*, if* $C_i(n_t T) < -V\bar{\alpha} - \Gamma$*.*

Proof. In TS-OC, we determine $P_{b,i}^*(t)$ by solving (4.20). From the equivalent problem (4.22), we can see that the determination of $P_{b,i}^*(t)$ is decoupled across BSs, and it depends on the first derivative of $G^{\mathrm{rt}}(\cdot)$. By (4.21), the maximum possible gradient for $G^{\mathrm{rt}}(\cdot)$ is $V\bar{\alpha}$. It then follows that if $V\bar{\alpha} + Q_i(n_t T) < 0$, we must have $P_{b,i}^*(t) = P_b^{\max}$. Similarly, if $V\underline{\beta} + Q_i(n_t T) > 0$, we must have $P_{b,i}^*(t) = P_b^{\min}$. Given that $Q_i(t) = C_i(t) + \Gamma$, the lemma follows readily. □

Lemma 8 reveals partial characteristics of the dynamic TS-OC policy. Specifically, when the energy queue (i.e., battery SoC) is large enough, the battery must be discharged

as much as possible; that is, $P^*_{b,i}(t) = P^{\min}_b$. On the other hand, when the energy queue is small enough, the battery must be charged as much as possible; i.e., $P^*_{b,i}(t) = P^{\max}_{b,i}$. Alternatively, such results can be justified by the economic interpretation of the virtual queues. Specifically, $-\frac{Q_i(t)}{V}$ can be viewed as the instantaneous discharging price. For high prices $-\frac{Q_i(t)}{V} > \bar{\alpha}$, the TS-OC dictates full charge. Conversely, the battery units can afford full discharge if the price is low.

Based on the structure in Lemma 8, we can thus establish the following result.

Proposition 1. *Under the conditions (4.13)–(4.14), the TS-OC algorithm with any pair* (Γ, V) *specified in (4.15) guarantees* $C^{\min} \leq C_i(t) \leq C^{\max}$, $\forall i$, $\forall t$.

Proof. See Appendix A.0.8. □

Remark 5. *Note that Proposition 1 is a* sample path *result; meaning, the bounded energy queues* $C_i(t) \in [C^{\min}, C^{\max}]$, $\forall i$, *hold per time slot under* arbitrary, *even non-stationary,* $\{\boldsymbol{A}_n, \alpha^{\rm lt}_n, \beta^{\rm lt}_n, \alpha^{\rm rt}_t, \beta^{\rm rt}_t, \mathbf{H}_t\}$ *processes. In other words, under the mild conditions (4.13)–(4.14), the proposed TS-OC with proper selection of* (Γ, V) *always yields a feasible control policy for (4.12).*

4.4.2 Asymptotic Optimality

To facilitate the analysis, we assume that the random processes $\{\boldsymbol{\xi}^{\rm lt}_n\}$ and $\{\boldsymbol{\xi}^{\rm rt}_t\}$ are both i.i.d. over slow and fast timescales, respectively. Define $\bar{C}_i := \frac{1}{NT}\sum_{t=0}^{NT-1}\mathbb{E}\{C_i(t)\}$ and $\bar{P}_{b,i} := \frac{1}{NT}\sum_{t=0}^{NT-1}\mathbb{E}\{P_{b,i}(t)\}$. Since $P_{b,i}(t) \in [P^{\min}_b, P^{\max}_b]$ and $C_i(t+1) = \eta C_i(t) + P_{b,i}(t)$, it holds that

$$\bar{P}_{b,i} = \frac{1}{NT}\sum_{t=0}^{NT-1}\mathbb{E}\{C_i(t+1) - \eta C_i(t)\} = (1-\eta)\bar{C}_i. \tag{4.28}$$

As $C_i(t) \in [C^{\min}, C^{\max}]$, $\forall t$, (4.28) then implies

$$(1-\eta)C^{\min} \leq \bar{P}_{b,i} \leq (1-\eta)C^{\max}, \quad \forall i. \tag{4.29}$$

Consider now the following problem

$$\tilde{\Phi}^{opt} := \min_{\mathcal{X}} \lim_{N\to\infty} \frac{1}{NT} \sum_{t=0}^{NT-1} \sum_{i\in\mathcal{I}} \mathbb{E}\{\Phi_i(t)\} \\ \text{s. t.} \quad (4.5), (4.6), (4.9), (4.10), \ \forall t, \quad (4.29). \tag{4.30}$$

Note that the constraints in (4.8), $\forall t$, are replaced by (4.29); i.e., the queue dynamics that need to be performed per realization per slot are replaced by a time-averaged constraint per BS i. The problem (4.30) is thus a relaxed version of (4.12) [109]. Specifically, any feasible solution of (4.12), satisfying (4.8), $\forall t$, also satisfies (4.29) in (4.30), due to the boundedness of $P_{b,i}(t)$ and $C_i(t)$. It then follows that $\tilde{\Phi}^{opt} \leq \Phi^{opt}$.

Variables $\{C_i(t)\}$ are removed from (4.30), and other optimization variables are "decoupled" across time slots due to the removal of constraints (4.8). This problem has an easy-to-characterize stationary optimal control policy as formally stated in the next lemma.

Lemma 9. *If $\boldsymbol{\xi}_n^{\mathrm{lt}}$ and $\boldsymbol{\xi}_t^{\mathrm{rt}}$ are i.i.d., there exists a stationary control policy $\mathcal{P}^{stat}$ that is a pure (possibly randomized) function of the current $(\boldsymbol{\xi}_{n_t}^{\mathrm{lt}}, \boldsymbol{\xi}_t^{\mathrm{rt}})$, while satisfying (4.5), (4.6), (4.9), (4.10), and providing the following guarantees per t:*

$$\mathbb{E}\{\sum_{i\in\mathcal{I}} \Phi_i^{stat}(t)\} = \tilde{\Phi}^{opt} \\ (1-\eta)C^{\min} \leq \mathbb{E}\{P_{b,i}^{stat}(t)\} \leq (1-\eta)C^{\max}, \ \ \forall i \tag{4.31}$$

where $P_{b,i}^{stat}(t)$ denotes the decided (dis)charging amount, $\Phi_i^{stat}(t)$ the resultant transaction cost by policy $\mathcal{P}^{stat}$, and expectations are taken over the randomization of $(\boldsymbol{\xi}_{n_t}^{\mathrm{lt}}, \boldsymbol{\xi}_t^{\mathrm{rt}})$ and (possibly) $\mathcal{P}^{stat}$.

Proof. The proof argument is similar to that in [113, Theorem 4.5]; hence, it is omitted for brevity. □

Lemma 9 in fact holds for many non-i.i.d. scenarios as well. Generalizations to other stationary processes, or even to non-stationary processes, can be found in [113] and [114].

It is worth noting that (4.31) not only assures that the stationary control policy $\mathcal{P}^{stat}$ achieves the optimal cost for (4.30), but also guarantees that the resultant expected transaction cost per slot t is equal to the optimal time-averaged cost (due to the stationarity of $\boldsymbol{\xi}_{n_t}^{\mathrm{lt}}$, $\boldsymbol{\xi}_t^{\mathrm{rt}}$ and $\mathcal{P}^{stat}$). This plays a critical role in establishing the following result.

Proposition 2. *Suppose that conditions (4.13)–(4.15) hold. If $\boldsymbol{\xi}_n^{\mathrm{lt}}$ and $\boldsymbol{\xi}_t^{\mathrm{rt}}$ are i.i.d. across time, then the time-averaged cost under the proposed TS-OC algorithm satisfies*

$$\lim_{N\to\infty}\frac{1}{NT}\sum_{t=0}^{NT-1}\sum_{i\in\mathcal{I}}\mathbb{E}\{\Phi_i^*(t)\}\leq\Phi^{opt}+\frac{M_1+M_2+M_3}{V}$$

where the constants[2]

$$M_1:=\frac{IT(1-\eta)}{2\eta(1-\eta^T)}M_B \tag{4.32}$$

$$M_2:=\frac{I[T(1-\eta)-(1-\eta^T)]}{(1-\eta)(1-\eta^T)}M_B \tag{4.33}$$

$$M_3:=I(1-\eta)M_C \tag{4.34}$$

with M_B and M_C given by

$$M_B:=\max\{[(1-\eta)\Gamma+P_b^{\min}]^2,[(1-\eta)\Gamma+P_b^{\max}]^2\}$$

$$M_C:=\max\{(\Gamma+C^{\min})^2,(\Gamma+C^{\max})^2\};$$

$\Phi_i^*(t)$ denotes the resultant cost with the TS-OC, and Φ^{opt} is the optimal value of (4.12) under any feasible control algorithm, including the one knowing all future realizations.

Proof. See Appendix A.0.9. □

Remark 6. *Proposition 2 asserts that the proposed TS-OC algorithm ends up with a time-averaged cost having optimality gap smaller than $\frac{M_1+M_2+M_3}{V}$. The novel TS-OC can also be viewed as a modified version of a classic queue-length based stochastic optimization scheme, where queue lengths play the role of "stochastic" Lagrange multipliers with*

[2]Note that $\lim_{\eta\to1}\frac{1-\eta^T}{1-\eta}=T$, and $\lim_{\eta\to1}\frac{T(1-\eta)-(1-\eta^T)}{(1-\eta)(1-\eta^T)}=\frac{T-1}{2}$.

a dual-subgradient solver to the regularized dual problem by subtracting an ℓ_2-norm of Lagrange multipliers. Intuitively, the gap M_1/V is inherited from the underlying stochastic subgradient method. The gap M_2/V is introduced by the inaccurate queue lengths in use (since we use $Q_i(nT)$, instead of $Q_i(t)$, for all $t = nT, \ldots, (n+1)T-1$), while the gap M_3/V is incurred by the presence of the ℓ_2 regularizer in the dual function (a. k. a. the price of battery imperfections).

4.4.3 Main Theorem for the Proposed TS-OC

Based on Propositions 1 and 2, it is now possible to arrive at our main result.

Theorem 3. *Suppose that conditions (4.13)–(4.15) hold and $(\boldsymbol{\xi}_n^{\mathrm{lt}}, \boldsymbol{\xi}_t^{\mathrm{rt}})$ are i.i.d. over slots. Then the proposed TS-OC yields a feasible dynamic control scheme for* (4.12)*, which is asymptotically near-optimal in the sense that*

$$\Phi^{opt} \leq \lim_{N\to\infty} \frac{1}{NT} \sum_{t=0}^{NT-1} \sum_{i\in\mathcal{I}} \mathbb{E}\{\Phi_i^*(t)\} \leq \Phi^{opt} + \frac{M}{V}$$

where $M := M_1 + M_2 + M_3$, as specified in Proposition 2.

The asymptotic behavior of the proposed dynamic approach is more complicated than that of existing alternatives due to the nature of multi-scale scheduling and battery imperfections. Interesting comments on the minimum optimality gap with the TS-OC are now in order.

1) When $\eta = 1$ (perfect battery), the optimality gap between the TS-OC and the offline optimal scheduling reduces to

$$\frac{M}{V} = \frac{M_1 + M_2}{V} = \frac{IT}{2V} \max\{(P_b^{\min})^2, (P_b^{\max})^2\}.$$

The typical tradeoff from the stochastic network optimization holds in this case [113]: an $\mathcal{O}(V)$ battery size is necessary, when an $\mathcal{O}(1/V)$ close-to-optimal cost is

achieved. Clearly, the minimum optimality gap is given by $M/V^{\max}$, which vanishes as $V^{\max} \to \infty$. By (4.18), such an asymptotic optimality can be achieved when we have very small price difference $(\bar{\alpha} - \underline{\beta})$, or very large battery capacities $C^{\max}$.

2) When $\eta \in (0, 1)$, the constants M_1, M_2 and M_3 are in fact functions of Γ, whereas the minimum and maximum values of Γ also depend on V [cf. (4.16)–(4.17)], thus the typical tradeoff in the case 1) is no longer correct. For a given $V^{\max}$, the minimum optimality gap, $G^{\min}(V^{\max})$, can be obtained by solving the following problem:

$$\min_{(V,\Gamma)} \ \frac{M}{V} = \frac{M_1(\Gamma)}{V} + \frac{M_2(\Gamma)}{V} + \frac{M_3(\Gamma)}{V}, \ \text{s. t.} \ \ (4.15). \tag{4.35}$$

For $V \geq 0$, we know that the quadratic-over-linear functions $\frac{[(1-\eta)\Gamma + P_b^{\min}]^2}{V}$ and $\frac{[(1-\eta)\Gamma + P_b^{\max}]^2}{V}$ are jointly convex in V and Γ [84]. As a point-wise maximum of these two convex functions, $\frac{M_B(\Gamma)}{V}$ is also convex [84]. Then $\frac{M_1(\Gamma)}{V}$ and $\frac{M_2(\Gamma)}{V}$ are clearly convex by (4.32)-(4.33); and likewise for $\frac{M_3(\Gamma)}{V}$. Since the objective is convex and the constraints in (4.15) are linear, problem (4.35) is a convex program which can be efficiently solved by general interior-point methods. Note that $G^{\min}(V^{\max})$ no longer monotonically decreases with respect to $V^{\max}$ (or $C^{\max}$); see also [109]. This makes sense intuitively because for a large battery capacity, the impact of using inaccurate queue lengths (battery SoC) and the dissipation loss due to battery imperfections will also be enlarged. The smallest possible optimality gap can be numerically computed by one dimensional search over $G^{\min}(V^{\max})$ with respect to $V^{\max}$.

4.5 Numerical Tests

In this section, simulated tests are presented to evaluate our proposed TS-OC algorithm, and justify the analytical claims in Section 4.4.

Table 4.1: Parameter Values for the CoMP network. All units are kWh.

Constant energy consumption of BSs P_c	10
Maximum energy consumption of BSs $P_g^{\max}$	50
Minimum charging amount of battery $P_b^{\min}$	-2
Maximum charging amount of battery $P_b^{\max}$	2
Minimum energy level of battery $C^{\min}$	0
Maximum energy level of battery $C^{\max}$	80
Initial energy level of battery $C_i(0)$	0

4.5.1 Experiment Setup

The considered CoMP network includes $I = 2$ BSs each with $M = 2$ transmit antennas, and $K = 3$ mobile users. The system bandwidth is 1 MHz, and each element in channel vectors $\boldsymbol{h}_{ik,t}, \forall i, k, t$, is a zero-mean complex-Gaussian random variable with unit variance. Each coarse-grained interval consists of $T = 5$ time slots. The limits of $P_{g,i}$, $P_{b,i}$ and C_i, as well as the values of the initial SoC $C_i(0)$ and P_c are listed in Table 4.1. The battery storage efficiency is $\eta = 0.95$. The ahead-of-time and real-time energy purchase prices α_n^{lt} and α_t^{rt} are generated from folded normal distributions, with $\mathbb{E}\{\alpha_n^{\text{lt}}\} = 1.15$ and $\mathbb{E}\{\alpha_t^{\text{rt}}\} = 2.3$. The selling prices are set as $\beta_n^{\text{lt}} = 0.9 \times \alpha_n^{\text{lt}}$ and $\beta_t^{\text{rt}} = 0.3 \times \alpha_t^{\text{rt}}$. The harvested energy $A_{i,n}$ is also generated from a folded normal distribution. Finally, the Lyapunov control parameter V is chosen as $V = V^{\max}$. The proposed TS-OC algorithm is compared with three baseline schemes to benchmark its performance. ALG 1 is a one-scale scheme without ahead-of-time energy planning; ALG 2 performs two-scale online control without leveraging the renewable energy or energy storage devices; and the offline benchmark is an ideal scheme with a-priori knowledge of future channel states, energy prices and RES arrival realizations.

4.5.2 Numerical Results

Fig. 4.3 shows the running-average transaction costs of the proposed algorithm, ALGs 1-2, as well as the offline benchmark. It is seen that within 500 time slots, the proposed approach converges the closest to the lower bound, while ALGs 1-2 incur about 71% and 31% larger costs than the proposed one. However, note that the optimal offline counterpart cannot work in practice due to the lack of future. In addition, the optimality gap can be reduced as the battery efficiency η approaches 1. Among online schemes, the TS-OC algorithm intelligently takes advantage of the ahead-of-time energy planning, and the renewable energy and batteries, to hedge against future potential high energy cost, while ALGs 1-2 have to purchase much more expensive energy from the real-time energy market and result in a higher transaction cost.

The theoretical optimality-gap [cf. (4.35)] between the TS-OC and the offline optimal scheduling is depicted in Fig. 4.4 under different battery capacities $C^{\max}$. As analyzed after Theorem 1, the optimality-gap M/V for $\eta = 1$ diminishes as $C^{\max}$ (or $V^{\max}$) grows; whereas the gaps for $\eta = 0.9$ and $\eta = 0.95$ are no longer monotonically decreasing. Specifically, both of them first decrease and then increase, reaching the lowest points (where the optimality gaps are minimized) at $C^{\max} = 40$ kWh and $C^{\max} = 55$ kWh, respectively. As expected, the gap for the worst storage efficiency $\eta = 0.9$ remains the largest across the entire spectrum of battery capacity.

In Fig. 4.5, the average transaction cost of the TS-OC is compared under different battery efficiencies $\eta = 0.9, 0.95, 1$. Clearly, the average costs monotonically decrease as $C^{\max}$ grows. The BSs with imperfect batteries ($\eta = 0.9, 0.95$) require larger budgets for energy purchase than the ones with perfect batteries ($\eta = 1$), thus compensating for the battery degeneration losses. In particular, when $C^{\max} = 120$ kWh, the costs for $\eta = 0.9$ and $\eta = 0.95$ are 41.8% and 33.8% larger than that of the perfect battery case, respectively.

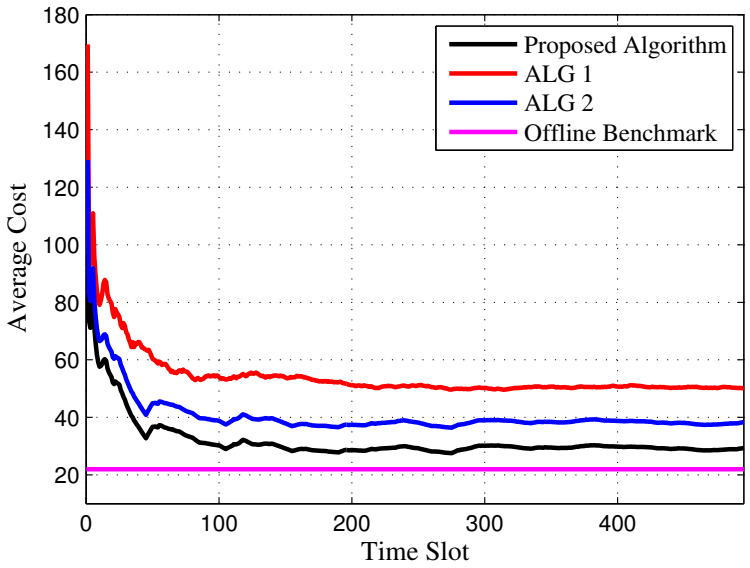

Figure 4.3: Comparison of average transaction cost.

The evolutions of battery SoC $C_1(t)$ with different storage efficiencies η are compared in Fig. 4.6. Clearly, all the three lines fluctuate within the feasible region; i.e., $C^{\min} \leq C_1(t) \leq C^{\max}$. Among the three cases, the battery with $\eta = 1$ maintains the highest energy level, followed by those with $\eta = 0.95$ and $\eta = 0.9$. Intuitively speaking, keeping a high energy level in an imperfect battery results in much higher energy dissipation losses. As a result, the TS-OC algorithm tends to maintain a low energy level in such cases (e.g., around 30 kWh for $\eta = 0.9$) to reduce average energy loss, and (dis)charge the battery less frequently.

The previous remarks are further substantiated by Fig. 4.7, where the instantaneous discharging price, or, the "stochastic" Lagrange multiplier $-\frac{Q_1(t)}{V}$ is compared with the running-average purchase and selling prices $\bar{\alpha}_t^{\text{rt}} := (1/t)\sum_{\tau=1}^{t} \alpha_\tau^{\text{rt}}$ and $\bar{\beta}_t^{\text{rt}} := (1/t)\sum_{\tau=1}^{t} \beta_\tau^{\text{rt}}$. It is interesting to observe that with a perfect battery ($\eta = 1$), the instantaneous discharging price $-\frac{Q_1(t)}{V}$ is hovering between the average purchase and selling prices, which features a frequent (dis)charging operation. For $\eta = 0.95$ or $\eta = 0.9$, $-\frac{Q_1(t)}{V}$ is relatively

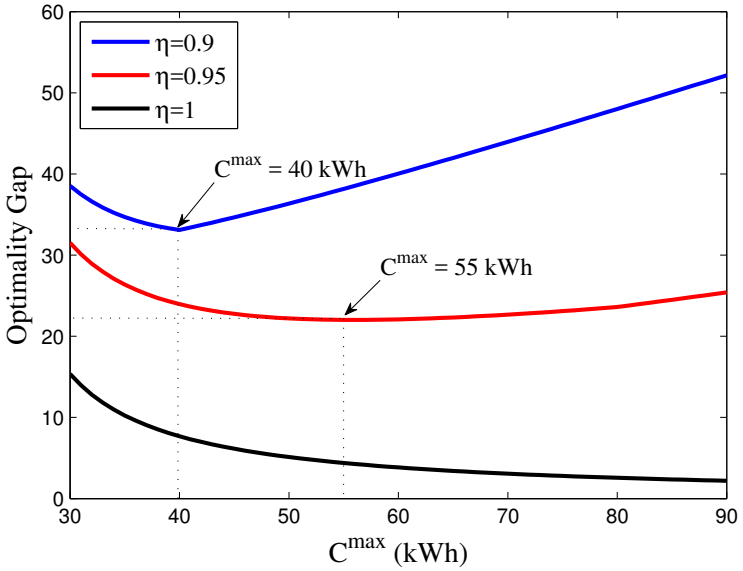

Figure 4.4: Optimality-gap versus battery capacity $C^{\max}$.

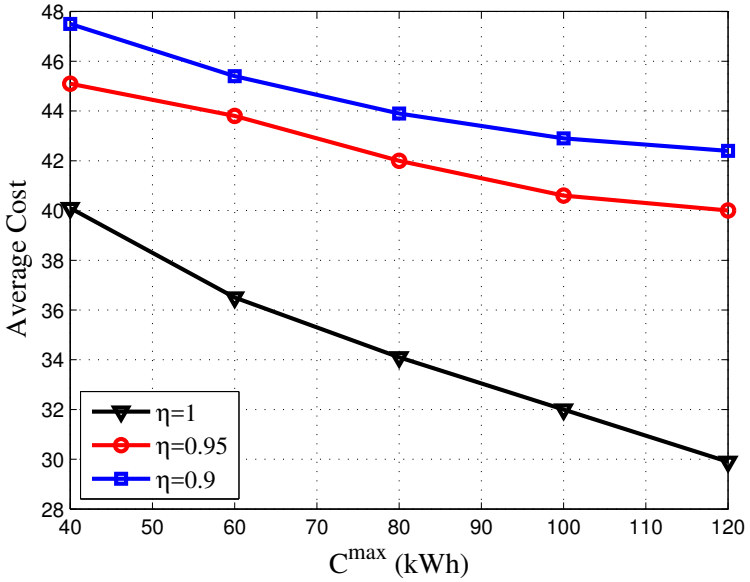

Figure 4.5: Average transaction cost versus battery capacity $C^{\max}$.

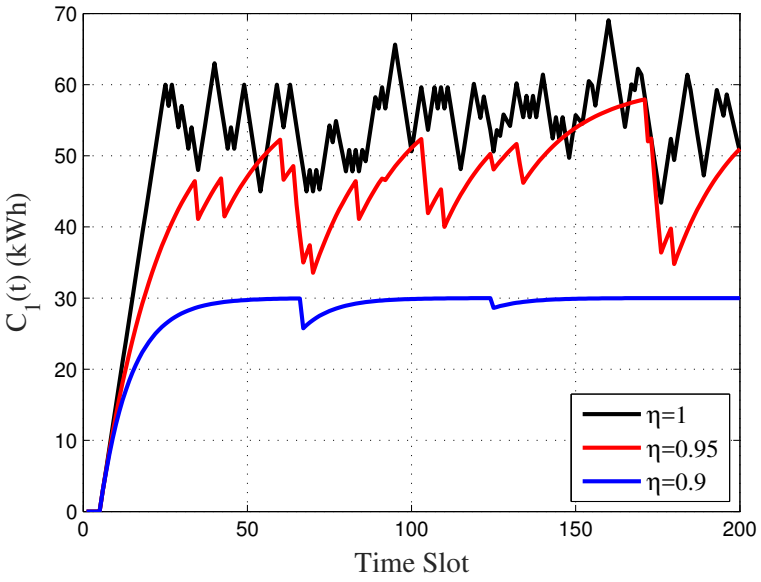

Figure 4.6: TS-OC based schedule of the battery SoC $C_1(t)$.

high compared to the average purchase and selling prices, which discourages frequent (dis)charging; see also Fig. 4.6. Note that the evolution of $-\frac{Q_1(t)}{V}$ can be further linked to the standard results from sensitivity analysis, which implies that the subdifferential of the objective $\lim_{N\to\infty}\frac{1}{NT}\sum_{t=0}^{NT-1}\sum_i \mathbb{E}\{\Phi_i(t)\}$ with respect to $P_{b,i}(t)$ (the convex hull of average purchase and selling prices) coincides with the negative of the optimal dual variable corresponding to (4.28) [84]. Building upon this claim, the asymptotic optimality can be easily verified for $\eta = 1$ since the "stochastic" Lagrange multiplier $-\frac{Q_1(t)}{V}$ converges to a neighborhood of the optimal dual variable; and a large optimality gap is also as expected for the imperfect batteries $\eta < 1$ due to the distance between $-\frac{Q_1(t)}{V}$ and the average purchase and selling prices.

Taking a deeper look, the battery SoC $C_1(n_tT)$ and the real-time battery (dis)charging $P^*_{b,1}(t)$ are jointly depicted in Fig. 4.8 to reveal the (dis)charging characteristics stated in Lemma 8. It can be observed that the TS-OC dictates the full discharge $P^*_{b,1}(t) = P_b^{\min}$ in the incoming 5 fine-grained slots $t \in [20, 24]$ when $C_1(n_tT) > -V\underline{\beta} - \Gamma$ at $n = 4$, while

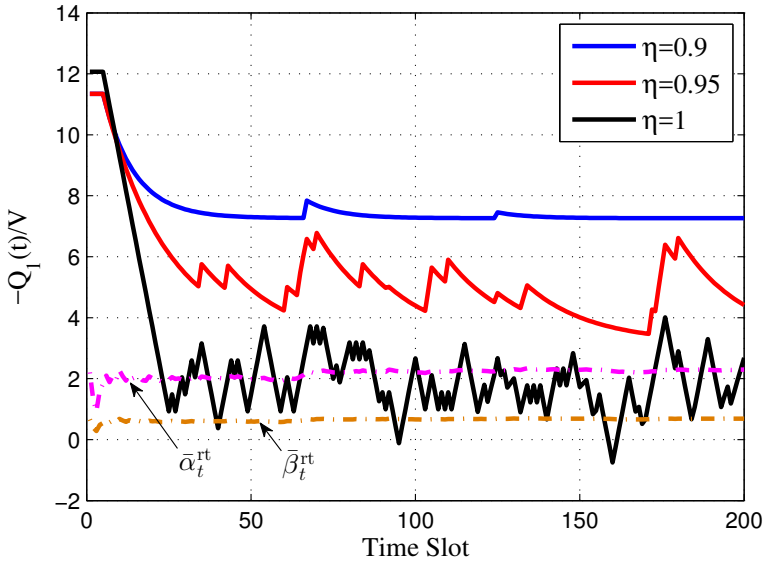

Figure 4.7: The evolution of $-Q_1(t)/V$ and running-average of energy prices.

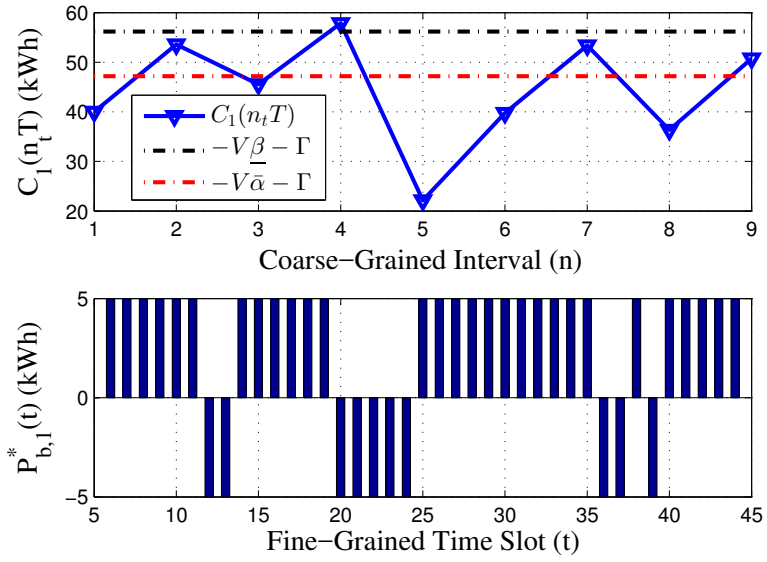

Figure 4.8: TS-OC based schedule of the battery SoC $C_1(n_tT)$ and battery (dis)charging actions $P_{b,1}^*(t)$, where $P_b^{\max} = 5$ kWh and $P_b^{\min} = -5$ kWh.

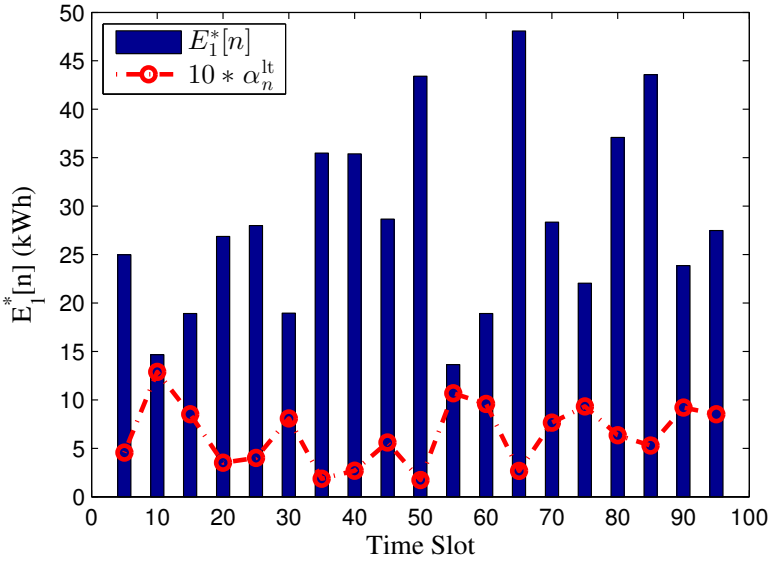

Figure 4.9: TS-OC based schedule of the optimal energy planning $E_1^*[n]$.

the battery is fully charged $P_{b,1}^*(t) = P_b^{\max}$ when $C_1(n_tT) < -V\bar{\alpha} - \Gamma$ at $n = 1, 3, 5, 6, 8$. In addition, when $C_1(n_tT) \in [-V\bar{\alpha} - \Gamma, -V\underline{\beta} - \Gamma]$ at $n = 2, 7$, $P_{b,1}^*(t)$ must be obtained by solving (4.22) numerically.

Fig. 4.9 shows the optimal energy planning $E_1^*[n]$ over a 100-slot period, along with the fluctuating ahead-of-time energy purchase prices α_n^{lt} for the resultant online policy. One observation is that the ahead-of-time energy purchase $E_1^*[n]$ highly depends on the long-term price α_n^{lt}. Specifically, the proposed scheme tends to request more energy for future T slots when α_n^{lt} is lower (e.g., $n = 10, 13, 17$), and tends to purchase less energy when α_n^{lt} is higher (e.g., $n = 2, 11$).

4.6 Conclusions

A two-scale dynamic resource allocation task was considered for RES-integrated CoMP transmissions. Taking into account the variability of channels, RES and ahead-of-time/real-time electricity prices, as well as battery imperfections, a stochastic optimization problem

was formulated to minimize the long-term average energy transaction cost subject to the QoS requirements. Capitalizing on the Lyapunov optimization technique and the stochastic subgradient iteration, a two-scale online algorithm was developed to make control decisions 'on-the-fly.' It was analytically established that the novel approach yields feasible and asymptotically near-optimal resource schedules without knowing any statistics of the underlying stochastic processes. Simulated tests confirmed the merits of the proposed approach and highlighted the effect of battery imperfections on the proposed online scheme. This novel two-scale optimization framework opens up some interesting research directions, which include incorporating the power network constraints and/or transmission losses in the formulation, pursuing a fast convergent approach by learning from historical system statistics, and reducing the battery size leveraging the so-called predictive scheduling.

Chapter 5

Thesis Conclusion and Future Work

5.1 Thesis Conclusions

EH is a key factor in building self-sustainable networks. It helps communication networks get rid of the limits of the grid, enabling people to provide network services in remote areas without grid coverage or in harsh areas. In addition, EH helps reduce carbon emissions and enables green communications. To deal with the inherent randomness and instability of environmental energy sources in EH-powered wireless communication systems, this thesis developed optimal data transmission schedules and resource allocation to ensure reliable and efficient communications, thus optimizing system performances.

In Chapter 2, we considered EH-powered WSN links, where data has strict deadline constraints and the power supply is unreliable. In the presence of circuit power consumption, a new DST algorithm was proposed, which generates the optimal transmit schedule in a computationally efficient, graphical manner by recursively updating the energy constraint curve on-the-go. We also extended the algorithm to online scenarios. The online algorithm follows the optimal rules we derived, generating transmission schedules in real time without a-priori knowledge of data or energy arrivals. Simulations showed that our

algorithm reduces the average complexity by almost two orders of magnitude compared to the standard convex solvers. The effective transmit region can also be substantially enlarged by our algorithm.

In Chapter 3, real-time resource allocation was developed for smart-grid powered MIMO downlink transmissions. Taking into account the time variations of channels, harvested renewables and electricity prices, a stochastic optimization problem was formulated to maximize the expected throughput while satisfying the energy cost constraints. Adopting the so-termed "virtual queue" relaxation techniques in [71,73,74], we decoupled the optimization variables across the infinite time horizon, and reformulated the problem as a state-independent stochastic programming. Then leveraging the dual relaxation and stochastic approximation methods, we developed a novel online control algorithm. It was proven that the novel approach yields feasible and asymptotically optimal resource schedules without knowing any statistics of the underlying stochastic processes. Simulations further corroborated the merits of the proposed scheme in non i.i.d. cases, where the underlying randomness is highly correlated over time.

In Chapter 4, a two-scale dynamic resource allocation task was considered for RES-integrated CoMP transmissions. Taking into account the variability of channels, RES and ahead-of-time/real-time electricity prices, as well as battery imperfections, a stochastic optimization problem was formulated to minimize the long-term average energy transaction cost subject to the QoS requirements. Based on [70, 71], a novel two-scale optimization framework was developed to facilitate the dynamic resource management for smart-grid powered CoMP systems with RES and channel dynamics at different time scales. While [71, 76] and [77] did not account for battery degeneration (energy leakage), we integrated the modified Lyapunov optimization technique into the two-scale stochastic optimization approach to leverage the diversity of energy prices along with the energy leakage effects on the dynamic energy management task. Simulated tests confirmed the

merits of the proposed approach and highlighted the effect of battery imperfections on the proposed online scheme.

5.2 Future Research Directions

Based on the work of this thesis, prospective future directions include

- modeling more practical battery unit with finite capacity and energy leakage, accounting for charging/discharging loss;
- extrapolation of the optimal transmission scheduling and energy management to large-scale EH powered networks;
- EH processes with multiple (discrete and/or continuous) power sources, and their impact on QoS;
- upper layer adaptation to the EH powered transmissions, including routing, prioritization, and QoS provision over EH powered wireless networks;
- incorporating the power network constraints and/or transmission losses in the formulations; and
- pursuing fast convergent approaches by learning from historical system statistics for energy management, etc.

Appendix A

Proofs of lemmas, propositions and theorems

A.0.1 Proof of Lemma 1

Define $\xi_{ee}(r) := \frac{P(r)+\rho}{r}$. Taking the first derivative of $\xi_{ee}(r)$, we have:

$$\frac{d\xi_{ee}(r)}{dr} = \frac{P'(r)r - (P(r)+\rho)}{r^2}. \tag{A.1}$$

Due to its "convex-over-linear" form, we can show that $\xi_{ee}(r)$ first decreases and then increases with r, and it reaches the minimum at r_{ee}. This implies:

$$\begin{cases} P'(r)r - (P(r)+\rho) < 0, & \text{if} \quad r < r_{ee}, \\ P'(r)r - (P(r)+\rho) = 0, & \text{if} \quad r = r_{ee}, \\ P'(r)r - (P(r)+\rho) > 0, & \text{if} \quad r > r_{ee}. \end{cases} \tag{A.2}$$

If we have an $r_i^* < r_{ee}$ when $l_i^* > 0$, it follows from (A.2) that $P'(r_i^*)r_i^* - (P(r_i^*)+\rho) < 0$. But when $P'(r_i^*)r_i^* - (P(r_i^*)+\rho) < 0$, (2.15) implies that $l_i^* = 0$, which leads to a contradiction. Hence, $r_i^* < r_{ee}$ is not allowed when $l_i^* > 0$.

When $r_i^* > r_{ee}$, we have $P'(r_i^*)r_i^* - (P(r_i^*)+\rho) > 0$ according to (A.2). This together with (2.15) then dictates $l_i^* = L_i$. In the case of $r_i^* = r_{ee}$, we have $P'(r_i^*)r_i^* - (P(r_i^*)+\rho) = 0$,

so any $l_i^* \in [0, L_i]$ is a minimizer in (2.15).

A.0.2 Proof of Lemma 2

Clearly, $r_i^* = P'^{-1}(w_i)$ changes only when w_i changes its value. By the definition of w_i in (2.5), if $(\lambda_n^c)^*, (\lambda_n^d)^*, (\mu_n^c)^* = 0, \forall n = 1, \ldots, N-1$, then a constant $w = [(\lambda_N^d)^* - (\lambda_N^c)^*]/[1 + (\mu_N^c)^*]$ will be used over all the epochs. We will have a change only when one of the Lagrange multipliers is positive for a certain $n \in [1, N-1]$, which occurs at the corresponding t_n. In addition, it follows from the complementary slackness conditions (2.11)-(2.13) that we have the corresponding constraints met with equality at such a t_n.

If the rate changes at t_n where $\sum_{i=1}^{n}(r_i^* l_i^*) = \sum_{i=0}^{n-1} A_i$, the corresponding $(\lambda_n^c)^* > 0$. For the epoch n, we have $w_n = \sum_{l=n}^{N}[(\lambda_l^d)^* - (\lambda_l^c)^*]/[1 + \sum_{l=n}^{N}(\mu_l^c)^*]$. On the other hand, we have $w_{n+1} = \sum_{l=n+1}^{N}[(\lambda_l^d)^* - (\lambda_l^c)^*]/[1 + \sum_{l=n+1}^{N}(\mu_l^c)^*]$ for the epoch $(n+1)$; thus, $w_{n+1} - w_n = (\lambda_n^c)^*/[1 + \sum_{l=n+1}^{N}(\mu_l^c)^*] > 0$. We can conclude that the rate increases after this t_n as $P'^{-1}(w_i)$ is an increasing function of w_i.

If a change occurs at a certain t_n where $\sum_{i=1}^{n}(r_i^* l_i^*) = \sum_{i=1}^{n} D_i$, then $(\lambda_n^d)^* > 0$. We can similarly obtain that $w_{n+1} - w_n = -(\lambda_n^d)^*/[1 + \sum_{l=n+1}^{N}(\mu_l^c)^*] < 0$, which indicates the rate decreases after this t_n.

If a change occurs at a certain t_n where $\sum_{i=1}^{n}[(P(r_i^*) + \rho) l_i^*] = \sum_{i=0}^{n-1} E_i$, then $(\mu_n^c)^* > 0$. We can derive that $1/w_n - 1/w_{n+1} = (\mu_n^c)^* / \sum_{l=n+1}^{N}[(\lambda_l^d)^* - (\lambda_l^c)^*] > 0$, which indicates the rate increases after this t_n.

A.0.3 Proof of Theorem 1

Given the rules in Algorithm 1, it can be shown that the rate-changing pattern in the transmit schedule $\mathcal{R} := (\boldsymbol{r}^*, \boldsymbol{l}^*)$ produced by Algorithm 1 is consistent with the optimal structure revealed in Lemma 2 [5], i.e., (i) if the rate in use is first r and then changed to $\tilde{r}$ at t_τ where $\sum_{i=1}^{\tau}(r l_i^*) = \sum_{i=0}^{\tau-1} A_i$ or $\sum_{i=1}^{\tau}\{[P(r) + \rho] l_i^*\} = \sum_{i=0}^{\tau-1} E_i$, then we must have

$\tilde{r} > r$; and (ii) if the rate r is changed at t_τ where $\sum_{i=1}^{\tau}(rl_i^*) = \sum_{i=1}^{\tau} D_i$, then we must have the next rate $\tilde{r} < r$.

Suppose that the rate changes M times in $\mathcal{R}$ yielded by Algorithm 1 at time instants $\{t_{\tau_1}, t_{\tau_2}, \ldots, t_{\tau_M}\}$. We divide the schedule into $M+1$ phases: rate $r_i^* = \check{r}_1$ over epochs $i \in [1, \tau_1]$, $r_i^* = \check{r}_2$ over epochs $i \in [\tau_1{+}1, \tau_2], \ldots, r_i^* = \check{r}_{M+1}$ over epochs $i \in [\tau_M{+}1, N]$. We can then construct a set of Lagrange multipliers $\mathbf{\Lambda^*} := \{(\lambda_n^c)^*, (\lambda_n^d)^*, (\mu_n^c)^*, n = 1, \ldots, N\}$ as follows:

For convenience, let Δ_1 denote $[P'(\check{r}_{m+1}) - P'(\check{r}_m)]$ and Δ_2 denote $[\frac{1}{P'(\check{r}_m)} - \frac{1}{P'(\check{r}_{m+1})}]$. For a certain τ_m, $\forall m = 1, \ldots, M$,

1. if $\sum_{i=1}^{\tau_m}(r_i^* l_i^*) = \sum_{i=0}^{\tau_m - 1} A_i$, then
$$(\lambda_{\tau_m}^c)^* = \Delta_1 \cdot [1 + \sum_{l=\tau_m}^{N} (\mu_l^c)^*];$$
2. if $\sum_{i=1}^{\tau_m}(r_i^* l_i^*) = \sum_{i=1}^{\tau_m} D_i$, then
$$(\lambda_{\tau_m}^d)^* = -\Delta_1 \cdot [1 + \sum_{l=\tau_m}^{N} (\mu_l^c)^*];$$
3. if $\sum_{i=1}^{\tau_m}\{[P(r_i^*) + \rho] l_i^*\} = \sum_{i=0}^{\tau_m - 1} E_i$, then
$$(\mu_{\tau_m}^c)^* = \Delta_2 \cdot \sum_{l=\tau_m}^{N} [(\lambda_l^d)^* - (\lambda_l^c)^*];$$

We have shown that the rate $\check{r}_{m+1} > \check{r}_m$ if the data or energy causality constraint is tight at t_{τ_m}, and $\check{r}_{m+1} < \check{r}_m$ if the deadline constraint is tight at t_{τ_m}. Recalling that $P'(r)$ is increasing in r, it readily follows that $(\lambda_{\tau_m}^c)^* > 0$, $(\lambda_{\tau_m}^d)^* > 0$, or $(\mu_{\tau_m}^c)^* > 0$, depending on which type of constraint is tight at t_{τ_m}. Besides, let $(\lambda_N^d)^* = P'(\check{r}_{M+1}) > 0$. Except these $M+1$ positive $(\lambda_N^d)^*$, $(\lambda_{\tau_m}^c)^*$, $(\lambda_{\tau_m}^d)^*$ and $(\mu_{\tau_m}^c)^*$, all other Lagrange multipliers in $\mathbf{\Lambda^*}$ are set to zero.

With such a $\mathbf{\Lambda^*}$, the complementary slackness conditions (2.11)-(2.13) clearly hold. Using such a $\mathbf{\Lambda^*}$ leads to $w_i := \sum_{n=i}^{N}[(\lambda_n^d)^* - (\lambda_n^c)^*]/[1 + \sum_{n=i}^{N}(\mu_n^c)^*] = P'(\check{r}_m), \forall i \in [\tau_{m-1}+$

$1, \tau_m]$ (with $\tau_0 := 1$ and $\tau_{M+1} := N$). This implies that $r_i^* = \check{r}_m = [\log(|h|^2 w_i)]_+, \forall i \in [\tau_{m-1}+1, \tau_m]$. In addition, the construction of $\mathcal{R}$ ensures $l_i^* = L_i$ when $r_i^* = \check{r}_m > r_{ee}$, and computes a feasible set of $l_i^* \leq L_i$ when $r_i^* = \check{r}_m = r_{ee}$ in each phase m. This guarantees that each pair of (r_i^*, l_i^*) satisfies (2.10); thus, $(\boldsymbol{r^*}, \boldsymbol{l^*})$ follows the optimal structure in Lemma 1.

A.0.4 Proof of Lemma 4

From recursions (3.13), we deduce

$$\begin{aligned}(\hat{\lambda}_2^{t+1})^2 &\leq [\hat{\lambda}_2^t - \mu(P_c + P_{x,t}(\hat{\boldsymbol{\lambda}}^t) - P_t(\hat{\boldsymbol{\lambda}}^t)]^2 \\ &= (\hat{\lambda}_2^t)^2 - 2\mu\hat{\lambda}_2^t[P_c + P_{x,t}(\hat{\boldsymbol{\lambda}}^t) - P_t(\hat{\boldsymbol{\lambda}}^t)] \\ &\quad + \mu^2[P_c + P_{x,t}(\hat{\boldsymbol{\lambda}}^t) - P_t(\hat{\boldsymbol{\lambda}}^t)]^2 \\ &\leq (\hat{\lambda}_2^t)^2 - 2\mu\hat{\lambda}_2^t[P_c + P_{x,t}(\hat{\boldsymbol{\lambda}}^t) - P_t(\hat{\boldsymbol{\lambda}}^t)] \\ &\quad + \mu^2(\max\{P_{b,i}^{\max}, -P_{b,i}^{\min}\})^2\end{aligned} \tag{A.3}$$

where the last inequality holds due to (3.9d). Similarly, it follows that

$$\begin{aligned}(\hat{\lambda}_1^{t+1})^2 \leq (\hat{\lambda}_1^t)^2 - 2\mu\hat{\lambda}_1^t[G^{\max} - G(P_t(\hat{\boldsymbol{\lambda}}^t)] + \mu^2[(G^{\max})^2 \\ + (\max\{\alpha^{\max}(P_g^{\max} + P_b^{\max}), \beta^{\max}(E^{\max} - P_b^{\min})\})^2].\end{aligned} \tag{A.4}$$

Considering now the Lyapunov function $V(\hat{\boldsymbol{\lambda}}^t) := \frac{1}{2}[(\hat{\lambda}_1^t)^2 + (\hat{\lambda}_2^t)^2]$, it readily follows that

$$\begin{aligned}-\triangle V(\hat{\boldsymbol{\lambda}}^t) &:= -V(\hat{\boldsymbol{\lambda}}^{t+1}) + V(\hat{\boldsymbol{\lambda}}^t) \\ &\geq \mu\hat{\lambda}_2^t[P_c + P_{x,t}(\hat{\boldsymbol{\lambda}}^t) - P_t(\hat{\boldsymbol{\lambda}}^t)] \\ &\quad + \mu\hat{\lambda}_1^t[G^{\max} - G(P_t(\hat{\boldsymbol{\lambda}}^t)] - \mu^2 M.\end{aligned} \tag{A.5}$$

Taking expectations and adding $\mu\mathbb{E}[R_t(P_{x,t}(\hat{\boldsymbol{\lambda}}^t))]$ to both sides, we arrive at

$$\begin{aligned}
&\mathbb{E}[-\triangle V(\hat{\boldsymbol{\lambda}}^t)] + \mu\mathbb{E}[R_t(P_{x,t}(\hat{\boldsymbol{\lambda}}^t))] \\
&\geq \mu\Big(\mathbb{E}[R_t(P_{x,t}(\hat{\boldsymbol{\lambda}}^t))] + \hat{\lambda}_2^t[P_c + P_{x,t}(\hat{\boldsymbol{\lambda}}^t) - P_t(\hat{\boldsymbol{\lambda}}^t)] \\
&\qquad + \hat{\lambda}_1^t[G^{\max} - G(P_t(\hat{\boldsymbol{\lambda}}^t)]\Big) - \mu^2 M \qquad \text{(A.6)} \\
&= \mu L(\boldsymbol{X}(\hat{\boldsymbol{\lambda}}^t), \hat{\boldsymbol{\lambda}}^t) - \mu^2 M \\
&= \mu D(\hat{\boldsymbol{\lambda}}^t) - \mu^2 M \\
&\geq \mu\tilde{R}^* - \mu^2 M
\end{aligned}$$

where we used the definition of $L(\boldsymbol{X}, \boldsymbol{\lambda})$ in (3.11); $\boldsymbol{X}(\hat{\boldsymbol{\lambda}}^t)$ denotes the optimal primal variable set given by (3.15) for $\boldsymbol{\lambda} = \hat{\boldsymbol{\lambda}}^t$ (hence, $L(\boldsymbol{X}(\hat{\boldsymbol{\lambda}}^t), \hat{\boldsymbol{\lambda}}^t) = D(\hat{\boldsymbol{\lambda}}^t)$); $\tilde{R}^*$ denotes the optimal value for problem (3.10); and the last inequality is due to the weak duality: $D(\boldsymbol{\lambda}) \geq \tilde{R}^*$, $\forall\boldsymbol{\lambda}$.

Summing over all t, we then have

$$\begin{aligned}
&\sum_{t=0}^{T-1}\mathbb{E}[-\triangle V(\hat{\boldsymbol{\lambda}}^t)] + \mu\sum_{t=0}^{T-1}\mathbb{E}[R_t(P_{x,t}(\hat{\boldsymbol{\lambda}}^t))] \\
&= -\mathbb{E}[V(\hat{\boldsymbol{\lambda}}^T)] + V(\hat{\boldsymbol{\lambda}}^0) + \mu\sum_{t=0}^{T-1}\mathbb{E}[R_t(P_{x,t}(\hat{\boldsymbol{\lambda}}^t))] \qquad \text{(A.7)} \\
&\geq T(\mu\tilde{R}^* - \mu^2 M)
\end{aligned}$$

which leads to

$$\begin{aligned}
\frac{1}{T}\sum_{t=0}^{T-1}\mathbb{E}[R_t(P_{x,t}(\hat{\boldsymbol{\lambda}}^t))] &\geq \tilde{R}^* - \mu M - \frac{V(\hat{\boldsymbol{\lambda}}^0)}{\mu T} \\
&\geq R^* - \mu M - \frac{V(\hat{\boldsymbol{\lambda}}^0)}{\mu T}. \qquad \text{(A.8)}
\end{aligned}$$

The lemma follows by taking the limit $T \to \infty$.

A.0.5 Proof of Lemma 5

Recall that $P_{b,t} = P_t - P_c - P_{x,t}$. Given $\hat{\boldsymbol{\lambda}}^t$, we can rewrite the maximization problem in (3.15) in terms of $\{P_{x,t}, P_{b,t}\}$ as

$$\begin{aligned} \max_{P_{x,t},P_{b,t}} \; & R_t(P_{x,t}) - \hat{\lambda}_1^t G(P_{b,t} + P_c + P_{x,t}) - \hat{\lambda}_2^t P_{b,t} \\ \text{s. t. } \; & 0 \le P_{x,t} \le P_g^{\max} - P_c, \quad P_b^{\min} \le P_{b,t} \le P_b^{\max}. \end{aligned} \tag{A.9}$$

Consider the following two cases [cf. (3.5)]

i) If $P_{b,t} + P_c + P_{x,t} \ge E_t$, then $G(P_{b,t} + P_c + P_{x,t}) = \alpha_t(P_{b,t} + P_c + P_{x,t} - E_t)$. The problem (A.9) can be decomposed into two subproblems, namely

$$\max_{0 \le P_{x,t} \le P_g^{\max} - P_c} \; R_t(P_{x,t}) - \hat{\lambda}_1^t \alpha_t P_{x,t} \tag{A.10}$$

$$\max_{P_b^{\min} \le P_{b,t} \le P_b^{\max}} \; -(\hat{\lambda}_1^t \alpha_t + \hat{\lambda}_2^t) P_{b,t}. \tag{A.11}$$

Let $R_t'^{-1}$ denote the inverse function of R_t'. It is easy to see that we must have

$$P_{x,t}(\hat{\boldsymbol{\lambda}}^t) = \max\{0, \min\{P_g^{\max} - P_c, R_t'^{-1}(\hat{\lambda}_1^t \alpha_t)\}\}.$$

$$P_{b,t}(\hat{\boldsymbol{\lambda}}^t) = \begin{cases} P_b^{\min}, & \text{if } \hat{\lambda}_1^t \alpha_t + \hat{\lambda}_2^t > 0 \\ P_b^{\max}, & \text{if } \hat{\lambda}_1^t \alpha_t + \hat{\lambda}_2^t < 0. \end{cases} \tag{A.12}$$

ii) If $P_{b,t} + P_c + P_{x,t} < E_t$, then $G(P_{b,t} + P_c + P_{x,t}) = \beta_t(P_{b,t} + P_c + P_{x,t} - E_t)$; and we similarly arrive at

$$P_{x,t}(\hat{\boldsymbol{\lambda}}^t) = \max\{0, \min\{P_g^{\max} - P_c, R_t'^{-1}(\hat{\lambda}_1^t \beta_t)\}\}.$$

$$P_{b,t}(\hat{\boldsymbol{\lambda}}^t) = \begin{cases} P_b^{\min}, & \text{if } \hat{\lambda}_1^t \beta_t + \hat{\lambda}_2^t > 0 \\ P_b^{\max}, & \text{if } \hat{\lambda}_1^t \beta_t + \hat{\lambda}_2^t < 0. \end{cases} \tag{A.13}$$

Combining cases i) and ii), we deduce that per slot t, if $\hat{\lambda}_1^t > \max\{R_t'(0)/\alpha_t, R_t'(0)/\beta_t\} = R_t'(0)/\beta_t$, then $P_{x,t}(\hat{\boldsymbol{\lambda}}^t) = 0$. Similarly, if $\hat{\lambda}_2^t > \max\{-\hat{\lambda}_1^t \alpha_t, -\hat{\lambda}_1^t \beta_t\} = -\hat{\lambda}_1^t \beta_t$, then $P_{b,t}(\hat{\boldsymbol{\lambda}}^t) = P_b^{\min}$; and if $\hat{\lambda}_2^t < \min\{-\hat{\lambda}_1^t \alpha_t, -\hat{\lambda}_1^t \beta_t\} = -\hat{\lambda}_1^t \alpha_t$, then c.

A.0.6 Proof of Lemma 6

Due to the projection operation, it is clear $\hat{\lambda}_1^t \geq 0$. We next establish the upper bound for $\hat{\lambda}_1^t$ by induction. First, set $\hat{\lambda}_1^0 \leq \frac{R'(0)}{\beta^{\min}} + \max\{0, \mu(\alpha^{\max}(P_g^{\max} + P_b^{\max}) - G^{\max})\}$, and suppose that this holds for all $\hat{\lambda}_1^t$ at slot t. We show that the bound holds for $\hat{\lambda}_1^{t+1}$ as well, in the following two cases.

c1) If $\hat{\lambda}_1^t \in [0, \frac{R'(0)}{\beta^{\min}}]$, we have $\hat{\lambda}_1^{t+1} = [\hat{\lambda}_1^t + \mu(G(P_t(\hat{\boldsymbol{\lambda}}^t)) - G^{\max})]^+ \leq \frac{R'(0)}{\beta^{\min}} + \max\{0, \mu(\alpha^{\max}(P_g^{\max} + P_b^{\max}) - G^{\max})\}$, since $G(P_t(\hat{\boldsymbol{\lambda}}^t)) \leq \alpha^{\max}(P_g^{\max} + P_b^{\max})$ due to $P_t(\hat{\boldsymbol{\lambda}}^t) \leq P_g^{\max} + P_b^{\max}$ by the constraints (3.9c)–(3.9d), and $G(P_t)$ is increasing in P_t.

c2) If $\alpha^{\max}(P_g^{\max} + P_b^{\max}) - G^{\max} \geq 0$ and $\hat{\lambda}_1^t \in (\frac{R'(0)}{\beta^{\min}}, \frac{R'(0)}{\beta^{\min}} + \mu(\alpha^{\max}(P_g^{\max} + P_b^{\max}) - G^{\max})]$, then we must have $P_{x,t}(\hat{\boldsymbol{\lambda}}^t) = 0$ by Lemma 4; thus, $P_t(\hat{\boldsymbol{\lambda}}^t) \leq P_c + P_b^{\max}$. It follows that $\hat{\lambda}_1^{t+1} = [\hat{\lambda}_1^t + \mu(G(P_t(\hat{\boldsymbol{\lambda}}^t)) - G^{\max})]^+ \leq [\frac{R'(0)}{\beta^{\min}} + \mu(\alpha^{\max}(P_g^{\max} + P_b^{\max}) - G^{\max}) + \mu(\alpha^{\max}(P_c + P_b^{\max}) - G^{\max})]^+ \leq \frac{R'(0)}{\beta^{\min}} + \mu(\alpha^{\max}(P_g^{\max} + P_b^{\max}) - G^{\max})$, since $\alpha^{\max}(P_c + P_b^{\max}) \leq G^{\max}$.

A.0.7 Proof of Lemma 7

The proof again proceeds by induction. First, set $\hat{\lambda}_2^0 \in [-\alpha^{\max}(\frac{R'(0)}{\beta^{\min}} + \mu\delta_{\lambda_1}) + \mu P_b^{\min}, \mu C^{\max} - \mu C^{\min} - \alpha^{\max}(\frac{R'(0)}{\beta^{\min}} + \mu\delta_{\lambda_1}) + \mu P_b^{\min}]$, and suppose that this holds for all $\hat{\lambda}_2^t$ at slot t. Define short-hand notation $\lambda_1^{\max} := \frac{R'(0)}{\beta^{\min}} + \mu\delta_{\lambda_1}$. We next show that the bounds hold for $\hat{\lambda}_2^{t+1}$ as well, in subsequent instances.

c1) If $\hat{\lambda}_2^t \in (0, \mu C^{\max} - \mu C^{\min} - \alpha^{\max}\lambda_1^{\max} + \mu P_b^{\min}]$, it is clear that $\hat{\lambda}_2^t > 0 > \max\{-\hat{\lambda}_1^t\beta^t, \forall t\}$. It then follows from Lemma 5 that $\hat{\lambda}_2^{t+1} = \hat{\lambda}_2^t + \mu P_b^{\min} \in [-\alpha^{\max}\lambda_1^{\max} + \mu P_b^{\min}, \mu C^{\max} - \mu C^{\min} - \alpha^{\max}\lambda_1^{\max} + \mu P_b^{\min}]$, since $P_b^{\min} < 0$.

c2) If $\hat{\lambda}_2^t \in [-\alpha^{\max}\lambda_1^{\max}, 0]$, then $\hat{\lambda}_2^{t+1} = \hat{\lambda}_2^t + \mu P_b^t(\hat{\boldsymbol{\lambda}}^t) \in [\hat{\lambda}_2^t + \mu P_b^{\min}, \hat{\lambda}_2^t + \mu P_b^{\max}] \subseteq [-\alpha^{\max}\lambda_1^{\max} + \mu P_b^{\min}, \mu P_b^{\max}] \subseteq [-\alpha^{\max}\lambda_1^{\max} + \mu P_b^{\min}, \mu C^{\max} - \mu C^{\min} - \alpha^{\max}\lambda_1^{\max} +$

$\mu P_b^{\min}]$, where the upper bound holds when $\mu \geq \underline{\mu} \geq \frac{\alpha^{\max}\lambda_1^{\max}}{C^{\max}-C^{\min}+P_b^{\min}-P_b^{\max}}$.

c3) If $\hat{\lambda}_2^t \in [-\alpha^{\max}\lambda_1^{\max} + \mu P_b^{\min}, -\alpha^{\max}\lambda_1^{\max})$, it holds that $\hat{\lambda}_2^t < -\alpha^{\max}\lambda_1^{\max} < \min\{-\hat{\lambda}_1^t\alpha^t, \forall t\}$. By Lemma 5, we have $\hat{\lambda}_2^{t+1} = \hat{\lambda}_2^t + \mu P_b^{\max} \in [-\alpha^{\max}\lambda_1^{\max} + \mu P_b^{\min} + P_b^{\max}, -\alpha^{\max}\lambda_1^{\max} + P_b^{\max}) \subseteq (-\alpha^{\max}\lambda_1^{\max} + \mu P_b^{\min}, \mu C^{\max} - \mu C^{\min} - \alpha^{\max}\lambda_1^{\max} + \mu P_b^{\min})$, where the last step follows from the facts $P_b^{\max} > 0$, and $-\alpha^{\max}\lambda_1^{\max} + P_b^{\max} \leq P_b^{\max} \leq \mu C^{\max} - \mu C^{\min} - \alpha^{\max}\lambda_1^{\max} + \mu P_b^{\min}$ when $\mu \geq \underline{\mu}$.

A.0.8 Proof of Proposition 1

The proof proceeds by induction. First, set $C_i(0) \in [C^{\min}, C^{\max}]$, $\forall i$, and suppose that this holds for all $C_i(nT)$ at slot nT. We will show the bounds hold for $C_i(t)$, $\forall t = nT+1, \ldots, (n+1)T$, as well as in subsequent instances.

By $C_i(t+1) = \eta C_i(t) + P_{b,i}^*(t)$, we have

$$C_i(t) = \eta^{t-nT} C_i(nT) + \sum_{\tau=nT}^{t-1} [\eta^{t-1-\tau} P_{b,i}^*(\tau)], \quad \forall t = nT+1, \ldots, (n+1)T. \tag{A.14}$$

Note that by the definitions of $\Gamma^{\min}$ and $\Gamma^{\max}$ in (4.16)-(4.17), we have $C^{\min} \leq -V\bar{\alpha} - \Gamma < -V\underline{\beta} - \Gamma \leq C^{\max}$. We then consider the following three cases.

c1) If $C_i(nT) \in [C^{\min}, -V\bar{\alpha} - \Gamma)$, then Lemma 3 implies that $P_{b,i}^*(t) = P_b^{\max}$, $\forall t = nT, \ldots, (n+1)T-1$. From (A.14), we have, $\forall t = nT+1, \ldots, (n+1)T$,

i) $C_i(t) \geq \eta^{t-nT} C^{\min} + \frac{1-\eta^{t-nT}}{1-\eta} P_b^{\max} \geq C^{\min}$, due to the condition (4.13);

ii) $C_i(t) \leq \eta^{t-nT}(-V\bar{\alpha} - \Gamma) + \frac{1-\eta^{t-nT}}{1-\eta} P_b^{\max} \leq \eta^{t-nT}(-V\underline{\beta} - \Gamma) + \frac{1-\eta^{t-nT}}{1-\eta} P_b^{\max} \leq C^{\max}$, due to $\underline{\beta} < \bar{\alpha}$, $\Gamma \geq \Gamma^{\min}$, and the definition of $\Gamma^{\min}$ in (4.16).

c2) If $C_i(nT) \in [-V\bar{\alpha} - \Gamma, -V\underline{\beta} - \Gamma]$, then $P_{b,i}^*(t) \in [P_b^{\min}, P_b^{\max}]$. We have, $\forall t = nT+1, \ldots, (n+1)T$,

i) $C_i(t) \geq \eta^{t-nT}(-V\bar{\alpha} - \Gamma) + \frac{1-\eta^{t-nT}}{1-\eta} P_b^{\min} \geq C^{\min}$, due to $\Gamma \leq \Gamma^{\max}$ and the definition of $\Gamma^{\max}$ in (4.17);

ii) $C_i(t) \leq \eta^{t-nT}(-V\underline{\beta} - \Gamma) + \frac{1-\eta^{t-nT}}{1-\eta} P_b^{\max} \leq C^{\max}$, as with c1-ii); and

c3) If $C_i(nT) \in (-V\underline{\beta} - \Gamma, C^{\max}]$, it follows from Lemma 3 that $P_{b,i}^*(t) = P_b^{\min}$, $\forall t = nT, \ldots, (n+1)T - 1$. We have, $\forall t = nT + 1, \ldots, (n+1)T$

i) $C_i(t) \geq \eta^{t-nT}(-V\underline{\beta} - \Gamma) + \frac{1-\eta^{t-nT}}{1-\eta} P_b^{\min} \geq \eta^{t-nT}(-V\bar{\alpha} - \Gamma) + \frac{1-\eta^{t-nT}}{1-\eta} P_b^{\min} \geq C^{\min}$, due to $\underline{\beta} < \bar{\alpha}$ and c2-i);

ii) $C_i(t) \leq \eta^{t-nT} C^{\max} + \frac{1-\eta^{t-nT}}{1-\eta} P_b^{\min} \leq C^{\max}$, due to $\eta \leq 1$, and $P_b^{\min} < 0$.

Cases c1)–c3) together prove the proposition.

A.0.9 Proof of Proposition 2

The evolution of $Q_i(t)$ in the TS-OC is given by $Q_i(t+1) = C_i(t+1) + \Gamma = \eta C_i(t) + P_{b,i}^*(t) + \Gamma = \eta Q_i(t) + (1-\eta)\Gamma + P_{b,i}^*(t)$. Hence, we have

$$\begin{aligned}
[Q_i(t+1)]^2 &= [\eta Q_i(t) + (1-\eta)\Gamma + P_{b,i}^*(t)]^2 \\
&= \eta^2 [Q_i(t)]^2 + 2\eta Q_i(t)[(1-\eta)\Gamma + P_{b,i}^*(t)] \\
&\quad + [(1-\eta)\Gamma + P_{b,i}^*(t)]^2 \\
&\leq \eta^2 [Q_i(t)]^2 + 2\eta Q_i(t)[(1-\eta)\Gamma + P_{b,i}^*(t)] \\
&\quad + \max\{[(1-\eta)\Gamma + P_b^{\min}]^2, [(1-\eta)\Gamma + P_b^{\max}]^2\}
\end{aligned} \tag{A.15}$$

where the last inequality holds due to (4.9).

With $\mathbf{Q}(t) := [Q_1(t), \ldots, Q_I(t)]'$, consider the Lyapunov function $L(\mathbf{Q}(t)) := \frac{1}{2}\sum_i [Q_i(t)]^2$.

Using the short-hand notation $\boldsymbol{Q}[n] := \boldsymbol{Q}(nT)$, it readily follows that

$$\begin{aligned}
&\triangle_T(\mathbf{Q}[n]) := L(\mathbf{Q}[n+1]) - L(\mathbf{Q}[n]) \\
&\leq -\frac{1}{2}(1-\eta^2) \sum_{t=nT}^{(n+1)T-1} \sum_{i\in\mathcal{I}} [Q_i(t)]^2 + \frac{IT}{2} M_B \\
&\quad + \sum_{t=nT}^{(n+1)T-1} \sum_{i\in\mathcal{I}} \{\eta Q_i(t)[(1-\eta)\Gamma + P^*_{b,i}(t)]\} \qquad \text{(A.16)} \\
&\leq \frac{IT}{2} M_B + \sum_{t=nT}^{(n+1)T-1} \sum_{i\in\mathcal{I}} \{\eta Q_i(t)[(1-\eta)\Gamma + P^*_{b,i}(t)]\}.
\end{aligned}$$

Since $Q_i(t+1) = \eta Q_i(t) + (1-\eta)\Gamma + P^*_{b,i}(t)$ and $P_b^{\min} \leq P^*_{b,i}(t) \leq P_b^{\max}$, we have: $\forall t = nT, \ldots, (n+1)T-1$,

$$\begin{aligned}
&\eta^{t-nT} Q_i[n] + \frac{1-\eta^{t-nT}}{1-\eta}[(1-\eta)\Gamma + P_b^{\min}] \leq Q_i(t) \\
&\quad \leq \eta^{t-nT} Q_i[n] + \frac{1-\eta^{t-nT}}{1-\eta}[(1-\eta)\Gamma + P_b^{\max}]. \qquad \text{(A.17)}
\end{aligned}$$

This implies that $\forall t = nT, \ldots, (n+1)T-1$,

$$\begin{aligned}
&Q_i(t)[(1-\eta)\Gamma + P^*_{b,i}(t)] \leq \eta^{t-nT} Q_i[n][(1-\eta)\Gamma + P^*_{b,i}(t)] \\
&+ \frac{1-\eta^{t-nT}}{1-\eta} \max\{[(1-\eta)\Gamma + P_b^{\min}]^2, [(1-\eta)\Gamma + P_b^{\max}]^2\}. \qquad \text{(A.18)}
\end{aligned}$$

Consequently, it follows that

$$\begin{aligned}
\triangle_T(\mathbf{Q}[n]) &\leq \frac{IT}{2} M_B + \sum_{t=nT}^{(n+1)T-1} \sum_{i\in\mathcal{I}} \{\frac{\eta(1-\eta^{t-nT})}{1-\eta} M_B \\
&\quad + \sum_{t=nT}^{(n+1)T-1} \sum_{i\in\mathcal{I}} \{\eta^{t-nT+1} Q_i[n][(1-\eta)\Gamma + P^*_{b,i}(t)]\} \\
&\leq \frac{IT}{2} M_B + \frac{I\eta[T(1-\eta) - (1-\eta^T)]}{(1-\eta)^2} M_B \qquad \text{(A.19)} \\
&\quad + \sum_{t=nT}^{(n+1)T-1} \sum_{i\in\mathcal{I}} \{\eta^{t-nT+1} Q_i[n][(1-\eta)\Gamma + P^*_{b,i}(t)]\}.
\end{aligned}$$

Taking expectations and adding $\sum_{t=nT}^{(n+1)T-1}\sum_i[\eta^{t-nT+1}V\mathbb{E}\{\Phi_i^*(t)\}]$ to both sides, we arrive at (with short-hand notation $M_\triangle := \frac{IT}{2}M_B + \frac{I\eta[T(1-\eta)-(1-\eta^T)]}{(1-\eta)^2}M_B$):

$$\begin{aligned}
&\mathbb{E}\{\triangle_T(\mathbf{Q}[n])\} + \sum_{t=nT}^{(n+1)T-1}\eta^{t-nT+1}\sum_{i\in\mathcal{I}}[V\mathbb{E}\{\Phi_i^*(t)\}] \\
&\leq M_\triangle + \sum_{t=nT}^{(n+1)T-1}[\eta^{t-nT+1}\sum_{i\in\mathcal{I}}Q_i[n](1-\eta)\Gamma] \\
&\quad + \sum_{t=nT}^{(n+1)T-1}[\eta^{t-nT+1}\sum_{i\in\mathcal{I}}\mathbb{E}\{V\Phi_i^*(t)+Q_i[n]P_{b,i}^*(t)\}] \\
&= M_\triangle + \sum_{t=nT}^{(n+1)T-1}[\eta^{t-nT+1}\sum_{i\in\mathcal{I}}Q_i[n](1-\eta)\Gamma] \\
&\quad + \frac{\eta(1-\eta^T)}{(1-\eta)T}\sum_{t=nT}^{(n+1)T-1}[\sum_{i\in\mathcal{I}}\mathbb{E}\{V\Phi_i^*(t)+Q_i[n]P_{b,i}^*(t)\}] \\
&\leq M_\triangle + \sum_{t=nT}^{(n+1)T-1}[\eta^{t-nT+1}\sum_{i\in\mathcal{I}}Q_i[n](1-\eta)\Gamma] \\
&\quad + \frac{\eta(1-\eta^T)}{(1-\eta)T}\sum_{t=nT}^{(n+1)T-1}[\sum_{i\in\mathcal{I}}\mathbb{E}\{V\Phi_i^{stat}(t)+Q_i[n]P_{b,i}^{stat}(t)\}] \\
&= M_\triangle + \sum_{t=nT}^{(n+1)T-1}[\eta^{t-nT+1}\sum_{i\in\mathcal{I}}\mathbb{E}\{V\Phi_i^{stat}(t)\}] \\
&\quad + \sum_{t=nT}^{(n+1)T-1}[\eta^{t-nT+1}Q_i[n]\{(1-\eta)\Gamma+P_{b,i}^{stat}(t)\}] \\
&\leq M_\triangle + I\eta(1-\eta^T)M_C + \frac{\eta(1-\eta^T)}{1-\eta}V\tilde{\Phi}^{opt}
\end{aligned} \tag{A.20}$$

where the two equalities hold since both $\sum_{i\in\mathcal{I}}\mathbb{E}\{V\Phi_i^*(t)+Q_i[n]P_{b,i}^*(t)\}$ for the TS-OC and $\sum_{i\in\mathcal{I}}\mathbb{E}\{V\Phi_i^{stat}(t)+Q_i[n]P_{b,i}^{stat}(t)\}$ for $\mathcal{P}^{stat}$ are in fact the same for slots $t=nT,\ldots,(n+1)T-1$, when $\boldsymbol{\xi}_t^{\mathrm{rt}}$ is i.i.d. over slots; the second inequality is because the TS-OC algorithm minimizes the third term $\sum_i\mathbb{E}\{V\Phi_i(t)+Q_i[n]P_{b,i}(t)\}]$ among all policies satisfying (4.5), (4.6), (4.9), and (4.10), including $\mathcal{P}^{stat}$; and the last inequality is due to (4.31) and $Q_i[n]\in[C^{\min}+\Gamma, C^{\max}+\Gamma]$ under conditions (4.13)–(4.15) per Proposition 1.

Again, note that $\sum_i[V\mathbb{E}\{\Phi_i^*(t)\}]$ for the TS-OC is the same for slots $t=nT,\ldots,(n+$

$1)T-1$, when $\boldsymbol{\xi}_t^{\mathrm{rt}}$ is i.i.d. over slots. Summing over all $n=1,2,\ldots$, we then have

$$\begin{aligned}
&\sum_{n=0}^{N-1}\mathbb{E}\{\triangle_T(\mathbf{Q}[n])\}+\sum_{n=0}^{N-1}\sum_{t=nT}^{(n+1)T-1}\eta^{t-nT+1}\sum_{i\in\mathcal{I}}[V\mathbb{E}\{\Phi_i^*(t)\}]\\
&=\mathbb{E}[L(\mathbf{Q}[N])]-L(\mathbf{Q}[0])+\frac{\eta(1-\eta^T)}{(1-\eta)T}\sum_{t=0}^{NT-1}\sum_{i\in\mathcal{I}}[V\mathbb{E}\{\Phi_i^*(t)\}] \qquad \text{(A.21)}\\
&\leq N[M_\triangle+I\eta(1-\eta^T)M_C+\frac{\eta(1-\eta^T)}{1-\eta}V\tilde{\Phi}^{opt}]
\end{aligned}$$

which leads to

$$\begin{aligned}
&\frac{1}{NT}\sum_{t=0}^{NT-1}\mathbb{E}[\sum_{i\in\mathcal{I}}\mathbb{E}\{\Phi_i^*(t)\}]\\
&\quad\leq\tilde{\Phi}^{opt}+\frac{M_1+M_2+M_3}{V}+\frac{(1-\eta)}{\eta(1-\eta^T)}\frac{L(\mathbf{Q}[0])}{NV} \qquad \text{(A.22)}\\
&\quad\leq\Phi^{opt}+\frac{M_1+M_2+M_3}{V}+\frac{(1-\eta)}{\eta(1-\eta^T)}\frac{L(\mathbf{Q}[0])}{NV}
\end{aligned}$$

and the proposition follows by taking the limit as $N\to\infty$.

Appendix B

List of Acronyms

5G	fifth-generation
AWGN	Additive White Gaussian Noise
BC	broadcast channel
BS	base station
CoMP	coordinated multi-point
C-RAN	cloud/collaborative/clean radio access network
CS/CB	coordinated scheduling/beamforming
CSCG	circularly symmetric complex Gaussian
CSI	channel state information
DPC	dirty paper coding
DSM	demand-side management
DST	dynamic string tautening
EE	energy efficiency
EH	energy harvesting
HetNets	heterogeneous networks
ICT	information and communication technology

IEEE	Institute of Electrical and Electronics Engineers
i.i.d.	independent and identically distributed
IoT	Internet of Things
JP/JT	joint processing/transmission
KKT	Karush-Kuhn-Tucker
MACs	multi-access channels
MIMO	multiple-input multiple-output
OPEX	operational expenditure
QoS	quality of service
RES	renewable energy sources
RF	radio frequency
SGOC	stochastic subgradient based online control
SINR	signal-to-interference-plus-noise ratio
SISO	single-input single-output
SoC	state of charge
TS-OC	two-scale online control
WSN	wireless sensor network

Appendix C

List of Notations

x	Scalar x
$\boldsymbol{x}$	Vector $\boldsymbol{x}$
$\boldsymbol{X}$	Matrix $\boldsymbol{X}$
$\mathbb{C}^{M\times N}$	$M \times N$ dimensional complex matrices
$\mathbb{R}^{M\times N}$	$M \times N$ dimensional real matrices
$(\cdot)'$	Transpose
$(\cdot)^\dagger$	Conjugate transpose
$\mathrm{diag}(a_1, \ldots, a_M)$	Diagonal matrix with diagonal elements $a_1, \ldots, a_M$
$\lvert \cdot \rvert$	Magnitude of a complex scalar
$\mathrm{tr}(\boldsymbol{A})$	Trace operator for matrix $\boldsymbol{A}$
$\boldsymbol{A} \succeq \boldsymbol{0}$	Square matrix $\boldsymbol{A}$ is positive semi-definite
$\mathbb{E}$	Expectation

References

[1] X. Chen, W. Ni, X. Wang, and Y. Sun, "Optimal quality-of-service scheduling for energy-harvesting powered wireless communications," *IEEE Trans. Wireless Commun.*, vol. 15, no. 5, pp. 3269–3280, May 2016.

[2] X. Wang, T. Chen, X. Chen, X. Zhou, and G. B. Giannakis, "Dynamic resource allocation for smart-grid powered mimo downlink transmissions," *IEEE J. Sel. Areas Commun.*, vol. 34, no. 12, pp. 3354–3365, Aug. 2016.

[3] X. Wang, X. Chen, T. Chen, L. Huang, and G. B. Giannakis, "Two-scale stochastic control for integrated multipoint communication systems with renewables," *IEEE Trans. Smart Grid*, vol. 9, no. 3, pp. 1822–1834, Mar. 2018.

[4] Y. He, X. Cheng, W. Peng, and G. L. Stuber, "A survey of energy harvesting communications: models and offline optimal policies," *IEEE Commun. Mag.*, vol. 53, no. 6, pp. 79–85, June 2015.

[5] X. Chen, X. Wang, and Y. Sun, "Energy-harvesting powered transmissions of bursty data packets with strict deadlines," in *Proc. of ICC*, 2014, pp. 4060–4065.

[6] "*Pennsylvania-New Jersey-Maryland interconnection (PJM) hourly prices*," Available online: http://www.pjm.com/markets-and-operations/energy/realtime/monthlylmp.aspx.

[7] M. Webb, "Smart 2020: Enabling the low carbon economy in the information age," *Climate Group*, vol. 1, pp. 1–1, Jan. 2008.

[8] G. Fettweis and E. Zimmermann, "ICT energy consumption – trends and challenges," in *Proc. WPMC*, 2008, pp. 8–11.

[9] L. Suarez, L. Nuaymi, and J. M. Bonnin, "An overview and classification of research approaches in green wireless networks," *Eurasip Journal on Wireless Communications & Networking*, vol. 2012, no. 1, p. 142, Jan. 2012.

[10] I. Chihlin, C. Rowell, S. Han, Z. Xu, G. Li, and Z. Pan, "Toward green and soft: A 5G perspective," *IEEE Commun. Mag.*, vol. 52, no. 2, pp. 66–73, Feb. 2014.

[11] E. Oh, B. Krishnamachari, X. Liu, and Z. Niu, "Toward dynamic energy-efficient operation of cellular network infrastructure," *IEEE Commun. Mag.*, vol. 49, no. 6, pp. 56–61, June 2011.

[12] P. Skillermark and P. Frenger, "Enhancing energy efficiency in LTE with antenna muting," in *Vehicular Technology Conference*, 2012, pp. 1–5.

[13] C. M. R. Institute, "C-RAN: The road towards green RAN," Available online: labs.chinamobile.com/cran.

[14] IEEE, Available online: http://ieeexplore.ieee.org/.

[15] C. R. Valenta, "Harvesting wireless power: Survey of energy-harvester conversion efficiency in far-field, wireless power transfer systems," *IEEE Microwave Mag.*, vol. 15, no. 4, pp. 108–120, Apr. 2014.

[16] D. Gunduz, K. Stamatiou, N. Michelusi, and M. Zorzi, "Designing intelligent energy harvesting communication systems," *IEEE Commun. Mag.*, vol. 52, no. 1, pp. 210–216, Jan. 2014.

[17] C. Knight, J. Davidson, and S. Behrens, "Energy options for wireless sensor nodes," *Sensors*, vol. 8, no. 12, pp. 8037–8066, Dec. 2008.

[18] M. Rahimi, H. Shah, G. Sukhatme, and J. Heideman, "Studying the feasibility of energy harvesting in a mobile sensor network," in *Proc. ICRA*, 2003, pp. 19–24 vol.1.

[19] S. Chalasani and J. M. Conrad, "A survey of energy harvesting sources for embedded systems," in *Southeastcon*, 2008, pp. 442–447.

[20] M. A. Abdullah, A. H. M. Yatim, and C. W. Tan, "A study of maximum power point tracking algorithms for wind energy system," in *Clean Energy and Technology*, 2011, pp. 321–326.

[21] N. Bhatnagar and B. Venkatesh, "Energy storage and power systems," in *Electrical & Computer Engineering*, 2012, pp. 1–4.

[22] Z. Chen and E. Spooner, "Grid power quality with variable-speed wind turbines," *IEEE Power Engr. Review*, vol. 21, no. 6, pp. 70–70, June 2007.

[23] R. Rao, S. Vrudhula, and D. N. Rakhmatov, "Battery modeling for energy-aware system design," *Computer*, vol. 36, no. 12, pp. 77–87, Dec. 2003.

[24] S. Faias, P. Santos, F. Matos, J. Sousa, and C. Rui, "Evaluation of energy storage devices for renewable energies integration: Application to a portuguese wind farm," in *Proc. Eem*, 2008, pp. 1–7.

[25] S. Basagni, M. Y. Naderi, C. Petrioli, and D. Spenza, *Wireless Sensor Networks with Energy Harvesting.* John Wiley & Sons, Inc., 2013.

[26] E. Uysalbiyikoglu, B. Prabhakar, and A. El Gamal, "Energy-efficient packet transmission over a wireless link," *IEEE/ACM Trans. Netw.*, vol. 10, no. 4, pp. 487–499, Apr. 2002.

[27] U. M. Colesanti, S. Santini, and A. Vitaletti, "DISSense: An adaptive ultralow-power communication protocol for wireless sensor networks," in *Proc. DCOSS*, 2011, pp. 1–10.

[28] C. Isheden, Z. Chong, E. Jorswieck, and G. Fettweis, "Framework for link-level energy efficiency optimization with informed transmitter," *IEEE Trans. Wireless Commun.*, vol. 11, no. 8, pp. 2946–2957, Aug. 2012.

[29] D. Gunduz, K. Stamatiou, N. Michelusi, and M. Zorzi, "Designing intelligent energy harvesting communication systems," *IEEE Commun. Mag.*, vol. 52, no. 1, pp. 210–216, Jan. 2014.

[30] M. Grant and S. Boyd, *CVX: Matlab software for disciplined convex programming.* http://cvxr.com/cvx/, Mar. 2015.

[31] M. Agiwal, A. Roy, and N. Saxena, "Next generation 5G wireless networks: A comprehensive survey," *IEEE Commun. Surveys Tuts.*, vol. 18, no. 3, pp. 1617–1655, Mar. 2017.

[32] T. Han and N. Ansari, "Powering mobile networks with green energy," *IEEE Wireless Commun.*, vol. 21, no. 1, pp. 90–96, Jan. 2014.

[33] G. Lee, W. Saad, M. Bennis, and A. Mehbodniya, "Online ski rental for scheduling self-powered, energy harvesting small base stations," in *Proc. ICC*, 2016, pp. 1–6.

[34] X. Chen, W. Ni, X. Wang, and Y. Sun, "Provisioning quality-of-service to energy harvesting wireless communications," *IEEE Commun. Mag.*, vol. 53, no. 4, pp. 102–109, April 2015.

[35] H. A. Inan and A. Ozgur, "Online power control for the energy harvesting multiple access channel," in *Proc. WiOpt*, 2016, pp. 1–6.

[36] X. Fang, S. Misra, G. Xue, and D. Yang, "Smart grid – the new and improved power grid: A survey," *IEEE Commun. Surveys Tuts.*, vol. 14, no. 4, pp. 944–980, Apr. 2012.

[37] J. Xu and R. Zhang, "Cooperative energy trading in CoMP systems powered by smart grids," *IEEE Trans. Veh. Technol.*, vol. 65, no. 4, pp. 2142–2153, Apr. 2016.

[38] Z. Ghebretensae, J. Harmatos, and K. Gustafsson, "Mobile broadband backhaul network migration from TDM to carrier ethernet," *IEEE Commun. Mag.*, vol. 48, no. 10, pp. 102–109, Oct. 2010.

[39] A. Mahmood, N. Javaid, and S. Razzaq, "A review of wireless communications for smart grid," *Renewable & Sustainable Energy Reviews*, vol. 41, pp. 248–260, 2015.

[40] R. S. Kshetrimayum, *Fundamentals of MIMO Wireless Communications*, 2017.

[41] F. Rashid-Farrokhi, L. Tassiulas, and K. J. R. Liu, "Joint optimal power control and beamforming in wireless networks using antenna arrays," *IEEE Trans. Commun.*, vol. 46, no. 10, pp. 1313–1324, Oct. 1996.

[42] D. Gesbert, M. Kountouris, R. W. Heath, and C. B. Chae, "Shifting the MIMO paradigm," *IEEE Signal Process. Mag.*, vol. 24, no. 5, pp. 36–46, May 2007.

[43] G. Nigam, P. Minero, and M. Haenggi, "Coordinated multipoint joint transmission in heterogeneous networks," *IEEE Trans. Commun.*, vol. 62, no. 11, pp. 4134–4146, Nov. 2014.

[44] R. Irmer, H. Droste, P. Marsch, M. Grieger, G. Fettweis, S. Brueck, H. P. Mayer, L. Thiele, and V. Jungnickel, "Coordinated multipoint: Concepts, performance, and field trial results," *IEEE Commun. Mag.*, vol. 49, no. 2, pp. 102–111, Feb. 2011.

[45] H. Dahrouj and W. Yu, "Coordinated beamforming for the multicell multi-antenna wireless system," *IEEE Trans. Wireless Commun.*, vol. 9, no. 5, pp. 1748–1759, May 2010.

[46] J. Zhang, R. Chen, A. Ghosh, A. Ghosh, and R. W. Heath, "Networked MIMO with clustered linear precoding," *IEEE Trans. Wireless Commun.*, vol. 8, no. 4, pp. 1910–1921, Apr. 2009.

[47] C. T. K. Ng and H. Huang, "Linear precoding in cooperative MIMO cellular networks with limited coordination clusters," *IEEE J. Sel. Areas Commun.*, vol. 28, no. 9, pp. 1446–1454, Sept. 2010.

[48] J. Yang and S. Ulukus, "Optimal packet scheduling in an energy harvesting communication system," *IEEE Trans. Commun.*, vol. 60, no. 1, pp. 220–230, Jan. 2012.

[49] K. Tutuncuoglu and A. Yener, "Optimum transmission policies for battery limited energy harvesting nodes," *IEEE Trans. Wireless Commun.*, vol. 11, no. 3, pp. 1180–1189, Mar. 2012.

[50] O. Ozel, K. Tutuncuoglu, J. Yang, S. Ulukus, and A. Yener, "Transmission with energy harvesting nodes in fading wireless channels: Optimal policies," *IEEE J. Sel. Areas Commun.*, vol. 29, no. 8, pp. 1732–1743, Aug. 2011.

[51] J. Xu and R. Zhang, "Throughput optimal policies for energy harvesting wireless transmitters with non-ideal circuit power," *IEEE J. Sel. Areas Commun.*, vol. 32, no. 2, pp. 322–332, Feb. 2014.

[52] Q. Bai, J. Li, and J. A. Nossek, "Throughput maximizing transmission strategy of energy harvesting nodes," in *Proc. IWCLD*, 2011, pp. 1–5.

[53] O. Orhan, D. Gunduz, and E. Erkip, "Throughput maximization for an energy harvesting communication system with processing cost," in *Proc. ITW*, 2012, pp. 84–88.

[54] M. Gregori and M. Payaro, "On the optimal resource allocation for a wireless energy harvesting node considering the circuitry power consumption," *IEEE Trans. Wireless Commun.*, vol. 13, no. 11, pp. 5968–5984, Nov. 2014.

[55] Z. Ding, S. Perlaza, I. Esnaola, and H. Poor, "Power allocation strategies in energy harvesting wireless cooperative networks," *IEEE Trans. Wireless Commun.*, vol. 13, no. 2, pp. 846–860, Feb. 2014.

[56] D. N. K. Jayakody, J. Thompson, S. Chatzinotas, and S. Durrani, *Wireless Information and Power Transfer: A New Paradigm for Green Communications.* Springer International Publishing AG, July 2017.

[57] D. W. K. Ng, T. Q. Duong, C. Zhong, and R. Schober, *Wireless Information and Power Transfer: Theory and Practice.* Wiley-IEEE Press, 2018.

[58] X. Wang and Z. Li, "Energy-efficient transmissions of bursty data packets with strict deadlines over time-varying wireless channels," *IEEE Trans. Wireless Commun.*, vol. 12, no. 5, pp. 2533–2543, May 2013.

[59] Z. Nan, X. Wang, and W. Ni, "Energy-efficient transmission of delay-limited bursty data packets under non-ideal circuit power consumption," in *Proc. of ICC*, 2014, pp. 4957–4962.

[60] G. Miao, N. Himayat, and G. Y. Li, "Energy-efficient link adaptation in frequency-selective channels," *IEEE Trans. Commun.*, vol. 58, no. 2, pp. 545–554, Feb. 2010.

[61] M. A. Zafer and E. Modiano, "A calculus approach to minimum energy transmission policies with quality of service guarantees," in *Proc. INFOCOM*, vol. 1, 2005, pp. 548–559.

[62] P. Youssef-Massaad, L. Zheng, and M. Medard, "Bursty transmission and glue pouring: on wireless channels with overhead costs," *IEEE Trans. Wireless Commun.*, vol. 7, no. 12, pp. 5188–5194, Dec. 2008.

[63] D. Shuman, M. Liu, and O. Wu, "Energy-efficient transmission scheduling with strict underflow constraints," *IEEE Trans. Inf. Theory*, vol. 57, no. 3, pp. 1344–1367, Mar. 2011.

[64] M. A. Antepli, E. Uysalbiyikoglu, and H. Erkal, "Optimal packet scheduling on an energy harvesting broadcast link," *IEEE J. Sel. Areas Commun.*, vol. 29, no. 8, pp. 1721–1731, Aug. 2010.

[65] J. Yang, O. Ozel, and S. Ulukus, "Broadcasting with an energy harvesting rechargeable transmitter," *IEEE Trans. Wireless Commun.*, vol. 11, no. 2, pp. 571–583, Feb. 2012.

[66] O. Ozel, J. Yang, and S. Ulukus, "Optimal broadcast scheduling for an energy harvesting rechargeable transmitter with a finite capacity battery," *IEEE Trans. Wireless Commun.*, vol. 11, no. 6, pp. 2193–2203, Jun. 2012.

[67] X. Wang, Z. Nan, and T. Chen, "Optimal MIMO broadcasting for energy harvesting transmitter with non-ideal circuit power consumption," *IEEE Trans. Wireless Commun.*, vol. 14, no. 5, pp. 2500–2512, May 2015.

[68] S. Bu, F. R. Yu, Y. Cai, and X. P. Liu, "When the smart grid meets energy-efficient communications: Green wireless cellular networks powered by the smart grid," *IEEE Trans. Wireless Commun.*, vol. 11, no. 8, pp. 3014–3024, Aug. 2012.

[69] J. Xu and R. Zhang, "CoMP meets smart grid: A new communication and energy cooperation paradigm," *IEEE Trans. Veh. Technol.*, vol. 64, no. 6, pp. 2476–2488, June 2013.

[70] X. Wang, Y. Zhang, G. B. Giannakis, and S. Hu, "Robust smart-grid-powered cooperative multipoint systems," *IEEE Trans. Wireless Commun.*, vol. 14, no. 11, pp. 6188–6199, Nov. 2015.

[71] X. Wang, Y. Zhang, T. Chen, and G. B. Giannakis, "Dynamic energy management for smart-grid-powered coordinated multipoint systems," *IEEE J. Sel. Areas Commun*, vol. 34, no. 5, pp. 1348–1359, May 2016.

[72] S. Hu, X. Wang, Y. Zhang, and G. B. Giannakis, "Optimal resource allocation for smart-grid powered MIMO broadcast channels," in *Proc. WCSP*, 2015, pp. 1–5.

[73] R. Urgaonkar, B. Urgaonkar, M. J. Neely, and A. Sivasubramaniam, "Optimal power cost management using stored energy in data centers," *Proc. ACM SIGMETRICS*, vol. 39, no. 1, pp. 181–192, Jan. 2011.

[74] S. Lakshminarayana, T. Q. S. Quek, and H. V. Poor, "Cooperation and storage tradeoffs in power grids with renewable energy resources," *IEEE J. Sel. Areas Commun.*, vol. 32, no. 7, pp. 1386–1397, July 2014.

[75] S. Sun, M. Dong, and B. Liang, "Real-time power balancing in electric grids with distributed storage," *IEEE J. Sel. Topics Signal Process.*, vol. 8, no. 6, pp. 1167–1181, Jun. 2014.

[76] Y. Yao, L. Huang, A. Sharma, and L. Golubchik, "Data centers power reduction: A two time scale approach for delay tolerant workloads," in *Proc. INFOCOM*, 2012, pp. 1431–1439.

[77] W. Deng, F. Liu, H. Jin, C. Wu, and X. Liu, "Multigreen: cost-minimizing multi-source datacenter power supply with online control," in *Proc. of ACM e-Energy*, 2013, pp. 149–160.

[78] N. Prasad, M. Arslan, and S. Rangarajan, "A two time scale approach for coordinated multi-point transmission and reception over practical backhaul," in *Proc. of COMSNETS*, 2014, pp. 1–8.

[79] H. Yu, H. C. Man, L. Huang, and J. Huang, "Power-delay tradeoff with predictive scheduling in integrated cellular and Wi-Fi networks," *IEEE J. Sel. Areas Commun.*, vol. 34, no. 4, pp. 735–742, Apr. 2016.

[80] C. Valenta and G. Durgin, "Harvesting wireless power: Survey of energy-harvester conversion efficiency in far-field, wireless power transfer systems," *IEEE Microw. Mag.*, vol. 15, no. 4, pp. 108–120, May 2014.

[81] W. Ni, R. P. Liu, J. Biswas, X. Wang, I. B. Collings, and S. Jha, "Multiuser MIMO scheduling for mobile video applications," *IEEE Trans. Wireless Commun.*, vol. 13, no. 10, pp. 5382–5395, Oct. 2014.

[82] X. Chen, X. Wang, and X. Zhou, "Energy-harvesting powered transmissions of delay-limited data packets," in *Proc. Globecom*, 2014.

[83] X. Wang and G. B. Giannakis, "Resource allocation for wireless multiuser OFDM networks," *IEEE Trans. Inf. Theory*, vol. 57, no. 7, pp. 4359–4372, July 2011.

[84] S. Boyd and L. Vandenberghe, *Convex Optimization*. Cambridge University Press, 2004.

[85] T. M. Cover and J. A. Thomas, *Elements of information theory*. Tsinghua University Pres, 2003.

[86] L. Li and A. J. Goldsmith, "Capacity and optimal resource allocation for fading broadcast channels - part i: Ergodic capacity," *IEEE Trans. Inf. Theory*, vol. 47, no. 3, pp. 1083–1102, Mar. 2001.

[87] H. Weingarten, Y. Steinberg, and S. S. Shamai, "The capacity region of the gaussian multiple-input multiple-output broadcast channel," *IEEE Trans. Inf. Theory*, vol. 52, no. 9, pp. 3936–3964, Sept. 2006.

[88] A. Tolli, H. Pennanen, and P. Komulainen, "Decentralized minimum power multicell beamforming with limited backhaul signaling," *IEEE Trans. Wireless Commun.*, vol. 10, no. 2, pp. 570–580, Feb. 2011.

[89] Y. Zhang, N. Gatsis, and G. B. Giannakis, "Robust energy management for microgrids with high-penetration renewables," *IEEE Trans. Sustain. Energy*, vol. 4, no. 4, pp. 944–953, Apr. 2013.

[90] G. B. Giannakis, V. Kekatos, N. Gatsis, and S. J. Kim, "Monitoring and optimization for power grids: A signal processing perspective," *IEEE Signal Process. Mag.*, vol. 30, no. 5, pp. 107–128, May 2013.

[91] L. Georgiadis, M. J. Neely, and L. Tassiulas, "Resource allocation and cross-layer control in wireless networks," *Found. and Trends in Networking*, vol. 1, no. 1, pp. 1–144, Jan. 2006.

[92] U. Erez and S. Ten Brink, "A close-to-capacity dirty paper coding scheme," *IEEE Trans. Inf. Theory*, vol. 51, no. 10, pp. 3417–3432, Oct. 2005.

[93] N. Jindal, S. Vishwanath, and A. Goldsmith, "On the duality of gaussian multiple-access and broadcast channels," *IEEE Trans. Inf. Theory*, vol. 50, no. 5, pp. 768–783, May 2004.

[94] S. Vishwanath, N. Jindal, and A. Goldsmith, "Duality, achievable rates, and sum-rate capacity of gaussian mimo broadcast channels," *IEEE Trans. Inf. Theory*, vol. 49, no. 10, pp. 2658–2668, Oct. 2003.

[95] G. Scutari, D. P. Palomar, F. Facchinei, and J. S. Pang, "Convex optimization, game theory, and variational inequality theory," *IEEE Signal Process. Mag.*, vol. 27, no. 3, pp. 35–49, Mar. 2010.

[96] A. L. Stolyar, "Greedy primal-dual algorithm for dynamic resource allocation in complex networks," *Queueing Syst.*, vol. 54, no. 3, pp. 203–220, Mar. 2006.

[97] X. Wang, G. B. Giannakis, and A. G. Marques, "A unified approach to QoS-guaranteed scheduling for channel-adaptive wireless networks," *Proc. IEEE*, vol. 95, no. 12, pp. 2410–2431, Dec. 2007.

[98] A. Eryilmaz and R. Srikant, "Fair resource allocation in wireless networks using queue-length-based scheduling and congestion control," *IEEE Trans. Netw.*, vol. 15, no. 6, pp. 1333–1344, June 2007.

[99] Y. Zhang, N. Gatsis, and G. B. Giannakis, "Risk-constrained energy management with multiple wind farms," in *Proc. of 4th IEEE-PES on Innovative Smart Grid Tech.*, 2013, pp. 1–6.

[100] I. Hwang, B. Song, and S. S. Soliman, "A holistic view on hyper-dense heterogeneous and small cell networks," *IEEE Commun. Mag.*, vol. 51, no. 6, pp. 20–27, June 2013.

[101] R. Irmer, H. Droste, P. Marsch, M. Grieger, G. Fettweis, S. Brueck, H. P. Mayer, L. Thiele, and V. Jungnickel, "Coordinated multipoint: Concepts, performance, and field trial results," *IEEE Commun. Mag.*, vol. 49, no. 2, pp. 102–111, Feb. 2011.

[102] H. Dahrouj and W. Yu, "Coordinated beamforming for the multicell multi-antenna wireless system," *IEEE Trans. Wireless Commun.*, vol. 9, no. 5, pp. 1748–1759, May 2010.

[103] J. Zhang, R. Chen, A. Ghosh, A. Ghosh, and R. W. Heath, "Networked MIMO with clustered linear precoding," *IEEE Trans. Wireless Commun.*, vol. 8, no. 4, pp. 1910–1921, Apr. 2009.

[104] C. T. K. Ng and H. Huang, "Linear precoding in cooperative MIMO cellular networks with limited coordination clusters," *IEEE J. Sel. Areas Commun.*, vol. 28, no. 9, pp. 1446–1454, Sept. 2010.

[105] E. Oh, B. Krishnamachari, X. Liu, and Z. Niu, "Toward dynamic energy-efficient operation of cellular network infrastructure," *IEEE Commun. Mag.*, vol. 49, no. 6, pp. 56–61, June 2011.

[106] X. Liu, "Economic load dispatch constrained by wind power availability: A wait-and-see approach," *IEEE Trans. Smart Grid*, vol. 1, no. 3, pp. 347–355, Mar. 2010.

[107] "*Mobile networks go green*," Available online: http://www1.huawei.com/en/about-huawei/publications/communicate/hw-082734.htm.

[108] D. Li, W. Saad, I. Guvenc, A. Mehbodniya, and F. Adachi, "Decentralized energy allocation for wireless networks with renewable energy powered base stations," *IEEE Trans. on Commun.*, vol. 63, no. 6, pp. 2126–2142, June 2015.

[109] J. Qin, Y. Chow, J. Yang, and R. Rajagopal, "Distributed online modified greedy algorithm for networked storage operation under uncertainty," *IEEE Trans. Smart Grid*, vol. 7, no. 2, pp. 1106–1118, Feb. 2017.

[110] A. Wiesel, Y. C. Eldar, and S. Shamai, "Linear precoding via conic optimization for fixed MIMO receivers," *IEEE Trans. Signal Process.*, vol. 54, no. 1, pp. 161–176, Jan. 2005.

[111] H. Robbins and S. Monro, "A stochastic approximation method," *Annals of Mathematical Statistics*, vol. 22, no. 3, pp. 400–407, 1951.

[112] L. Huang, "Fast-convergent learning-aided control in energy harvesting networks," Available online: http://arxiv.org/abs/1503.05665.

[113] M. J. Neely, "Stochastic network optimization with application to communication and queueing systems," *Synthesis Lectures on Communication Networks*, vol. 3, no. 1, pp. 1–211, Jan. 2010.

[114] ——, "Stability and capacity regions or discrete time queueing networks," *Computer Science*, 2010.